L s z
9 000004 122389

OF 1915

ANALELE UNIVERSITATII BUCURESTI

fizica

Theoretical Physics ● Plasma Physics ● Liquid State Physics ● Solid State Physics ● Polimers Physics ● Eart Physics

ANUL XXXII — 1983

FIZICĂ

COMITETUL DE REDACȚIE

Redactor responsabil : Prof. dr. *C. Plăvițu*
Redactor responsabil adj. : Conf. dr. *I. Licea*
Membri : Prof. dr. *I. Petrea*
Prof. dr. *I. Iova*
Prof. dr. *V. Gheorghe*
Prof. dr. *V. Grecu*
Conf. dr. *C. Vrejoiu*
Secretar de redacție : Conf. dr. *L. Georgescu*

REDACȚIA

TIPOGRAFIA UNIVERSITĂȚII BUCUREȘTI
Șoseaua Panduri, nr. 90
Telefon 31.40.00/122

OF 1915

ANALELE UNIVERSITĂȚII BUCUREȘTI

BUDAPESTI MŰSZAKI ÉS GAZDASÁGTUDOMÁNYI EGYETEM
Országos Műszaki Információs Központ és Könyvtár
2001

FIZICĂ

1983

SUMAR ● CONTENTS

THEORETICAL PHYSICS

D. ȘTEFĂNESCU : Algebraic Methods for Finding Instantons . . . 3

PLASMA PHYSICS

G. G. BRĂTESCU, MAGDA CAZAN-CORBASCA : Potentiels explosifs dans des mélanges de krypton et de vapeurs de l'alcool isobutilique 7

LIQUID STATE PHYSICS

L. GEORGESCU, POPA-NIȚĂ VLAD : On a Statistical Description of the Surface Tension of a Three-Dimensional Liquid Phase Interface 11

SOLID STATE PHYSICS

S. I. SPÂNULESCU, I. SPÂNULESCU : On the Problem of Averaging with Negative Covariance of the Correlated Samples 17
I. MUNTEANU, I. DIMA, MOHAMED ISMAIL ABD EL ATI : Anomalous Photovoltaic Effect in CdTe and CdSe Thin Films . . 23
TALAL KHALASS, I. SPÂNULESCU, I. SECĂREANU, N. BĂLȚĂȚEANU: The Crystalline Structure of the Electron Irradiated CdSe Films . 31
B. LOGOFĂTU, D. BRÂNCUȘ, A. DAFINEI, MICHAELA LOGOFĂTU, I. DAFINEI : Growth of Polycrystalline $CuInSe_2$ 37

ATH. TRUŢIA, FLORIANA IOVA, ANA DANCU: Electron Transfer Bands of the Co^{2+}, Ni^{2+} and Cu^{2+} Ions in $CdCl_2$ and $CdBr_2$ Lattices . 43

POLIMERS PHYSICS

I. C. PETREA, M. LEANCĂ, G. E. GRIGORIU, A. GRIGORIU : The Structure and Properties of Oriented Polypropylene (PP) Films . 49

E. BARNA, LIVIA IONESCU, CARMEN RĂDULESCU, C. RĂDULESCU : Méthode d'analyse dérivatographique des mécanismes thermo-oxidatifs dans le polyéthylène 55

G. E. GRIGORIU, AURELIA GRIGORIU, M. LEANCĂ, I. C. PETREA : Structural Modifications at the Spinning of Polypropylene (PP) Yarns 63

L. GEORGESCU, SAEED BAFAYAD, V. POPA-NIŢĂ, M. I. CHIPARĂ, RODICA MOLDOVAN, L. BUCŞA, E.S.R. Studies on Liquid Crystals 69

EARTH PHYSICS

D. BORŞAN, SABINA ŞTEFAN, Determination of the Fog Intrinsic Parameters by Means of the Laser Radiation Extinction . . . 87

ELENA DECU, ŞT. LASCU : Correlated Analysis of Particle Concentration and Meteorological Parameters on the Măgurele Platform 91

ŞT. LASCU, ELENA DECU : Considerations upon the Variation of the Seismic Wave Velocity Beneath the Vrancea Zone 95

8482

Budapesti Műszaki Egyetem
Központi Könyvtára
Folyóiratosztály
P 138/1984

ANALELE UNIVERSITĂŢII BUCUREŞTI, FIZICA, XXXII, 1983, pag. 3—4

1989

ALGEBRAIC METHODS FOR FINDING INSTANTONS

D. ŞTEFĂNESCU
University of Bucharest, Faculty of Physics *

Abstract. We describe what algebraic objects are needed for obtaining local and general solutions of the Yang-Mills equations, the so-called instantons. Then we discuss some algebraic algorithms that are usefull in the study of the Yang-Mills fields.

1. Algebraic expression of Yang—Mills equations

C. N. Yang and R. L. Mills described in [3] some field equations which are a generalization of Maxwell's equations (in vacuum). Recently these equations were formulated in terms of Lie groups ([1], [2]). Such formulations first appeared in physics in the attempt of H. Weyl to unify general relativity and electro-magnetism ([9]).

Let G be a compact Lie group, L (G) its Lie algebra and let M^4 be the Minkowski space. A set of functions $A_i : M^4 \to L(G)$, $i = 1, 2, 3, 4$, is called a *gauge potential*. Let's consider the operator ∇_i defined on the vectorial functions on M^4 by

$$\nabla_i = \partial_i + A_i \text{ where } \partial_i = \frac{\partial}{\partial x_i},\ x = (x_1, \dots, x_4) \in M^4. \tag{1}$$

The *gauge field* F_{ij} is defined by

$$F_{ij} := [\nabla_i, \nabla_j] = \partial_i A_j - \partial_j A_i + [A_i, A_j] \tag{2}$$

where the commutator $[A_i, A_j]$ is taken in the Lie algebra L(G).

The field equations for a gauge theory, written with respect to the covariant derivative ∇_i and with the units such that the velocity of light is 1, are

$$[\nabla_i, [\nabla_j, \nabla_k]] + [\nabla_j, [\nabla_k, \nabla_i]] + [\nabla_k, [\nabla_i, \nabla_j]] = 0 \tag{3}$$

$$[\nabla_i, [\nabla_i, \nabla_j]] = 0 \tag{4}$$

---

* National Center of Physics, Bucharest-Măgurele, PO Box 5211.

The relation (3) is an identity. The relation (4) is called the *Yang-Mills equation.* For $G = U(1)$, the complex unitary group, one can deduce from (4) Maxwell's equations. A solution of (4) is called an *instanton.*

In the case G is a compact non-abelian Lie group the Yang-Mills equations are different from the classical case. For instance, in the case $G = SU(2)$ in [2] some instantons ar described. In the quaternionic notation we can describe them by $A^{(1)}(x) = \mathrm{Im}\, \frac{\bar{x}\, dx}{1 + |x|^2}$, $F^{(1)} = \frac{d\bar{x} \wedge dx}{(1 + |x|^2)^2}$ and $A^{(2)} = \mathrm{Im}\, \frac{x d\bar{x}}{1 + |x|^2}$, $F^{(2)} = \frac{dx \wedge d\bar{x}}{(1 + |x|^2)^2}$, where the symbol "$-$" denotes the quaternionic conjugation.

For obtaining general instantons it is necessary to use other algebraic and geometrical techniques: the 3—dimensional complex projective space (see, for instance, [4]), the holomorphic bundles. We describe below some algorithmic methods from the theory of polynomials and power series. They are usefull in the study of the projective space and of the singular points.

2. The division of polynomials in many variables

Let k be a field and let's consider the k-algebra $k[X_1, \dots X_n]$ of the polynomials in n variables with coefficients in the field k. If we consider two polynomials from $k[X_1, \dots X_n]$ we are interested to know how to divide one by another. For $n = 1$ this is a very well known fact, but for $n \geqslant 2$ there is no a „Canonical way" to do the division.

If we fix a polynomial f in n variables with coefficients in the field k we are interested to find a k-automorphism t of the k-algebra $k[x_1, \dots x_n]$ such that t(f) be almost monic with respect to one variable, for instance x_n. If this done, we can divide the images under t of the polynomials from $k[x_1, \dots x_n]$ by t(f) (division with respect to the variable x_n). We recuperate the initial polynomials by t^{-1}. Such a situation is described in the sequel.

2.1. Proposition. Let k be a commutative field of characteristic $\neq 2$, *let n, u be natural numbers ard let* $f_1, \dots, f_u$ *be nonconstant polynomials from* $k[x_1, \dots x_n]$. *Then there is a k-automorphism t of* $k[x_1, \dots x_n]$ *such that the polynomials* $t(f_1), \dots t(f_u)$ *be almost monic with respect to every variable* $x_1, \dots x_n$.

Proof. We first record that a polynomial f is called almost monic with respect to the variable x_n if there are $a_n \in k^*$, $g \in k[x_1, \dots, x_n]$ such that $f = a_n x_n^{\deg f} + g$ and $\deg x_n g < \deg f$.

Let K be a natural number such that $K > \max(\deg f_1, \ldots, \mathrm{def}\, f_u)$ and let $a = K^i$. As in the proof of the normalization lemma we consider the k-automorphism s of $k[x_1, \ldots . x_n]$ defined by $s(x_1, x_2, \ldots x_n) = (x_1, x_2 - x_1^{a_2}, \ldots, x_n - x_1^{a_n})$ (as in [5]). Let $f_j = \sum a_j x_1^{p_{j1}} \ldots x_n^{p_{jn}}$. Since all the sums $p_{j1} + a_2 p_{j2} + \ldots + a_n p_{jn}$ are distinct for $j = 1, 2, \ldots u$ there is an unique $(b_{j1}, \ldots, b_{jn})$ such that $\deg(x_1^{b_{j1}} \ldots x_n^{b_{jn}}) = \deg s(f_j)$. Let r be the k-automorphism of $k[x_1, \ldots . x_n]$ defined by $r(X_1, \ldots X_n) = (X_1 + \ldots + X_n, X_1 - X_2 + X_3 + \ldots X_n, \ldots, X_1 + \ldots X_{i-1} - X_i + X_{i+1} + \ldots + X_n, \ldots, X_1 + \ldots + X_{n-1} - X_n)$. It suffices to take $t = r^* s$.

3. A problem of linear algebra

In various practical and theoretical problems we must know if some linear systems with a great number of equations admit solutions (or nontrivial solutions). We describe a situation in which we can decide in a finite number of steps if a linear infinite homogeneous system admits nontrivial solutions.

Let n be a natural number, a an integer number, $i \geqslant a$ and let $(a_j)_{j \geqslant a}$ be a sequence of elements from the commutative field k of characteristic $p \neq 0$. We call the determinant

$$P_{i,n} = \begin{vmatrix} a_1 & a_{i+1}^{p} \ldots a_{i+n}^{p^n} \\ a_{i+1} & a_{i+2}^{p} \ldots a_{i+n+1}^{p^n} \\ \cdot & \cdot \quad \cdot \quad \cdot \quad \cdot \quad \cdot \\ a_{i+n} & a_{i+n+1}^{p} \ldots a_{i+2n}^{p^n} \end{vmatrix}$$

the *p*-Hankel (i, n)-determinant of the sequence $(a_j)_{j \geqslant a}$.

3.1. Lemma. With the above notation we have :

i) $P_{i,n} P_{i+2,n-2}^{p} + P_{i+2,n-1}^{p} P_{i,n-1} = P_{i+1,n-1}^{p+1}$.

ii) *If* $P_{j+m,n} = 0$ *for* $0 \leqslant m \leqslant r - 1$ *then all the determinants* $P_{j+m,n-1}$ $(1 \leqslant m \leqslant r)$ *are simultaneously zero or nonzero.* (For the proof we refer to [7]).

3.2. Proposition. Let $(a_j)_{j \geqslant a} \subset k$. *Then the homogeneous infinite linear system*

$$(*) \quad a_1 Y_0 + a_{i+1}^{p} Y_1 + \ldots + a_{i+n}^{p^n} Y_n = 0 \quad (i \geqslant a)$$

admits nontrivial solutions if there is a natural number $q \leqslant n$ *such that* $P_{i,q} = 0$, $P_{i,q-1} \neq 0$ *for every* $i \geqslant a$.

Proof. It suffices to show that a nontrivial solution of the system

$$\sum_{j=0}^{q} a_{i+j}^{p^j} Y_j = 0 (a \leqslant i \leqslant a+q)$$

is also a solution of the system

$$\sum_{j=0}^{q} a_{i+j}^{p^j} = 0 (a+1 \leqslant i \leqslant a+q+1).$$

Let $(c_0, \ldots, c_q)$ be such a solution. We consider $B_1 = (a_a, \ldots, a_{a+q}^{pq}), \ldots, B_{q+2} = = (a_{a+q+1}, \ldots, a_{a+2q+1}^{p^q}), C_1 = a_a, \ldots, a_{a+q-1}^{p^{q-1}}), \ldots, C_{q+1} = a_{a+q}, \ldots, a_{a+2q-1}^{p^{q-1}})$. Since $P_{i,q} = 0$ for $i \geqslant a$ it follows that the rows $B_1, \ldots, B_{q+1}$ are linearly dependent over k, i.e. there are $e_1, \ldots, e_{q+1} \in \mathbf{k}$, not all e_j zero, such that $e_1B_1 + \ldots + e_{q+1}B_{q+1} = 0$. If $e_{q+1} = 0$ it would follow that $C_1, \ldots, C_q$ were linearly dependent over k, fact that contradicts the assumption that $P_{a,q-1} \neq 0$. Therefore $e_{q+1} \neq 0$. Then there are $d_1, \ldots, d_q \in k$, not all d_j zero, ,such that $B_{q+1} = d_1B_1 + \ldots + d_qB_q$. Similarly there are $f_2, \ldots, f_{q+1} \in k$, not all f_j zero, such that $B_{q+2} = f_2B_2 + \ldots + f_{q+1}B_{q+1}$. It follows that $(c_0, \ldots, c_q)$ is a solution of the second system.

3.3. *Remarks*. i) The proposition 3.2. can be used for improving the criteria obtained in [6].

ii) Similar results can be obtained also for fields of characteristic zero by making use of the clasical Hankel determinants.

, iii) The former result can be used for proving that some power series are rational, fact which is important in the study of holomorphic bundles.

REFERENCES

1. M. F. ATIYAH, R. S. WARD. *Comm. Math. Phys. 55*, 117 (1977).
2. A. BELAVIN, A. POLYAKOV, A. ACHWARTZ, Y. TYUPKIN, *Phys. Lett. 59B*, 85 (1975).
3. R. L. MILLS, C. N. YANG, *Phys. Rev. 96*, 191 (1954).
4. R. PENROSE, *Rep. Math. Phys. 12, 65* (1977).
5. N. RADU, *Local rings*, v. 1, Ed. Acad. R. S. Romania (in Rumanian) (1968).
6. D. ŞTEFĂNESCU, *Bull. Math.* de la Soc. Math. de la R. S. Roumanie 26 *(74)*, 77 (1982).
7. D. ŞTEFĂNESCU, *Bull. Math.* de la Soc. Math. de la R. S. Roumanie (1983) (to appear).
8. G. 'T. HOOFT, Phys. Rev. D *14*, 3432 (1976).
9. H. WEYL, *Sitz. Köng. Preuss. Akad. Wiss., 26*, 465 (1918).

Received, 18 November, 1982

ANALELE UNIVERSITĂŢII BUCUREŞTI, FIZICA, XXXII, 1983, pag. 7—10

POTENTIELS EXPLOSIFS DANS DES MÉLANGES DE KRYPTON ET DE VAPEURS DE L'ALCOOL ISOBUTILIQUE

G. G. BRĂTESCU, MAGDA CAZAN-CORBASCA
Faculté de Physique, Université de Bucarest *

Résumé. On a calculé les potentiels explosifs et on a tracé les courbes de Paschen dans le krypton à l'état pur et dans des mélanges de proportions differentes du krypton avec des vapeurs de l'alcool isobutilique. Les électrodes employées sont de Al et de Ni.

1. Introduction

Dans cet ouvrage on s'est proposé, comme object d'étude, les mélanges de krypton et de vapeurs de l'alcool isobutilique, en utilisant des électrodes de Al et de Ni.

On a déterminé expérimentalement les potentiels explosifs, V_a, et en même temps on a tracé les courbes de Paschen dans le krypton à l'intention de comparer les résultats obtenus à ceux existants trouvés dans la littérature.

Les résulats concernant les vapeurs de l'alcool isobutilique à l'état pur sont mentionés dans un ouvrage anterieur /1/.

2. Résultats

Les déterminations ont été effectuées avec la même instalation, et de la même manière que dans le cas des divers alcools étudiés /1, 2, 3, 4, 5/.

Les courbes de Paschen $V_a = f(pd)$ (où p est la pression du gaz et d la distance entre les électrodes), pour le krypton, en employant des élecrtodes de Al et de Ni, sont présentées dans la figure 1.

---

* Centre National de Physique, Măgurele-Bucarest P.O. Box 5211.

On a obtenu les valeurs :

$V_{a_{min}} = 259 \pm 1$ V ; $(pd)_{min} = 11,90 \pm 0,1$ mm Torr pour les électrodes de Al,

$V_{a_{min}} = 296 \pm 1$ V ; $(pd)_{min} = 4,90 \pm 0,1$ mm Torr pour les électrodes Ni, les résultats étant appropriés à ceux trouvés dans la littérature de spécialite /6/.

On a tracé les courbes de Paschen dans les suivants mélanges :

14,18% alcool isobutilique en mélange et 6,27% krypton en mélange, pour des électrodes de Al (les courbes des figures 2, et 3) ;

26,40% alcool isobutilique en mélange, pour des électrodes de Ni (la courbe de la figure 4).

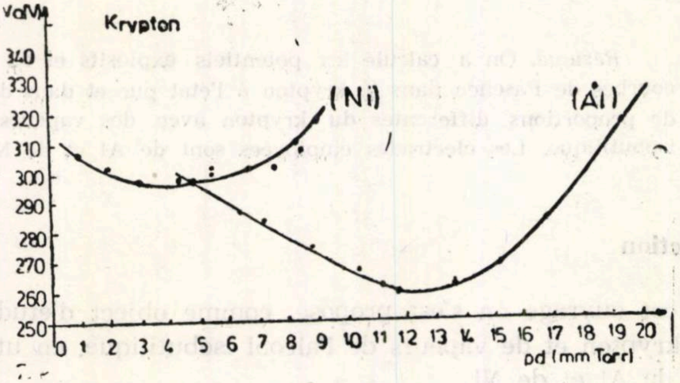

Fig. 1 Les courbes de Paschen pour le Kr, pour des électrodes de Al et de Ni.

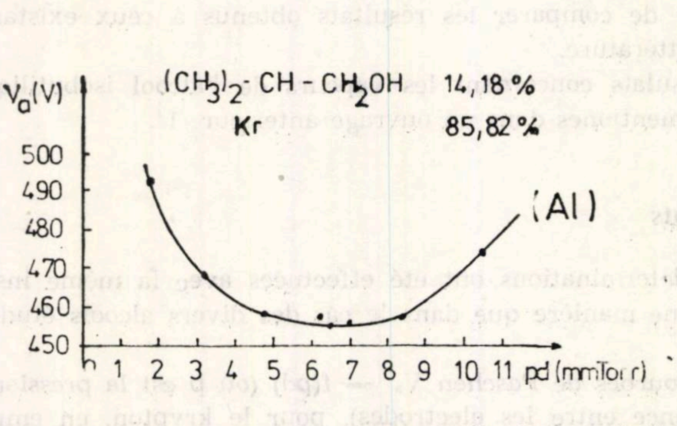

Fig. 2 La courbe de Paschen pour 14,18% alcool isobutilique dans le mélange avec le krypton, pour des électrodes de Al.

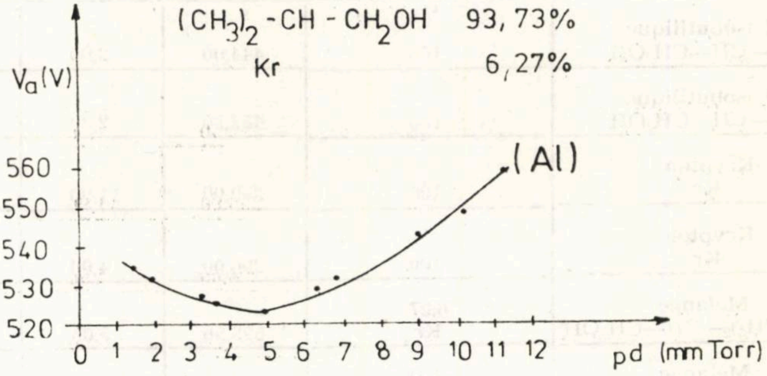

Fig. 3 La courbe de Paschen pour 6,27% krypton dans le mélange avec l'alcool isobutilique, pours des électrodes de Al.

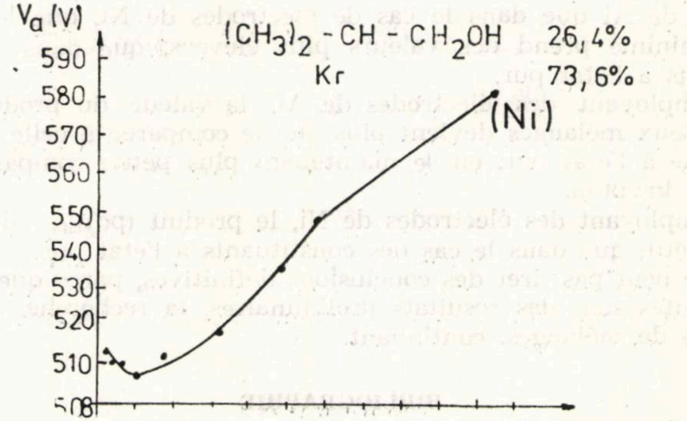

Fig. 4 La courbe de Paschen pour 26,40% alcool isobutilique dans le mélange avec le krypton, pour des électrodes de Ni

Dans le tableau I, on retrouve les valeurs du potentiel explosif minime et du produit $(pd)_{min}$ correspondant, pour les constituants du mélange à l'état pur, de même que pour les trois mélanges étudiés, pour des électrodes de Al et de Ni.

Tableau 1

Substance	Proportion %	V_{min}(V)	$(pd)_{min}$ mm Torr	Électrodes
Alcool isobutilique $(CH_3)_2$—CH—CH_2OH	100	444,00	3,00	Al
Alcool isobutilique $(CH_3)_2$—CH—CH_2OH	100	452,50	2,80	Ni
Krypton Kr	100	259,00	11,90	Al
Krypton Kr	100	296,00	4,90	Ni
Mélange Kr + $(CH_3)_2$—CH—CH_2OH	6,27 Kr	523,50	5,00	Al
Mélange Kr + $(CH_3)_2$—CH—CH_2OH	14,18 $(CH_3)_2$—CH—CH_2OH	454,80	6,50	Al
Mélange Kr + $(CH_3)_2$—CH—CH_2OH	26,48 $(CH_3)_2$—CH—CH_2OH	506,00	1,15	Ni

3. Discussion des résultats

On constate pour les trois mélanges, tant dans le cas de l'emploi des électrodes de Al que dans le cas de électrodes de Ni, que le potentiel explosif minime prend des valeurs plus élévées, que dans le cas des constituants à l'état pur.

En employant des électrodes de Al, la valeur du produit $(pd)_{min}$ pour les deux mélanges devient plus élevée comparée à celle de l'alcool isobutilique à l'état pur, en se maintenant plus petite comparativement à celle du krypton.

En employant des électrodes de Ni, le produit $(pd)_{min}$ du mélange est plus petit, que dans le cas des constituants à l'état pur.

On ne peut pas tirer des conclusions définitives, parce que les résultats présentés sont des résultats préliminaires, la recherche, concernant ces formes de mélanges, continuant.

BIBLIOGRAPHIE

1. G. G. BRĂTESCU, M. CAZAN-CORBASCA, Anal. Univ. București, Fizică, 31, 17 (1982)
2. G. G. BRĂTESCU, M. CAZAN-CORBASCA, Anal. Univ. București, Fizică, 27, 11 (1978)
3. G. G. BRĂTESCU, M. CAZAN-CORBASCA, Anal. Univ. București, Fizică, 9 (1980)
4. G. G. BRĂTESCU, M. CAZAN-CORBASCA, C. DAMACUS, Anal. Univ. București, Fizică, 30, 13 (1981).
5. G. G. BRĂTESCU, M. CAZAN-CORBASCA, C. MARMANDIU, Buletinul Institutului de Petrol și Gaze, Ploiești, XXVIII, 73 (1978).
6. A. A. KRUITHOFF, Physica, VII, 519 (1940).

ANALELE UNIVERSITĂȚII BUCUREȘTI, FIZICA, XXXII, 1983, pag. 11—16

ON A STATISTICAL DESCRIPTION OF THE SURFACE TENSION OF A THREE-DIMENSIONAL LIQUID PHASE INTERFACE

L. GEORGESCU and POPA NIȚĂ VLAD
Faculty of Physics, University of Bucarest *

Abstract. Let's consider the phase interface of the liquid vapour, a real, three-dimensional one. The surface tension of this phase is expressed by the intermediary of the radial distribution function taking into account that the density of the phase interface depends on the distance like the function hyperbolical tangent. The relation we thus obtain is explicity expressed for argon and neon and there after it is compared with the experimental data.

1. Introduction

Within the statistical description of the interface properties of the liquids, the surface tension of the liquid in contact with their vapours is expressed by the intermediary of the correlation functions through the relations [1], [2].

$$\gamma = \frac{1}{2}\int_{-\infty}^{\infty} dz_1 \iiint \nabla_1 \Phi(r_{12})\, \rho_{(2)}(z_1, \vec{r}_{12})\, \frac{x_{12}^2 - r_{12}^2}{r_{12}}\, d\vec{r}_{12} \tag{1}$$

where Φ is the pair interaction potential.

If the pressure and the temperature are chosen in such a manner that the liquid phase coexists in equilibrium with its vapours, then the presence of the gravitational field would determine a plane region of transition between the phases.

The local density of the particles in this region is $\rho_1(z_1) = \rho g_1(z_1)$, where $g_1(z_1)$ reprezents the single correlation function and it varies from the value in the liquid phase ρ_L to the value in the vapours ρ_V.

---

* National Center of Physics, Măgurele, Bucharest, Roumania, P. O. Box 5211.

The lack of homogeneity of the local density implies the anisotropy of the binary distribution, namely:

$$\rho_2(z_1, \vec{r}_{12}) = \rho_1(z_1)\rho_1(z_2)g_2(z_1, \vec{r}_{12}) \tag{2}$$

where $g_2(z_1, \vec{r}_{12})$ is the correlation function of the second degree.

In order to be able to calculate the surface tension of the liquids by the help of the relation (1) we have to know explicitly the function ρ_2, this fact implies to determine from the relation (2) the correlation function of the second degree $g_2(z_1, \vec{r}_{12})$ for the phase interface, which is known exactly neither theoretically nor experimentally.

In order to simplify the theory, Kirkwood, Buff and Fowler [3] [4] consider the liquid to be a column of an one-component fluid in contact with its vapours, along the OZ_1 axis (see figure 1), with the distribution function of the following form:

$$\rho_2(z_1) = \begin{cases} \rho_L & \text{for } z_1 \leqslant 0 \\ 0 & \text{for } z_1 > 0 \end{cases} \tag{3}$$

and

$$\rho_2(z_1, \vec{r}_{12}) = \rho_1(z_1)\rho_{(1)}(z_1 + z_{12})g_2^L(\vec{r}_{12}), \tag{4}$$

The relation (3) implies to neglect the vapour phase (the density) in comparison with the liquid phase. The relation (4) is equivalent to the approximation of the liquid phase interface with a surface of mathematical division, a gibbsian division, where the liquid is homogeneous up to the plane $z_1 = 0$ and the contribution of the interface layer is neglected (see fig. 1).

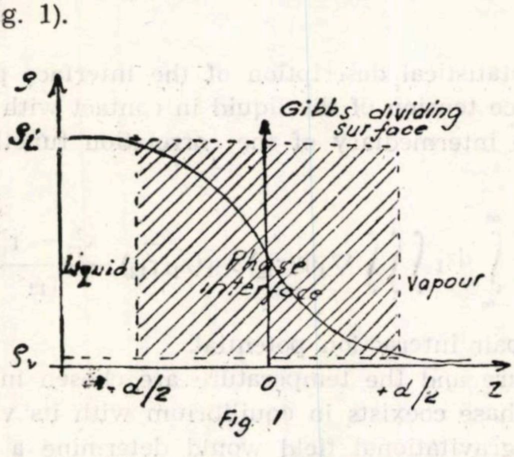

Fig. 1 The liquid, vapour and phase interface in equilibrium; the full line is the interfacial density profile for a Lennard — Jones fluid.

Introducing the approximation (3) and (4) into the relation (1) and integrating there after with respect to z_1 and to the angular variables, we obtain [1], [2], [5] the known relation:

$$\gamma = \frac{\pi \rho_L^2}{8} \int_0^\infty r_{12}^4 \nabla_1 \Phi (r_{12})\, g_2^L (r_{12})\, dr_{12} \tag{5}$$

If we calculate the surface tension of argon by the help of the relation (5) at a temperature of 90 K, we would obtain the theoretical value 14.9 dyn/cm [2], while the experimental one is 11.9 dyn/cm. Likewise for neon at a temperature of 27.2 K we determine the theoretical value 6.0 dyn/cm to 4.8 dyn/cm, which is the experimental value. As one can notice in these two examples, the difference between the theoretical and the experimental data is quite significant.

2. The surface tension of the three-dimensional phase interface

The surface model of gibbsian division is far from being a real three-dimensional phase. The system liquid phase in equilibrium with its vapours could be considered as three autonomous phases : the liquid phase, the vapours and the phase interface, which is a three-dimensional phase like the liquid and the vapours ones. Within this real model, the surface tension of a liquid in contact with its vapours is :

$$\gamma = \gamma_L + \gamma_V + \gamma_{12} \tag{6}$$

where γ_{12} is the surface tension of the phase interface. Its expresion is given by the following relation :

$$\gamma_{12} = \frac{\rho_V \rho_L}{2} \int_{-d/2}^{d/2} dz_1 \iiint \nabla_1 \Phi (r_{12})\, g_2^{(1,2)} (r_{12})\, \frac{x_{12}^2 - z_{12}^2}{r_{12}}\, d\vec{r}_{12} \tag{7}$$

γ_V, the surface tension of the vapours is three orders smaller than γ_L, so that it can be neglected in comparison with γ_L.

In the relation (7) the radial distribution function $g_2^{(1,2)} (\vec{r}_{12})$ of the phase interface is unknown and because of this it is expressed by the intermediary of the radial distribution functions of the liquid phase an of the vapour one. This dependence can have different forms but, when we tend to the liquid or to the vapour phase we must rediscover the radial distribution function of these phases.

The radial distribution function of the phase interface may have a simple form of the following type [7], [6].

$$g_2^{(1,2)} (r_{12}) = \frac{1}{2} g_2^L (r_{12}) \left(1 - \frac{2z_1}{d}\right) + \frac{1}{2} g_2^V (r_{12}) \left(1 + \frac{2z_t}{d}\right) \tag{8}$$

which satisfies the limit condition stated above.

We introduce the relation (8) into the relation (7) and we integrate with respect to z_1 and to angular variables. We obtain finally (see details in paper [7]),

$$\gamma_{12} = -\frac{2\pi \rho_V \rho_L}{5d} \int_0^\infty r_{12}^5 \nabla_1 \Phi(r_{12}) \left[g_2^V(r_{12}) - g_{(2)}^L(r_{12}) \right] dr_{12} \tag{9}$$

where d is the thickness of the phase interface. The relation (9) was determined considering the simplifying hypothesis that the densities ρ_L and ρ_V have remained constant up to the division gibbsian surface.

By the help of the relation (9) we have theoretically calculated the surface tension of the three-dimensional phase interface for argon and neon. For the radial distribution function of argon we worked with the relation :

$$g_2^V(r) = e^{-\beta\Phi(r)}$$

$$g_2^L(r) = \left(\frac{a_l}{r}\right)^s \exp\left[\left(\frac{a_m}{a_l}\right)^t - \left(\frac{a_m}{r}\right)^t\right] \tag{10}$$

where $a_l = 4.15$ Å, $t = 14$, $s = 7$ and $a_m = 3.55$ Å. For the pair interaction potential we have chosen a form that approaches the potential (6, 12) [8].

$$\Phi(r) = \left[\frac{8.62 \cdot 10^{-8}}{r^{11,4}} - \frac{1.11 \cdot 10^{-10}}{r^6}\right] \text{erg}$$

Calculating the surface tension of the phase interface for argon on the basis of the relation (9) and having also taken into account (8), for $d = 8$ Å we obtain the value $\gamma_{12} = \varphi 0.595$ dyn/cm. Therefore, considering the relation (6), the final value of the surface tension for argon is $\gamma = 14.3$ dyn/cm.

For neon, we have chosen for the radial distribution functions the following forms :

$$\begin{aligned} g_2^V(r) &= e^{-\beta\Phi(r)} \\ g_2^L(r) &= e^{-\beta\Phi(r)}\, g_{HS}(r) \end{aligned} \tag{11}$$

and the interaction potential of the form [8]:

$$\Phi(r) = -\left[\frac{6.1}{r^6} + \frac{8.8}{r^8}\right] 10^{-12} \text{ erg}$$

where

$$g_{HS}(r) = \left[\alpha + \beta\left(\frac{r}{\sigma}\right)^2 + \delta\left(\frac{r}{\sigma}\right)^3\right] \tag{12}$$

is the radial distribution function of a hard sphere particle in the Percus-Yevick approximation [9], with $\eta = \frac{\pi a^3 \rho}{6}$. The coefficients α, β, δ are approximated relying on the parameter η through the relation :

$$(1-\eta)^4\alpha = (1+2\eta)^2$$

$$(1-\eta)^4\beta = -6\eta\left(1+\frac{\eta}{2}\right)^2 \tag{13}$$

$$(1-\eta)^4\delta = \frac{1}{2}\,\eta(1+2\eta)^2$$

, Introducing the relation (11) into relation (9) and having also considered the relations (12) and (13) with $\sigma = 2.82$ Å we obtain for neon the following value for the surface tension $\gamma_{12} = -0.74\frac{\text{dyn}}{\text{cm}}$. From the relation (6) we determine the value of the total surface tension $\gamma = 5.35$ dyn/cm which approaches better the experimental value of 4.8 dyn/cm.

As stated above, we have calculated the surface tension of the three dimensional phase interface by the help of the relation (9) considering the desity of liquid to the gibbsian surface of division. This approximation is hardly to be precise for a real phase interface, especially as the density of the liquid in this phase powerfully varies until the value of the density for the vapour phase [10] (see fig. 1). In order to consider the variation of the density in the real phase, too, we approximate the relation (2) in this way :

$$\rho_2(z_1, \vec{r}_{12}) \approx \rho_1(z_1)\rho_1(z_1)g_2(\vec{r}_{12}) \tag{14}$$

where [11] :

$$\rho_1(z_1) = \frac{\rho_L+\rho_V}{2} - \frac{\rho_L+\rho_V}{2}\,\mathrm{th}[a(z_1-b)] \tag{15}$$

with

$$b = \frac{1}{\sqrt{3}}\left(\frac{1}{a_1}-\frac{1}{a_2}\right) \qquad \begin{array}{ll} \text{for } z_1 < b & a = a_1 \\ \phantom{\text{for }} z_1 > b & a = a_2 \end{array} \tag{16}$$

We introduce the relation (16) into the relation (15), we expand $\mathrm{th}[a(z_1-b)]$ in series and there after we integrate numerically the relation (9) for argon and neon, with the same expressions for the pair interaction potential $\Phi(r_{12})$ and for the radial distribution function (16) and (11).

We finally obtain the value of the surface tension of the phase interface for argon $\gamma_{12} = -1.95$ dyn/cm, with $d = 8$ Å and for neon $\gamma_{12} = -0.87$ dyn/cm with $d = 8$ Å. Using the relation (6) the total surface tension for argon and neon has the values 12.95 dyn/cm respectively. These values approache the experimental ones better.

The model of the phase interface, as a three-dimensional phase approaches better a real model for the liquid-vapour interface than model of the gibbsian division interface.

3. Conclusions

The phase interface of the liquid-vapour is a real, three-dimensional one, representing a more complex model than that of Gibbs. We have expressed the surface tension of the three-dimensional phase of the liquid-vapour interface by the intermediary of the radial distribution function. At the same time, we have also considered that the density of this phase powerfully depends on the distance. The obtained relations for the surface tension has been applied for argon and neon and we have found out a better correlation of the theoretical data with the experimental ones.

REFERENCES

1. I. Z. FISHER, *Statistical Theory of Liquids*, University of Chicago Press, Chicago, 1964.
2. C. A. CROXTON, *Statistical Mechanics of the Liquid State*, John Wiley Sons, 1980.
3. J. G. KIRKWOOD and F. P. BUFF, J. Chem. Phys., 17, 338 (1949).
4. R. H. FOWLER, Proc. Roy. Soc. A 159, 229 (1937).
5. L. GEORGESCU, I. C. PETREA și D. BORȘAN, *Fizica stării lichidt*, E.D.P., 1982.
6. L. GEORGESCU și I. STAMATIN, Rev. Roum. Phys., 25, 935 (1980).
7. S. TOXVAERD, J. Chem. Phys., 57, 4092 (1972).
8. J. Q. HIRSCHFELDER, C. F. CURTISS, R. B. BIRD, *Molecular Theory of Gases and Liquids*, John Wiley, New York, 1954.
9. M. S. WORTHEIM, Phys. Rev. Lett., 10, 321 (1963) ; L. VERLET and J. J. WEISS, Phys. Rev. A 5, 939 (1972).
10. S. TOXVAERD, J. Chem. Phys., 64, 2863 (1976).
11. S. TOXVAERD, J. Chem. Phys., 55, 3116 (1971) ; 57, 4092 (1972).

ANALELE UNIVERSITĂȚII BUCUREȘTI, FIZICA, XXXII, 1983, pag. 17–22

ON THE PROBLEM OF AVERAGING WITH NEGATIVE COVARIANCE OF THE CORRELATED SAMPLES

S. I. SPÂNULESCU
Research Apparatus and Equipment Entréprise — Bucharest*

I. SPÂNULESCU
Faculty of Physics, University of Bucharest**

Abstract. This paper presents some theoretical consideration on the problem of averaging with negative covariance of the correlated samples. The obtained conclusions are very important for the process of signals measurement.

1. Introduction

Statistical processing of signals by time averaging or sampled data averaging is a very important method for improving the signal to noise ratio in very sensitive measurement sistems.

Ensemble average of a given function $f[x(t_1), x(t_2), \ldots, x(t_n)]$ is definied by :

$$E\{f\} = \int_{-\infty}^{\infty} dx_1 \int_{-\infty}^{\infty} dx_2 \ldots \int_{-\infty}^{\infty} f \cdot p_n(x_1, t_1; x_2, t_2; \ldots; x_n, t_n) dx_n \qquad (1.1)$$

and this is not a random variable.

The first and second order average values are of great interest and their expressions are :

$\xi(t_1) = E\{x(t_1)\}$; — expected value

$E\{x^2(t_1)\}$; — mean square value.

It is defined also the dispersion (mean square error) as :

$$E\{[x(t_1) - \xi(t_1)]^2\} = E\{x^2(t_1)\} - \xi^2(t_1) = \mathrm{Disp}\,\{x(t_1)\} = \sigma_x^2(t_1) \qquad (1.2)$$

---

* Str. Fabricii nr. 47, sect. 7, Bucharest, Romania.

** National Centre of Physics, P.O. Box 5211 Măgurele, Bucharest, Romania.

On the other hand we can define the time averaging by the following theoretical expressions :

$$< x(t_1) > = \lim_{T\to\infty} \frac{1}{T} \int_{-\frac{T}{2}}^{\frac{T}{2}} x(t_1 + \lambda)\, d\lambda \tag{1.3}$$

$$< f > = < f\,[x(t_1), x(t_2), \ldots, x(t_n)] > = \lim_{T\to\infty} \frac{1}{T} \int_{-\frac{T}{2}}^{\frac{T}{2}} f(\lambda) d\lambda =$$

$$= \lim_{T\to\infty} \frac{1}{T} \int_{-\frac{T}{2}}^{\frac{T}{2}} f\,[x(t_1 + \lambda),\ x(t_2 + \lambda), \ldots,\ x(t_n + \lambda)]\ d\lambda. \tag{1.4}$$

All these expressions are valuable for infinite large random signals measurement and they are characteristics for the studied process. By adequate limiting the measurements we can use also the average values for finite samples or finite times so that the statistical processing should become practical. The main problem is that the results of such measurements are random variables presenting statistical fluctuations and they must be as near as possible by the expected value, for being its objective estimation.

Such estimations can be obtained by continuous or sample averaging of real data in finite time :

$$[f]_n = \frac{1}{n} \sum_{k=1}^{n} f(t_1 + k\,\Delta t,\ t_2 + k\,\Delta t, \ldots,\ t_n + k\,\Delta t) = \frac{1}{n} \sum_{k=1}^{n} f(k\Delta t) \tag{1.5}$$

$$< f >_T = \frac{1}{T} \int_0^T f(t_1 + \lambda,\ t_2 + \lambda, \ldots, t_n + \lambda)\, d\lambda = \frac{1}{T} \int_0^T f(\lambda)\, d\lambda \tag{1.6}$$

For the ideal and special class of the stationary processes, the evaluation of the expected value is absolute correct as :

$$E\{[f]_n\} = E\{< f >_T\} = E\{f\}. \tag{1.7}$$

2. Continuous measurement of the time average value

For the majority of the practical applications it is possible a time average operation by using adequate filters, producing a finite time weighted value :

$$z(t) = \int_0^T h(T-\lambda)\, f(\lambda)\, d\lambda = \int_0^T f(T-\zeta)\, h(\zeta)\, d\zeta \tag{2.1}$$

This is an enough good estimation of the ensemble average E{f} in the case of a stationary process.

For example for the usual low pass filter with transfer function :

$$H(j\omega) = \frac{1}{j\omega T_0 + 1}$$

and

$$h(\varsigma) = \frac{1}{T_0} e^{-\frac{\zeta}{T_0}}$$

furnishes the exponentially-weighted-past average value (EWP) :

$$z(T) = \frac{1}{T_0}\int_0^T e^{-\frac{T-\lambda}{T_0}} f(\lambda)\,d\lambda = \frac{1}{T_0}\int_0^T e^{-\frac{\xi}{T_0}} f(T-\zeta)\,d\zeta \tag{2.2}$$

In this case the past values of exceeding several times T_0 will have very small influence an (2.2) integral because of the exponential factor. We can approximate then (2.2) by :

$$z(T) = \frac{1}{T_0}\int_{-\infty}^T e^{-\frac{T-\lambda}{T_0}} f(\lambda)\,d\lambda = \frac{1}{T_0}\int_0^\infty e^{-\frac{\zeta}{T_0}} f(T-\zeta)\,d\zeta \tag{2.3}$$

Taking an enough long time T, low variance of the average values should be obtained :

$$\text{Disp.}\{\langle f\rangle_T\} = \frac{2}{T}\int_0^T \left(1 - \frac{\lambda}{T}\right) \text{Cov}\{f(0), f(\lambda)\}\,d\lambda \tag{2.4}$$

where the autocovariance function has one of the following forms :

$$\begin{aligned} \text{Cov}\{f(0), f(\lambda)\} &= E\{[f(0) - E\{f\}][f(\lambda) - E\{f\}]\} = \\ &= E\{f(0)f(\lambda)\} - [E\{f\}]^2 = R_{ff}(\lambda) - R_{ff}(0) \end{aligned} \tag{2.5}$$

and the autocorrelation function for stationary processes depend only by the delay $\lambda = t_2 - t_1$ between the sampling moments t_1 and t_2 :

$$R_{ff}(\lambda) = \lim_{T\to\infty} \frac{1}{T}\int_{-\frac{T}{2}}^{\frac{T}{2}} f(t+\lambda)f(t)\,dt$$

$$R_{ff}(0) = \lim_{T\to\infty} \frac{1}{T}\int_{-\frac{T}{2}}^{\frac{T}{2}} f^2(t)\,dt.$$

This kind of continuous time averaging is frequently met in applications and sometimes inherent in the measuring devices. In particular integration processes in the analog to digital convertors characterized by the weight function :

$$h(\zeta) = \begin{cases} 0 \mid \zeta < 0 \\ \text{ct.} \mid \zeta > 0 \end{cases}$$

furnishes the finite time average value :

$$< f >_T = \frac{1}{T}\int_0^T f(\lambda)d\lambda = \frac{1}{T}\int_0^T f(T - \zeta)d\zeta$$

3. Variance reduction by sampled-data averaging

There are some very critical situation when usual averaging already presented is totally inadequated. Thus, taking (2.4) and using the covariance function expression we obtain :

$$\text{Disp}\{< f >_T\} = \frac{2}{T}\int_0^T \left(1 - \frac{\lambda}{T}\right)[R_{ff}(\lambda) - R_{ff}(0)]d\lambda \tag{3.1}$$

Applying Wiener-Hincin relations it becomes :

$$\left.\begin{aligned} \text{Disp}\{< f >_T\} &= \frac{1}{2\pi}\int_{-\infty}^{\infty} |H(j\omega)|^2 \Phi_{ff}(\omega)d\omega - [E\{f\}]^2 \\ \text{Disp}\{< f >_{EWP}\} &= \frac{1}{2\pi}\int_{-\infty}^{\infty} \frac{1}{(\omega T_0)^2 + 1}\Phi(\omega)d\omega \end{aligned}\right\} \tag{3.2}$$

It can be observed the dependence of the statistical fluctuations by the spectral density Φ (ω) of the signal which can strongly increase the (3.2) integrals. In such situations it is better to make repeated measurements and take into acocunt their average value :

$$\left.\begin{aligned} \overline{x(t_1)} &= \frac{1}{n}[{}^1x(t_1) + {}^2x(t_2) + \ldots + {}^nx(t_n)] \\ \overline{f[x(t_1),\ x(t_2),\ \ldots]} &= \frac{1}{n}\sum_{k=1}^{n} {}^kf = \frac{1}{n}\sum_{k=1}^{n} f[{}^kx(t_1),\ {}^kx(t_2),\ \ldots] \end{aligned}\right\} \tag{3.3}$$

where ${}^1x(t)$, ${}^2x(t), \ldots$, are sampled functions having statisticaly independent groups ${}^ix(t_1)$, ${}^ix(t_2), \ldots$ and ${}^1x(t_1)$, ${}^2x(t_1), \ldots$ is a clasical n-dimension random sample. In this case the variance of estimate in n times reduced as :

$$\left.\begin{aligned} \text{Disp}\ \{\overline{x(t_1)}\} &= \frac{1}{n}\ \text{Disp}\ \{x(t_1)\} \\ \text{Disp}\ \{\bar{f}\} &= \frac{1}{n}\ \text{Disp}\ \{f\} \end{aligned}\right. \tag{3.4}$$

Let us notice that it is not a very efficient method, as a 10 times decreasing of the mean square error needs 100 times repeating of the measurement leading to a very small speed of collecting the results.

It can be expected now that an adequated interdependence of the signal samples should alter the (3.4) formula. Taking into account correlated samples we obtain :

$$\mathrm{Disp}\ \{\overline{f(x)}\} = E\{[\overline{f(x)}]^2\} - E^2\{\overline{f(x)}\} \tag{3.5}$$

$$E^2\{\overline{f(x)}\} = \frac{1}{n^2}\sum_{i=1}^{n}\sum_{k=1}^{n} E\{f({}^i x)\}E\{f({}^k x)\} \tag{3.6}$$

$$E\{[\overline{f(x)}]^2\} = \frac{1}{n^2}\sum_{i=1}^{n}\sum_{k=1}^{n} E\{f({}^i x)f({}^k x)\}. \tag{3.7}$$

In the case of the stationary processes, with :

$$E\{f(x)\} = E\{\overline{f(x)}\} \tag{3.8}$$

summing the terms with i<k, the (3.5), expression becomes :

$$\mathrm{Disp}\ \{\overline{f(x)}\} = \frac{1}{n^2}\sum_{i=1}^{n}\sum_{k=1}^{n} \mathrm{Cov}\ \{f({}^i x), f({}^k x)\} = \frac{2}{n^2}\sum_{i<k}\sum \mathrm{Cov}\{f({}^i x),\ f({}^k x)\} +$$

$$+ \frac{1}{n^2}\sum_{k=1}^{n} [E\{f({}^k x)\}f({}^k x)\} - E\{{}^k f\} \cdot E\{{}^k f\}] \tag{3.9}$$

Using tht autocovariance function expression we finally obtain :

$$\mathrm{Disp}\ \{\overline{f(x)}\} = \frac{1}{n}\mathrm{Disp}\ \{f(x)\} + \frac{2}{n^2}\sum_{i<}\sum_{k} \mathrm{Cov}\ \{f(\overset{i}{x}), f(\overset{k}{x})\} =$$

$$= \frac{1}{n}\mathrm{Disp}\,\{f(x)\} - \frac{2}{n}\sum_{i}\sum_{<k} [R_{ff}(0) - R_{ff}(\lambda)]. \tag{3.10}$$

This formula indicates that an appropiate correlation between the sample pairs will introduce negative covariance terms, strongly reducing the statistical fluctuation without biasing the estimation.

4. Conclusions

As it was seen, statistical average measuring is practically achieved in a finite time and it is characterized by more or less important fluctuations and sometimes by a bias of the estimations.

In the case of very low frequency components of the noise (often met in d.c. applications) the needed time of integration for reducing the fluctuation of estimate values under a fixed level, may increase undefinitely. Even accepting a compromise in the speed of results collecting it is possible a systematic error by affecting the stationarity hypothesis.

In these conditions the clasical averaging methods (for example by integration) is not efficient. Using appropiate correlated samples, satisfying the condition :

$$R_{ff}(0) > R_{ff}(\lambda)$$

by previous correlator testing of the signals can have very good results in system's performance increasing.

Received January, 5, 1983.

REFERENCES

1. A. PAPOULIS, *Probability, Random Variables and Stochastic Processes*, New-York, McGraw-Hill, 1965.
2. GH. MIHOC, *Statistică matematică*, București, Editura Didactică și Pedagogică, 1971.
3. GH. CARTIANU et al., *Semnale, circuite și sisteme*, București, Editura Tehnică, 1974.
5. G. A. KORN, *Simularea și măsurarea proceselor aleatoare*, București, Editura Tehnică, 1969.
6. A. I. RUBIN, *Continuous Data Analysis with Analog Computers Using Statistical and Regression Techniques*, in IRE, march 1963.
7. H. EKRE, *Polarity Coincidence Correlation Detection of a Weak Noise Source*, in IEEE Trans., jan. 1963.

ANALELE UNIVERSITĂȚII BUCUREȘTI, FIZICA, XXXII, 1983, pag. 23—30

ANOMALOUS PHOTOVOLTAIC EFFECT IN CdTe AND CdSe THIN FILMS

I. MUNTEANU, I. DIMA and MOHAMED ISMAIL ABD EL ATI *

Faculty of Physics, University of Bucharest **

Abstract. In some experimental conditions CdTe and CdSe thin films can be obtained in which the polarity of the photovoltaic effect changes depending on the incident light intensity. To explain the experimental results a model, which takes in acount both the anisotrope charge carrier diffusion and the barrier mechanism of the anomalous photovoltaic effect is proposed.

1. Introduction

In the case of the semiconducting thin films obtained in vacuum by thermal evaporation on the substrates which make an angle with the incident molecular beam, an anomalous photovoltaic effect (APE) is observed. If the substrate is perpendicular to the incident molecular beam, then the photovoltaic effect is very small or even unobservable.

On both, elementary semiconductors as Ge, Si, Se /1—4/ and binary semiconducting compounds $A^{II}B^{VI}$ /5—8/ and $A^{III}B^{V}$ /9—13/ the APE has been observed.

The APE has some interesting peculiarities compared with the normal photovoltaic effect :

(a) In the case of APE the photovoltage can overpass by a few orders of magnitude the photovoltage corresponding to the band-gap of the semiconductor from which the thin film is prepared.

(b) The polarity of the photovoltage depends on the deposition conditions of thin film.

(c) The photovoltages obtained by illuminating the thin film through the substrate or directly are different.

---

* Permanent address: Faculty of Science, Tanta University Egypt.

** National Centre of Physics, Bucharest — Măgurele, P.O. Box 5211, Romania.

(d) The polarity of the photovoltage can be changed depending on the spectral composition of the incident irradiation.

Due to these „strange“ properties, this photovoltaic effect was called "anomalous".

Although many mechanisms were been proposed to explain the physical background of the APE, there is not a model to clarify all the features of the APE as a function of all the experimental parameters.

In this paper we studied the APE in CdTe and CdSe thin films obtained by thermal evaporation under different angles between the substrate and the incident molecular beam. The obtained results put in evidence the fact that under some experimental conditions, one can get photovoltaic thin films which have another interesting property : the change of the polarity of the photovoltaic effect depending on the intensity of the incident irradiation. This property is very important, because it shows that the rise of the APE at least two physical processes are participating which act oppositely and with different rates depending on the intensity of incident irradiation.

In order to explain the experimental results, is proposed a model which considers both physical phenomena in the volume of the crystallites and the interfaces between crystallites.

2. The existent modeles for APE

The up to day models for APE could be classified in two groups :

(a) models in which the photovoltaic thin films is considered as an entity and

(b) models which are based on the hypothesis that the photovoltaic films is formed by many consecutive microcrystallites.

In the frame of the models from group (a) the rise of the APE is explained by the variation of the sample's thickness /14/, or by the variation of the distribution of recombination centers /15/ through the sample. The models of this group are already abandoned because they can not explain many peculiarities of the APE.

The models from group (b) are based on tht idea that the photovoltaic film is formed by many consecutive microphotoelements. Thus it is supposed that the films have a polycristalline structure and every microcrystallite can act as an microphotoelement under irradiation. Further the models from group (b) will be shortly described.

A. *p—n junction model*

In this model one considers that the APE is the sum of the elementary photovoltages of the p-n junction /4—5/, or of the potential barriers /6, 16—18/ between microcrystallites. Thus, the microphotoelement "i" will generate the photovoltage V_i^{p-n} given by

$$V_i^{p-n} = \frac{kT}{q} \ln\left(1+\frac{I_{sci}}{I_{rsi}}\right) \tag{1}$$

where I_{sci} is the short-circuit photocurrent, I_{ssi} is the saturation current of the junction reverse biased, k is the Boltzmann's constant, T is the absolute temperature and q is sthe electronic unit charge.

B. *The Dember-microphotoelements model*

This model is explained by Dember effect /1—3/ and elementary photovoltage is given by

$$V_i^D = \frac{kT}{q} \cdot \frac{1-b}{1+b} \ln \frac{\sigma_i}{\sigma_d} \tag{2}$$

where b is the ratio of the electron and hole mobilities, σ_i and σ_d are the electrical conductivity of the illuminated and nonilluminated regions respectively. In order to explain the polarity of the APE depending on the spectral dependence of the incident irradiation, the anomal Dember effect must be considered.

C. *The stacking faults model*

Some semiconducting materials can crystallize in both cubic and hexagonal phases. If the photovoltaic thin films is formed by microcrystallites in which different phases are consecutive, then at the interfaces between them appear potential barriers which can act as microphotoelements under irradiation /20/.

D. *The model of anisotrope photovoltaic effect*

In this model the generation of elementary photovoltage is due to the anisotrope diffusion of the charge carriers /21—23/. This effect is similar to the photoelectromagnetic effect and elementary photovoltage is given by

$$v_i^A = \frac{a_i \Phi}{A_i + B_i \Phi} \tag{3}$$

where a_i is a parameter of anisotrophy, Φ is the intensity of the incident light, and A_i,B_i are some constants depending on geometrical sizes of the microcrystallites and on the surface recombination rates.

No one of these models can explain all the features of the APE.

Further the experimental results will be presented which show that the nature of the APE is much complex and it can not be explained by one mechanism only.

3. Experimental results

In this paper CdTe and CdSe photovoltaic thin films obliquely deposited are studied. The films were deposited on glassy substrate heated at $T = 150^\circ C$ and the angle between the molecular beam and the substrate normal was 60°. The distance from the evaporation source to the substrate was 15 cm and the vacuum during deposition was 10^{-5} mmHg.

The deposition rate was 10 Å/s and the thickness of the obtained films was 1 µm. For the photovoltaic thin film illumination a tungsten lamp of 60 W has been used and the irradiation intensity was varied by changing the distance between light source and the sample. The photovoltage was measured with an amplifier with a great input impendance ($> 10^{14}\Omega$), and the photocurrent was measured with a picoammeter. All measurements were performed at room temperature. It the insert of Fig. 1 a scheme for the obtaining of thin films and the convention for the polarity of APE are presented. The farthest electrode from the evaporation source is considered to be positive and the nearest to be negative.

The short-circuit photocurrent dependence on the intensity of the incident irradiation is shown in Fig. 1. It can be seen that with the increasing light intensity the photocurrent goes through a minimum and then changes the sign.

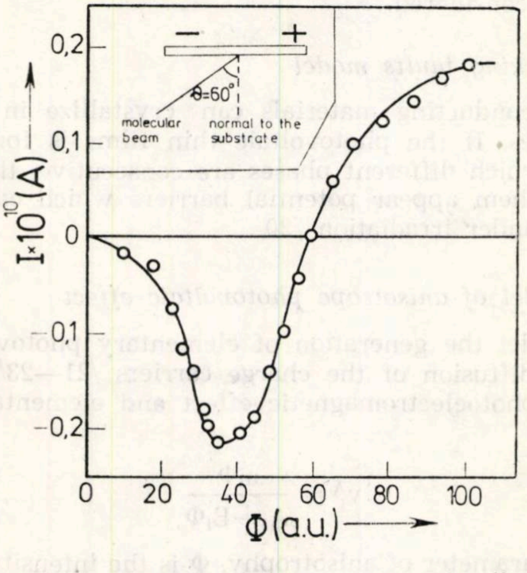

Fig. 1. Short-circuit photocurrent as a function of the incident light intensity. Insert shows the angle between the molecular beam and the normal to the substrate and the convention for the polarity of APE.

The open circuit photovoltage has a similar behaviour, as it can be seen from Fig. 2.

For a CdTe photovoltaic thin film, the photocurrent dependence on the intensity of the incident light for various biases is presented in Fig. 3. On CdSe photovoltaic thin films prepared in the same conditions, similar results were obtained.

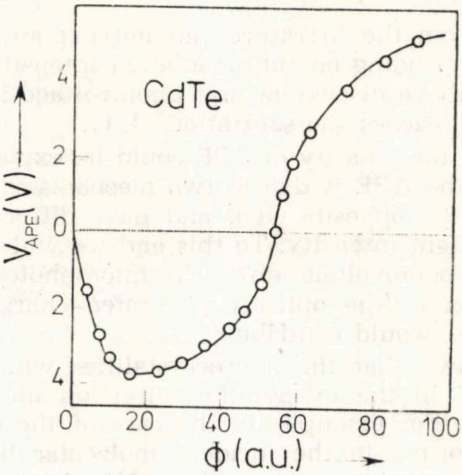

Fig. 2. Photovoltage versus light intensity for CdTe films.

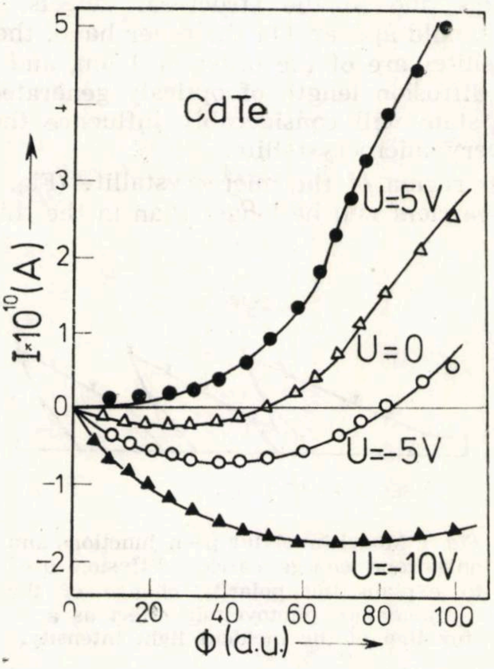

Fig. 3. Photocurrent dependence on the light intensity for various biases in the case of CdTe films.

4. The analysis of the experimental results

The models from the literature can not explain the change of the polarity of APE depending on the irradiation intensity. In all models, as follows from the above discussion, the photovoltage increases with light intensity and then reaches the sautration /4, 6/.

The change of the polarity of APE could be explained if we suppose that the origin of the APE is due to two mechanisms which give photovoltage effects of the opposite sign, and have different evolution rates depending on the light intensity. To this end we will suppose that to the formation of the photovoltaic effect in microphotoelements both, the anisotrope diffusion of the opticaly generated charge carriers and the barrier mechanisms would contribute.

It is well known that the microcrystallites which are forming the film grow parallel to the evaporation direction and have a shape as sketched in Fig. 4. For example, in the case of the CdTe thin films, if the substrate is normal to the incident molecular beam then the film has a polycrystalline structure and the (111) planes of the crystallites are parallel to the substrate surface. When the films, are obliquely deposited the (111) planes of the microcrystallites, are inclined to the evaporation direction (tend to be normal to the evaporation direction) and the inclining degree increases with microcrystallite dimensions /24/.

From these considerations follows that in the frontier regions between crystallites due to the structural defects, p-n junctions or potential barriers would appear. On the other hand, the geometrical sizes of the microcrystallites are of the order of 1 μm, and so they are comparable with the diffusion length of opticaly generated charge carriers. Thus the surface state will considerably influence the nonequilibrium processes from every microcrystallite.

In the thicker region of the microcrystallite (Fig. 4) the lifetime of generated charge carriers will be longer than in the thinner region. Thus due to the fact that the life-time is different for different regions of the microcrystallites the non-equilibrium charge carriers will diffuse into the regions with lower concentrations. So, along the thin film a diffusion of

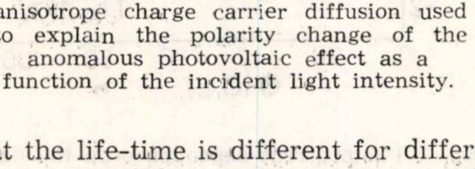

Fig. 4. Model involving p—n junctions and anisotrope charge carrier diffusion used to explain the polarity change of the anomalous photovoltaic effect as a function of the incident light intensity.

generated charge carriers will appear which at the equilibrium will be compensated by the internal photoelectric field from every crystallite.

Combining both the anisotrope diffusion and the barrier mechanisms one can understand the behaviour of the APE in our photovoltaic thin films.

The CdTe and CdSe thin films have a p-type conduction, so we may suppose that the volume of every crystallite is of p-type also. Under irradiation, the non-equilibrium charge carriers (in our case electrons) will diffuse from the right to the left (Fig. 4) and by summing the elementary photovoltages one obtaines a negative photovoltage. In the same time, under irradiation, the p-n junctions at the frontiers are active also and by summing elementary photovoltages one get a positive anomal photovoltage. When the irradiation intensity is weak the APE caused by the anisotrope diffussion will predominate, and at high intensity, the barrier mechanism will predominate. The photovoltage-intensity dependance can be written as

$$V_i^{p-n} = \frac{kT}{q} \ln(1 + b_i \Phi), \tag{4}$$

where b_i is a constant depending on the physical properties and geometrical parameters of the "i" crystallite.

Considering eq. (3) and (4) and supposing that along the mesuring direction there are N microcrystallites we can write for the total anomal photovoltage the relation

$$V_{APE} = \sum_{i=1}^{N} \left[\frac{kT}{q} \ln(1 + b_i \Phi) - \frac{a_i \Phi}{A_i + B_i \Phi} \right] \tag{5}$$

From the analyse results that the change of the sign of the APE could be explained only if the two mechanisms acting opositely are considered.

REFERENCES

1. H. KALLMAN, B. KRAMER, E. HAIDEMENAKIS, J. Electrochem. Soc. **108**, 247 (1961).
2. H. KALLMAN, G. MARMOR SPRUCH, S. TRESTER, J. Appl. Phys. **43**, 469 (1972).
3. M. TAKAHASHI, F. KOU, O. TADA, Japan. J. Appl. Phys. **7**, 1446 (1968).
4. *Fotoelectriceschie iavlenia v poluprovodnikah i optoelectronica, izdatelsto* „FAN", Tachkent, p. 143 (1972).
5. J. STARKIENICZ, L. SOSNOWSKI, O. SIMPSON, Natura, **156**, 6 (1946).
6. B. GOLDSTEIN, L. PENSAK, J. Appl. Phys., **30**, 155 (1959).
7. A. GAGLIANO, H. KALLMAN, B. KRAMER, J. Phys. Chem. Solids, **28**, 737 (1967).
8. V. A. IGNATIUK, F. NOVIK, Fiz. Tverd. Tela, **8**, 3661 (1966).
9. E. I. ADIROVICH, V. F. ROSLIAKOVA, Iu. M. Iuabov, Fiz. Tekh. Poluprov. **2**, **848**, (1968).

10. E. I. ADIROVICH, V. M. RUBINOV, IU. M. IUABOV, Fiz. Tverd. Tela. **6**, 3180 (1964).
11. U. A. ARIFOV, N. ABDULAEV, M. S. ARIFDJANOVA, Fiz. Tekh. Poluprov. **10**, 25 (1976).
12. M. D. MARTINUZZI, Compt. Rend. **258**, 1769 (1964).
13. M. D. USPENSKII, A. G. IVANOVA, I. E. MALKIS, Fiz. Tekh. Poluprov. **1**, 1020 (1968).
14. V. M. LIUBIN, G. A. FEDOROVA, Dokl. Akad. Nauk, USSR, **135**, 833 (1960).
15. G. BRINCOURT, S. MARTINUZZI, Compt. Rend. **266**, 1283 (1968).
16. A. R. HUTSON, Bull. Am. Phys. **6**, 110 (1961).
17. T. NOVIK, Fiz. Tverd. Tela, **5**. 3142 (1963).
18. R. H. WILLIAMS, H. R. JOHNSON, Solid State Commun. **16**, 873 (1975).
19. H. W. BRANDHORST, A. E. POTTER, J. Appl. Phys. **35**, 1997 (1964).
20. S. G. ELLIS, S. HERMAN, E. E. LÖBNER, W. J. MERZ, C. W. STRUK, J. G. WHITE, Phys. Rev. **108**, 1860 (1959).
21. I. P. ZHADKO, V. A. ROMANOV, Phys. Stat. Sol. **28**, 797 (1968).
22. R. M. SHAH, J. F. SCHETZINA, Phys. Rev. **B5**, 4014 (1972).
23. J. F. SCHETZINA, Phys. Rev. **B12**, 3339 (1975).
24. J. MATSUMA, M. INOUE, Japan. J. Appl. Phys. **6**, 297 (1967).

ANALELE UNIVERSITĂŢII BUCUREŞTI, FIZICA, XXXII, 1983, pag. 31—36

THE CRYSTALLINE STRUCTURE OF THE ELECTRON IRRADIATED CdSe THIN FILMS

TALAL KHALASS
Faculty of Science, University of October *
I. SPÂNULESCU, I. SECĂREANU
Faculty of Physics, University of Bucharest **
N. BĂLŢĂŢEANU
Central Institute of Physics, Măgurele — Bucharest ***

Abstract. In this paper the influence of 10 MeV electron radiation on the crystalline structure of CdSe thin films obtained by vacuum evaporation was studied. The crystalline lattice parameters of CdSe hexagonal and cubic crystals are computed.

1. Introduction

Thin films of the semiconductor compounds of the A^2B^6 type are intensively studied because of interesting electrophysic properties and their applications. Among these, the CdSe thin films have been less studied [1—5], though this material finds also many applications especially for the obtaining of luminofores and solar cells [6, 7].

Besause various devices performed with thin films may be used in radiation fields, this paper deals with the influence of irradiation with 10 MeV electron radiation on the crystalline structure of the CdSe thin films.

2. Experimental

The CdSe thin films were obtained by thermal evaporation and condensation in vacuum ($\approx 10^{-5}$ torr). As supports were used optical plane plates of silica glass heated at temperature varying between 25° and 380°C [8]. The layers thickness varied between 0.06 and 3.5 μm.

To prevent a strong dissociation of CdSe, this was evaporated at temperature of 700° and 760°C.

---

* University of October, Lattakia, Siria.

, * National Centre of Physics, P.O. Box MG-11, Măgurele, Bucharest, Romania.

The crystalline structure of CdSe thin films obtained in various experimental conditions has been studies through X-rays and electrons diffraction. In the X-ray diffraction analyse we used a Debye-Scherrer method with photographic recording as well the X-rays diffractometer with paper diagram recording.

The obtained CdSe thin films were subjected to irradiation with 10 MeV electrons supplied by an electron liniar accelerator.

The irradiation dose ranged from 10^7 to 10^9 rad.

3. Results and discussions

According to our experiments, the results of the irradiation are strongly dependent on samples preparation conditions especially on the substrate temperature, its cleanliness and pressure in the evaporation chamber.

The irradiation action provided to be important for the CdSe thin films obtained on low heated supports ($T_s = 25$—100°C). After the irradiation of these samples with 10^8 rad electron irradiation, one finds a worsening of the crystalline structure and the appearance of amorphous phase in the superficial layers of the sample, at least. As it is seen in figure 1,b after irradiation of the sample with 10 MeV elctron radiation of 5×10^7 rad dose, the intensity of the diffraction lines is appreciable

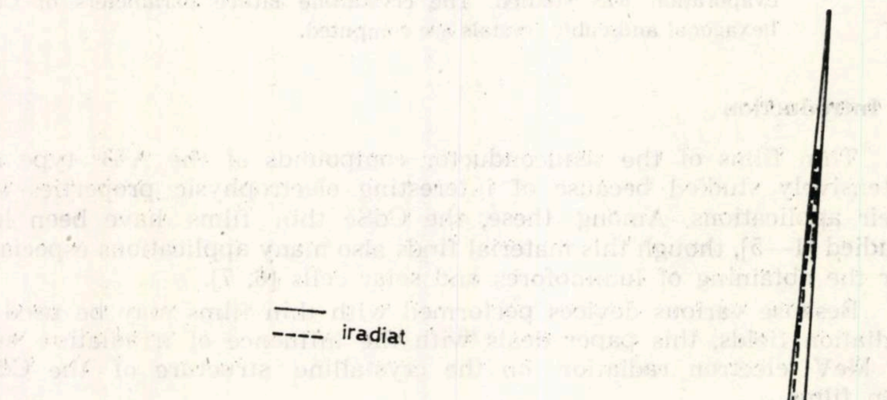

Figure 1. X-ray diffraction diagrams of a CdSe thin film obtained on a substrate heated to 80—100°C; a-before irradiation; b-after 10^8 rad dose electron irradiation.

diminished. This fact may be explained by the disappearance of some CdSe crystallites and the appearance of a structural defects in the studied films. The same results were obtained for the CdSe thin films prepared on a substrates heated to 150°C (fig. 2).

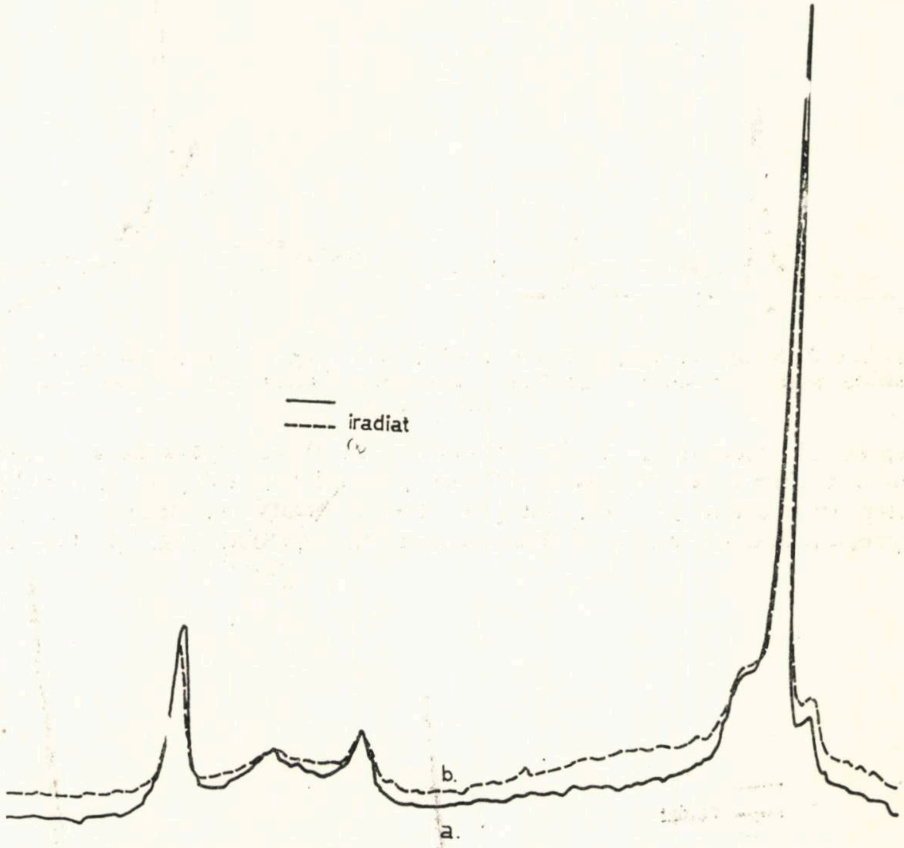

Figure 2. X-ray diffraction diagrams of a CdSe thin film obtained on a substrate heated to 150°C ; a-before irradiation ; b-after 10^8 rad dose electron irradiation.

The increasing of the substrate temperature about 200—250°C leads to the improvement of CdSe crystallites structure (Fig. 3,a). As seen in figure 3 the samples prepared for about 250°C substrate temperature, contain CdSe crystallites with cubic structure (Fig. 3,a), or a mixture of cubic and hexagonal crystallites. The crystallites contained in the respective films show a great resistance by irradiation. Though for such of layers one did not find important modification for 5 x 10^7 rad doses of 10 MeV electron radiation. At 10^8 rad doses (on an average) one finds an easy improvement of CdSe crystallites structure of respective layers (Fig. 3,b).

For high temperature of subtrate ($T_s = 300—350°C$) a good enough crystalline structure of CdSe crystallites in thin films are observed (Fig. 4, a. The improvement of the crystalline structure and the increased

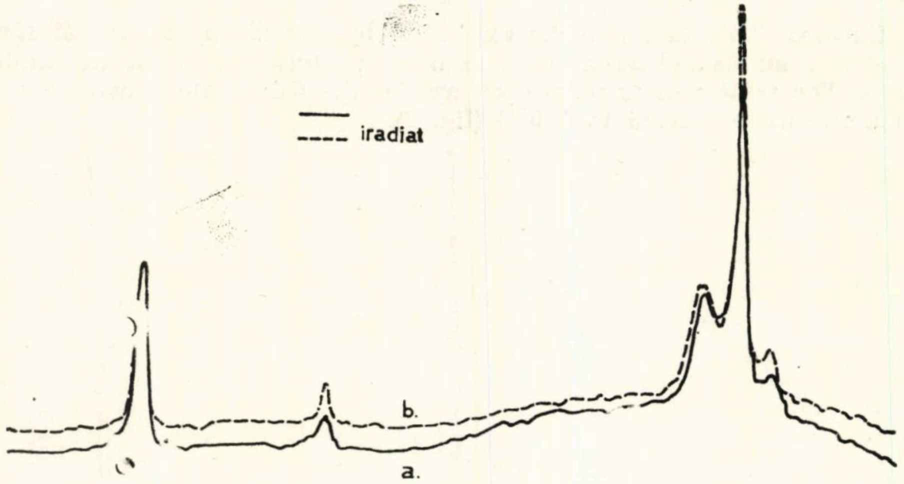

Figure 3. X-ray diffraction diagrams of a CdSe thin film obtained on a substrate heated to 250°C; a-before irradiation; b-after 10^8 rad dose electron irradiation.

degree of orientation of the crystallites in these layers became more obvious after irradiation with 10^8 rad doses of 10 MeV (Fig. 4, b). Thus, after irradiation of such samples, the intensity of diffraction lines increased and some new diffraction maxima appeared (Fig. 3,b, Fig. 4,b).

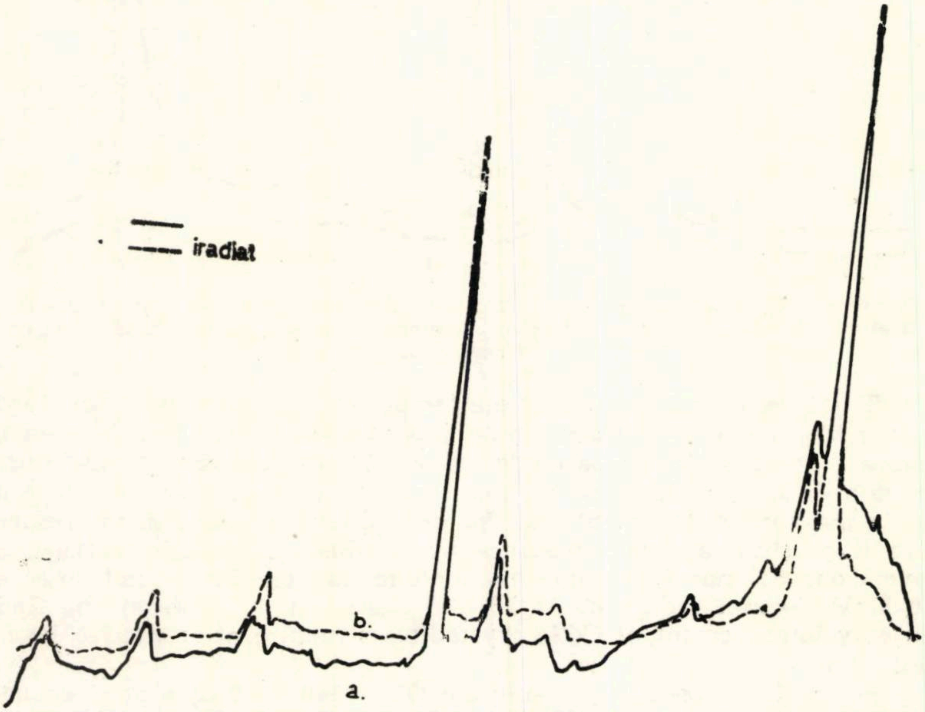

Figure 4. X-ray diffraction diagrams of a CdSe thin film obtained on a substrate heated to 300°C; a-before irradiation; b-after 10^8 rad dose irradiation.

The lattice-type identification and the calculus of the parameters of the crystalline lattice were being accomplished by X-rays diffraction analyse, using the Debye-Scherrer method.

In the table 1 are given containing the distances d (in Å) between the lattice plane and the diffraction lines identified on X-ray patterns of hexagonal crystals.

Table 1

Distance between the lattice planes in hexagonal CdSe crystals

nr.	sin θ	d (Å)	hkil
1	0,271440	2,838559	$10\bar{1}2$
2	0,38655	1,993273	$10\bar{1}3$
3	0,417549	1,845288	$11\bar{2}2$
4	0,448071	1,719592	$20\bar{2}1$
5	0,540974	1,424281	0004
6	0,5541182	1,390497	$20\bar{2}2$
7	0,602511	1,278813	$20\bar{2}3$
8	0,661311	1,165198	$10\bar{2}4$

For a calculation of the cubic lattice parameter the known formula

$$a = d(h^2 + k^2 + l^2)^{1/2}$$

together with Wulff-Bragg formula

$$2d\sin\theta = n\lambda$$

were used.

The value of the cubic lattice constant was found to be

$$a = (5.838 \pm 0.005)\ \text{Å}.$$

The hexagonal lattice parameters were calculated using the formulas

$$a_{ij}^2 = \frac{\lambda^2}{3}\ \frac{A_iB_j - A_jB_i}{B_j\sin^2\theta_i - B_i\sin^2\theta_j}$$

$$c_{ij}^2 = \frac{\lambda^2}{4} \cdot \frac{A_iB_j - A_jB_i}{A_i\sin^2\theta_j - A_j\sin^2\theta_i}$$

where

$$A = h^2 + hk + k^2\,; \qquad B = l^2.$$

The following values were found for the lattice parameters of CdSe hexagonal crystallites [8]

$$a = (4.32 \pm 0.005)\ \text{Å}$$

$$c = (7.06 \pm 0.005)\ \text{Å}$$

$$\frac{c}{a} = 1.63$$

4. Conclusions

The lattice perfection of crystallites contained in CdSe thin films strongly depends on the experimental conditions of preparation especially on the substrate temperature. At substrate temperature between 25°C and 200°C one obtain CdSe policrystalline thin films, whose crystallites contain a several defects structure especially packing defects on the crystalline planes. The increasing of the substrate temperatures of 250—350°C leads to a improvement of the CdSe crystallites structure in the studied samples.

The effect of electron irradiation of CdSe thin film with 10 MeV electron radiation depend on the preparation conditions, therefore the perfection of crystallites structure. For layers obtained at low support temperature ($T_s \approx 25$—150°C) with small, nonorientated crystallites and many defects one finds an apreciable increasing of defects number and the appearance of amorphous phase in the superficial regions of samples.

At higher support temperatures ($T_s \approx 250$—350°C), when the structure of CdSe films is more stable after irradiation in the same conditions of samples (by the same doses and energies), a more visible improvement of crystalline structure are observed.

It were identified the majority of the diffraction lines specific to the CdSe hexagonal crystallites contained in thin films obtained by thermal evaporation in vacuum and it was calculated the parameters of the crystalline lattice.

Received January, 6, 1983.

REFERENCES

1. I. P. KALINIKN et al., F.T.T., **3**, 2640 (1961).
2. J. NAKAI et al., Japan J. Appl. Phys., **4**, 545 (1965).
3. L. A. SERGHEEVA et al., Kristallografià, **10**, 237 (1965).
4. J. VIŠČKAS, A. MEDEIŠIS, Litovskii fiziceskii sbornik, **8**, 875 (1968).
5. V. RUXANDRA, *Teză de doctorat*, Universitatea Bucureşti, 1980.
6. D. BONNET, Proc. Photovoltaic Solar Energy Conf., 1977, Dordrecht, Boston, 1978, p. 630.
7. D. BONNET, Proc. Second European Community Photovoltaic Solar Energy Conf., Berlin, 23—26 April, 1979, p. 387.
8. T. KHALASS, *Thesis*, University of Bucharest, 1983.

ANALELE UNIVERSITĂŢII BUCUREŞTI, FIZICĂ, XXXII, 1983, pag. 37—41

GROWTH OF POLYCRYSTALLINE $CuInSe_2$

B. LOGOFĂTU, D. BRÂNCUŞ, A. DAFINEI, MICHAELA LOGOFATU
Faculty of Physics, University of Bucharest *

I. DAFINEI
Secondary School, Bucharest

Abstract. The fabrication of $CuInSe_2$ ternary compound is described. Samples were prepared by reacting the mixture of the elements at about 1100°C. X-ray analysis was used to confirm that the correct chalcopyrite structure was obtained. Besides this method, thermoelectric probe method (for conductivity type) and two point probe technique (for resistivity measurements) were used for rapid characterization of the samples.

1. Introduction

$CuInS_2$ belongs to the I III VI_2 family of chalcopyrite compounds which are semiconducting and optoelectronic materials. The chalcopyrite structure is derived from sphalerite, but its unit cell is twice that of sphalerite (fig. 1). Each atom of a given element is surrounded tetrahedrally by four atoms, four bonding electrons being required for each atom in the structure.

The semiconducting compounds CdS and $CuIneS_2$ appear attractive for solar energy conversion devices. CdS is the substrate material which can be deposited easily in the film form. $CuInSe_2$ is a choice for a good match to CdS. The band gap is 1.04 eV, close to $1.3 \div 1.5$ eV- the range of optimum conversion efficiency. $CuInSe_2$ has a direct band gap implying short light absorption length. There is an excellent lattice match between these materials ; the mismatch being very small ($\sim 1.2\%$), strain

---

* National Center of Physics, Măgurele, Bucharest, P.O. Box 5211.

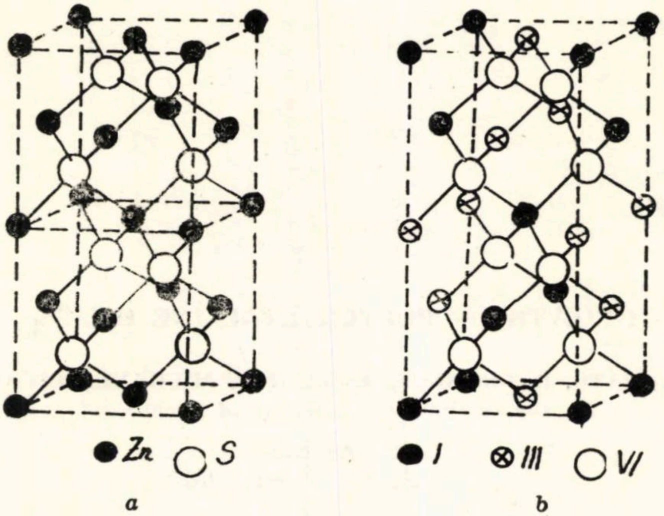

Fig. 1
The unit cell for (a) sphalerite (zinc blende) and (b) the chalcopyrite structure /1/.

induced interfacial defects are minimal. Solar cells with efficiency of 12% have been already reported /2/.

In the first step our attention was focused on the technological problems associated with the fabrication process of CuInSe$_2$.

2. Experimental

We used pseudo-binary phase diagram (fig. 2) for the system Cu$_2$Se-In$_2$Ce$_3$, /3/. A solid state transition associated with ordering on the Cu-In sublattice occurs at 810°C. The melting point of the CuInSe$_2$ compound

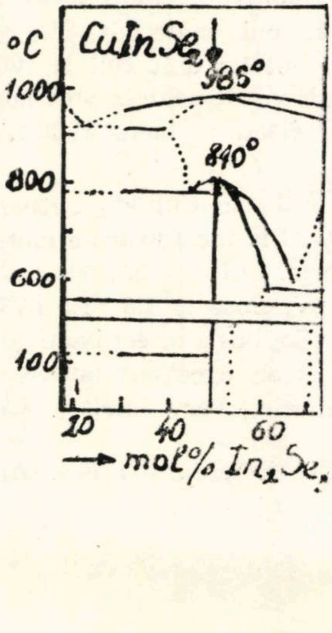

Fig. 2
The pseudo binary phase diagram for the system Cu$_2$Se-In$_2$Se$_3$ /3/.

is 986°C. The melting points of the elements are : 156°C (In), 217°C (Se), 1083°C (Cu).

One special problem was the exothermal reaction of In and Se ; this reaction, which starts at 217°C, can lead to generation of high Se vapour pressures and the explosion of the quartz ampoule. We employed the procedure described in /4/, in order to minimize the risk of cracking. Furthemore, we kept one end of the quartz ampoule at 710 ± 3°C ; the method assured a pressure that did not exceed 970 torr, the maximum pressure of the Se vapours at this temperature.

The fabrication process was carried out using the experimental system shown in fig. 3. The furnance was an horizontal one, with two zones. Two temperature controllers allowed maintaining the temperature at a precise value and heating at different temperature rates. Moreover, we controled the temperature of both ends of the quartz ampoule with two P/PtRd 10% thermocouples in connection with two electronic voltmeters.

Polycrystalline ingots were obtained by melt growth from mixtures of the elements, in stoichiometric compositions (mass %) : 18.9% Cu + 34.1% In + 47.0% Se. The mixtures was given in a sand blasted quartz crucibles, and than in a quartz ampoule evacuated to less 10^{-4} torr. The ampoule was heated at a rate of 3°C/min till 195°C ; the mixture was kept at this temperature for a period of 4h ; then, the temperature was increased to 205°C and was maintained for 2h. Heating was continued at a rate of 2.5°C/min up to 1100°C. The material was kept melted for a period of 8h. The reacted material was allowed to slow cool with 1.5°C/min to 500°C and 3°C/min to room temperature.

The crystal structure was obtained by X-ray analysis ; resistivity measurements were performed with two point probe technique and the carrier type was determined by thermoelectric probe.

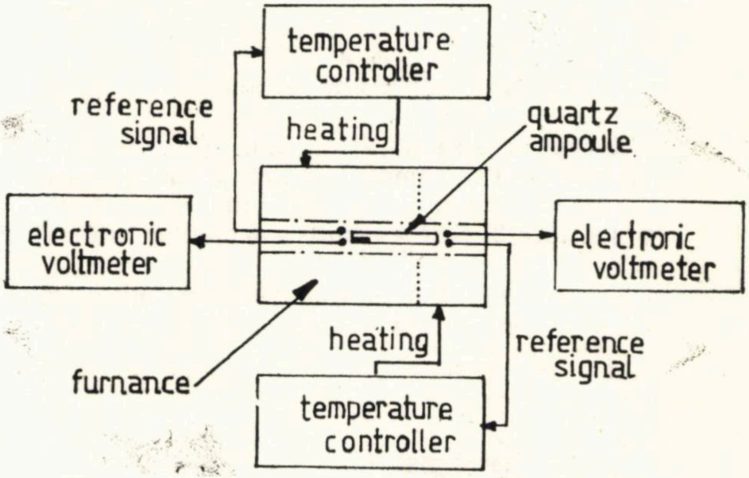

Fig. 3
Schematic diagram of growth apparatus.

3. Results and discussions

The X-ray diffraction pattern was obtained to confirm the crystal structure of the compound ; the structure of the wafers was polycrystalline. One typical diffraction pattern for our material is presented in fig. 4. Using the data available from the literature, we identified the Miller indicies. The determinations show that chalcopyrite crystalline structure was obtained.

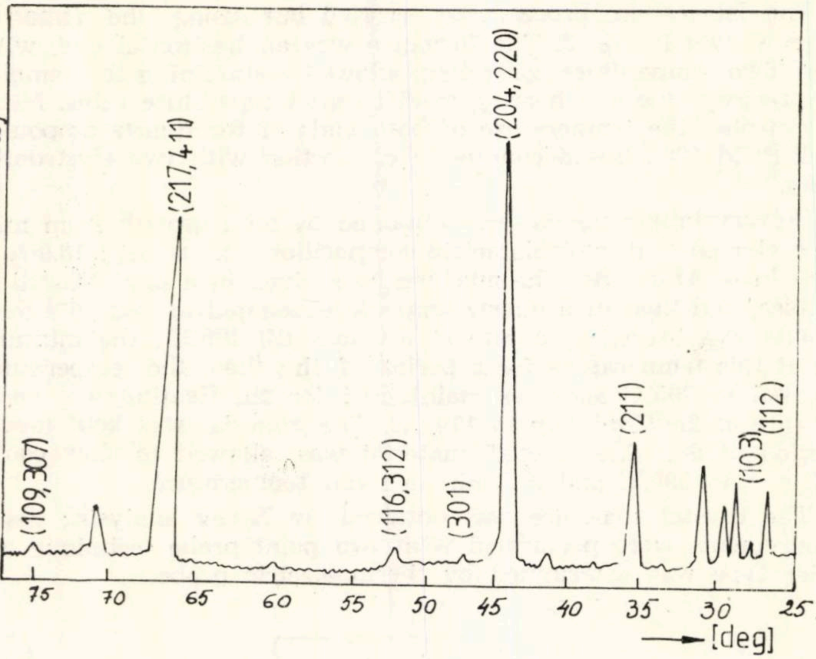

Fig. 4
X-ray diffraction pattern.

Samples with typical size $8\times5\times1.5$ mm (fig. 5), were used for resistivity measurements. The samples exhibit a more resistive surface layer ($\rho = 45$ Ω cm for the face 1) than the bulk of the material ($\rho = 30$ Ω cm for the face 2). These results are similar to those presented in the literature.

The thermoelectric probe showed that the ingots always have p-type conductivity. In the ternary compound CuInSe$_2$, Se vacancy would be

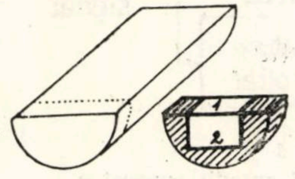

Fig. 5
Sample for resistivity measurement.

expected to act as a donor state and Cu or In vacancy as an acceptor state; meanwhile, Se interstitials would act as acceptor and Cu or In interstitials as donors. Our initial mixtures had Se in excess because this is the most volatile element. Thus, the p-type conductivity can be explained in terms of a compensation mechanism : Se in excess produces a reduction of the vacancy population on the anion sublattice and a possible introduction of Se interstitials.

4. Conclusions

This paper reports the preparation of the ternary compound $CuInSe_2$. The synthesis of this material was carried out by the method of sintering the stoichiometric mixture of the elements. X-ray diffractometry, thermoelectric probe and two point probe technique were used as relatively simple methods for rapid characterization of the samples. Samples were polycrystalline, with chalcopyrite structure, and with p-type conductivity.

We shall try to improve the $CuInSe_2$ fabrication process, because this material is of interest, expecially for efficient $CdS/CuInSe_2$ solar cells.

REFERENCES

1. J. L. SHAY, J. H. WERNICK, *Ternary Chalcopyrite Semiconductors,* Pergamon Press, 1975.
2. J. L. SHARP, S. WAGNER, H. M. KASPER, Appl. Phys. Lett. *22,* 89 (1975).
3. L. S. PALATNIK, E. J. ROGACHEVA, Dokl. AN SSSR, *174,* 80 (1967).
4. J. PARKES, R. D. TOMLINSON, M. J. HAMPSHIRE, Sol. State El. *16,* 773 (1973).
5. R. E. HONIG, D. J. KRAMER, RCA Rev. 285 (1969).

ANALELE UNIVERSITĂŢII BUCUREŞTI, FIZICA, XXXII, 983, pag. 43—48

ELECTRON TRANSFER BANDS OF THE Co^{2+}, Ni^{2+} AND Cu^{2+} IONS IN $CdCl_2$ AND $CdBr_2$ LATTICES

ATH. TRUTIA, FLORIANA IOVA and ANA DANCU
Faculty of Physics,, University of Bucharest *

Abstract. The ultraviolet spectra of $CdCl_2$ and $CdBr_2$ single crystals doped with Co^{2+}, Ni^{2+} and Cu^{2+} are measured. The absorption bands are assigned to dipol-allowed electron transfer transitions from halogen ions to 3d orbitals of metal ions.

1. Introduction

The electrostatic model of the "ligand field" has been replaced in recent years by the "angular overlap model" connected with the overlapping between orbitals centered on adjacent atoms (central metal ions and ligand ions) [1, 2].

The non-local transitions observed at high energies (electron transfer bands) are those for which the electron is concentrated around different atoms in its initial and final states [3, 4].

2. Measurements and results

The $CdCl_2$ and $CdBr_2$ single crystals with 1—2%M Co^{2+} or 0.5—1%M Ni^{2+} or 0.02—0.2%M Cu^{2+} added in the melt, were grown by the Bridgman method in our laboratory.

The optical absorption spectra at room temperature were measured with a "Cary" Model 118C spectrophotometer or a UV—VIS Specord "Zeiss" spectrophotometer. These spectra are shown in the figures 2—7. The electron transfer bands are indicated by vertical arrows. Their intensities are greater then those of the crystal field bands situated at lower energies.

3. Discussion

Fig. 1 shows the $(MX_6)^{4-}$ one electron molecular orbital scheme [1]. In these molecular orbitals, $(a_{1g}\sigma^b)$, $(e_g\sigma^b)$ and $(t_{1u}\sigma^b)$ mainly consist of

---

* National Center of Physics, Măgurele — Bucharest, P.O. Box 5211.

p_σ orbitals of halogen ions, while $(t_{2g}\pi^b)$, $(t_{1u}\pi^b)$ and non -bonding $(t_{2u}\pi)$, $(t_{1g}\pi)$ are mainly composed of p_π orbitals of halogen ions. The $(t_{2g}\pi^*)$ and $(e_g\sigma^*)$ are mainly composed of 3d orbitals of the transition mental ions, where the separation between $(t_{2g}\pi^*)$ and $(e_g\sigma^*)$ corresponds to the crystal field splitting $\Delta = 10$ Dq.

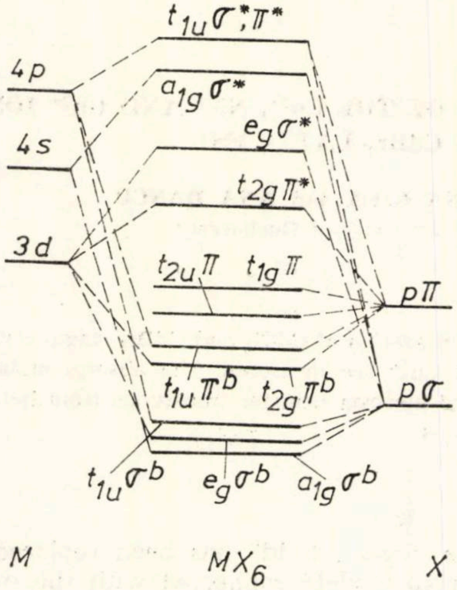

Fig. 1. The molecular orbital energy level scheme for MX_6 complex.

The dipole-allowed electron transfer transitions from halogen ions to 3d orbitals of metal ions are possible for Co^{2+} with the electronic configuration d^7 $(t_{2g}^5 e_g^2)$, from $(t_{1u}\sigma^b)$, $(t_{1u}\pi^b)$ or $(t_{2u}\pi)$ orbitals to the unfilled $(t_{2g}\pi^*)$ and $(e_g\sigma^*)$ orbitals.

For Ni^{2+} and Cu^{2+}, with the elctronic configuration d^8 and d^9 respectively $(t_{2g}^6\ e_g^2$ and $t_{2g}^6\ e_g^3)$, only the transitions to $e_g\sigma^*$ are possible because only this orbital is unfilled. [5]

The two π orbitals are less stabilized than the σ orbital formed from a given p —shell of the ligand (3p for Cl^- and 4p for Br^-). The absorption spectra suggest a difference of 10—15 kK between the two kind of orbitals in halide complexes [6].

The corrected wave-number $\tilde{\upsilon}_{corr}$ of the first Laporte-allowed electron transfer band ($\pi \rightarrow t$ or $\pi \rightarrow e$) is related to the difference :

$$\tilde{\upsilon}_{corr} = 30\text{kK}[x_{opt}(X) - x_{opt}(M)] \qquad (1\text{kK} = 1000\ \text{cm}^{-1}) \qquad (1)$$

where $x_{opt}(X)$ and $x_{opt}(M)$ are the optical electronegativities of the ligand and the metal ions respectively.

In the d group, the corrections to be performed are those for the spin pairing energy ΔE_{sp} and for Δ if the transition goes to the upper subshell [6].

$$\tilde{\upsilon}_{e.t.} = 30[x_{opt}(X) - x_{opt}(M)] + \Delta + \Delta E_{sp} \qquad (\text{kK}) \qquad (2)$$

Table I gives the values of $\tilde{\nu}_{obs}$ (from spectra) and $\tilde{\nu}_{est}$, estimated with the formula (2).

The values of x_{opt} are those given in literature, [6] and Δ values were obtained from the absorption spectra [7, 8]. ΔE_{sp}, the "spin — pairing" correction is the difference between the spin pairing energy of the ground and excitated configurations (1^q and 1^{q+1}) of the metal ion. [9]

Table 1

Metal ion	Lattice	$x_{opt}(M)$	$x_{opt}(X)$	Δ (κK)	$\tilde{\upsilon}$ (κK) obs	$\tilde{\upsilon}_{est}$(κK)	Transition
Co^{2+}	$CdCl_2$	2.0	3.0	6.9	37.0	35.3	π→t
					42.0	42.2	π→e
	$CdBr_2$		2.8	6.4	28.5	29.3	π→t
Ni^{2+}	$CdCl_2$	2.1	3.0	6.0	34.5	35.6	π→e
	$CdBr_2$		2.8	5.8	27.0	29.4	π→e

The apparent value for Δ derivated from the electron transfer bands is slighty decreased from the observated value by charge -separation effects [6].

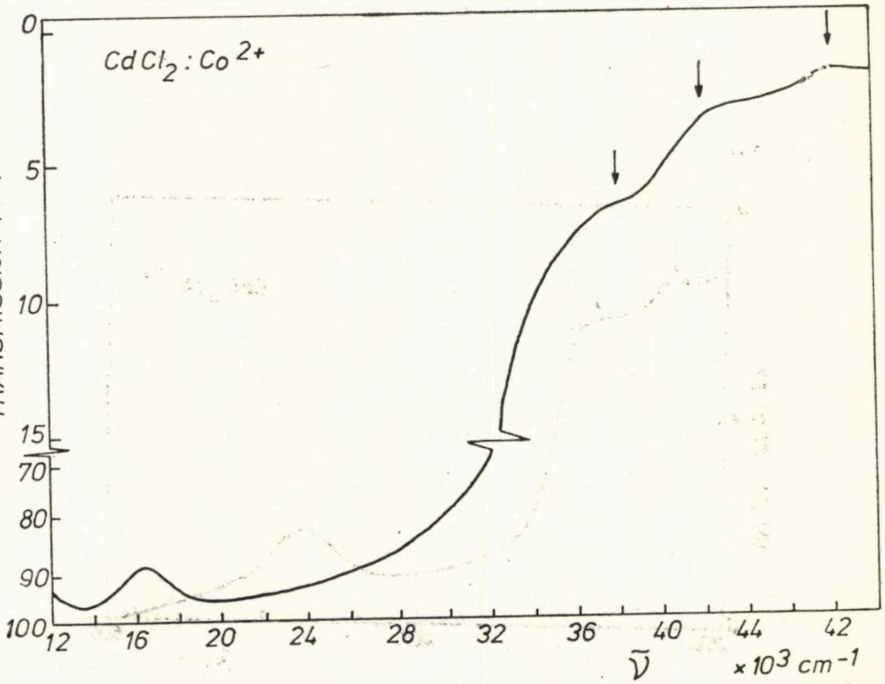

Fig. 2. Absorpion bands at 300 K of Co^{2+} in $CdCl_2$.

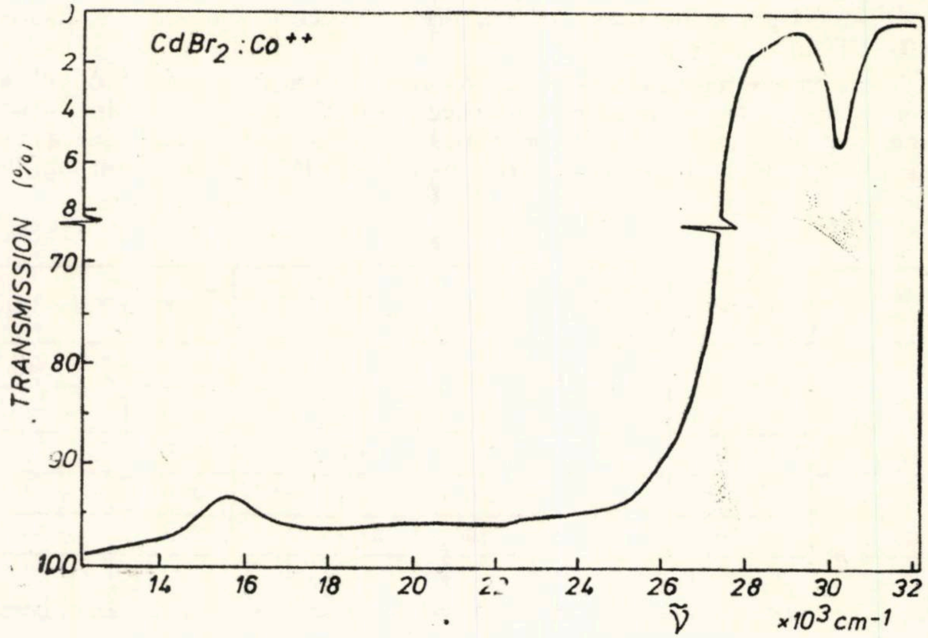

Fig. 3. **Absorpion bands at 300K of Co^{2+} in $CdBr_2$**

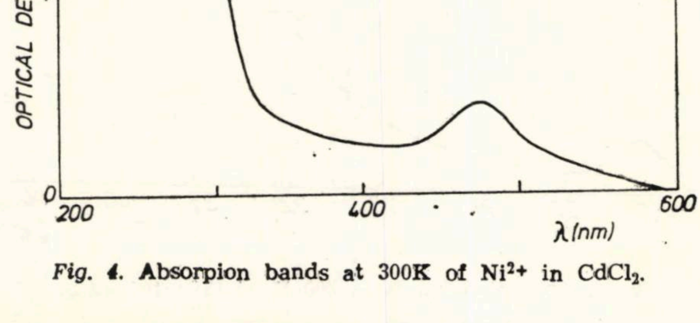

Fig. 4. **Absorpion bands at 300K of Ni^{2+} in $CdCl_2$.**

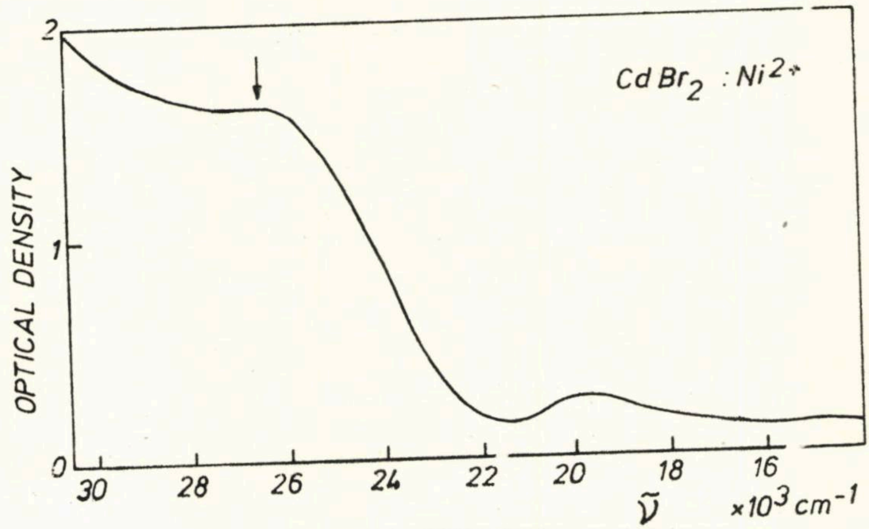

↑

Fig. 5. Absorption bands at 300K of Ni^{2+} in $CdBr_2$.

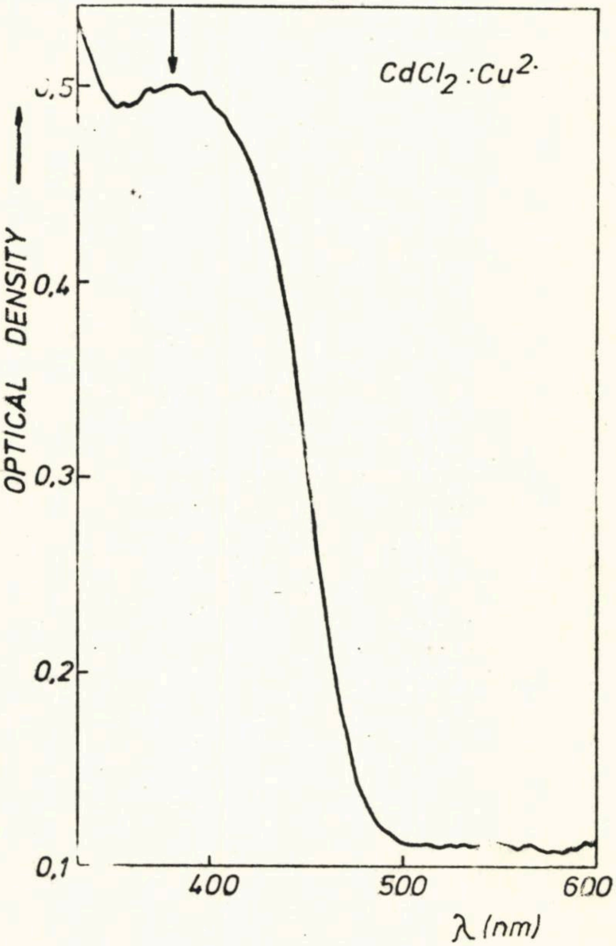

Fig. 6. Absorption bands at 300K of Cu^{2+} in $CdCl_2$ (0.2% in original melt). →

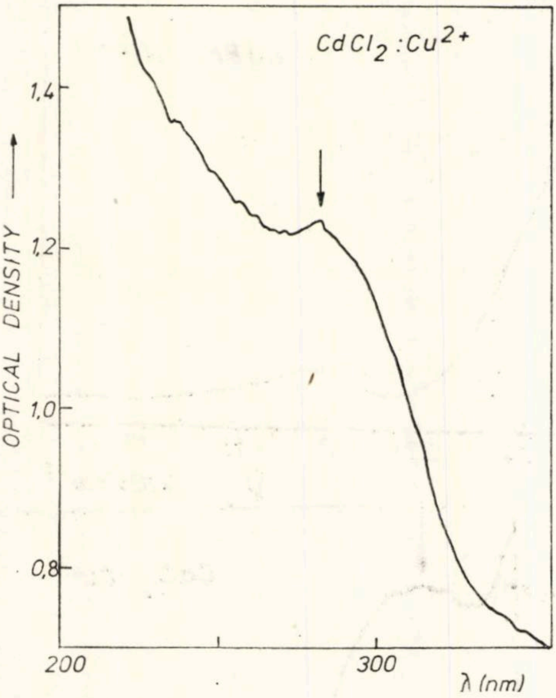

Fig. 7. Absorption bands at 300K of Cu^{2+} in $CdCl_2$ (0.02% in original melt).

Received, March 24, 1983

REFERENCES

1. C. J. BALLHAUSEN, *Introduction to Ligand Field Theory,* Ed. Mc. Graw Hill, New York (1962).
2. C. K. JØRGENSEN, *Modern Aspects of Ligand Field Theory,* North-Holland Publishing Company — Amsterdam (1971).
3. D. S. McCLURE, J. Lum. 18/19, 135 (1979).
4. ATH. TRUTIA, M. VODA. J. Chem Phys. 7, 2715 (1976).
5. SHIN-ICHI HIRAKO. RYUMYO ONAKA, J. Phys. Soc. Jap., 5, 1637 (1981).
6. C. K. JØRGENSEN, Progr. Inorg. Chem., 12, p. 101, ed. S. Lippard, New York (1970).
7. J. FERGUSON, D. L. WOOD, K. KNOX, J. Chem. Phys, 39, 881 (1963).
8. FLORIANA IOVA, Rev. Roum. Phys. 26, 525 (1981).
9. C. K. JORGENSEN, Solid State Phys., 13, 393 (1962).

ANALELE UNIVERSITĂȚII BUCUREȘTI, FIZICA, XXXII, 1983, pag. 49—54

THE STRUCTURE AND PROPERTIES OF ORIENTED POLYPROPYLENE (PP) FILMS

I. C. PETREA
Faculty of Physics, Bucharest University *

M. LEANCA
Combine for Synthetic Fibers of Jassy **

G. E. GRIGORIU
Institute for Macromolecular Chemistry "P. Poni" of Jassy ***

AURELIA GRIGORIU
Faculty of Technology and Chemistry for Textiles, Polytechnic Institute of Jassy ****

Abstract. We have investigated the changes in structure and mechanical properties of isotactic unoriented PP films, which have been obtained through melting extrusion and then stressed axially. The effect of draw temperature and draw ratio was determined. Structural characterization techniques used in this study include wide angle diffraction (WAXS), birefrigence measurements and IR spectroscopy in polarized and non-polarized light.

Introduction

To elucidate the behaviour at deformation of polycristalline polymers poses a lot of problems connected both with the techniques of the characterization of structural changes and with the theoretical interpretation of the results.

The PP films obtained by extrusion from melting with complex morphological structure including, at the supermolecular level, spherulites linked through interspherulites regions present a decreased order degree. In their turn, the spherulites are formed out of crystalline lamella (preferentially oriented towards radial directions) and non-crystalline polymers. By uniaxial deformation of the films the different structural units forming the spherulite substructure are rearranged to elongation direction. The structure of the films after deformation depends on the initial structure and the parameters of drawing (drawing ratio R_e, temperature, time, etc.).

---

* National Center of Physics, P.O. Box 5211, Măgurele, Bucharest.

** Soseaua Tutora no. 29, Jassy-6600.

*** Aleea Grigore Ghica-Vodă no. 41 A, Jassy-6600.

**** Calea 23 August no. 11, Jassy-6600

To measure the molecular orientation, methods are applied which are sensitive to crystalline orientation (X-ray diffraction, IR dichroism [/1—4/], amorphous (IR dichroism) and total orientation (birefringence, IR dichroism).

Experimental

The studied isotactic PP films (average viscosimetric molecular weight $\overline{M}_v = 130.000$) were obtained by drawing ($2 \leqslant R_e \leqq 7$) at temperatures of 100, 125, 140 and 150°C.

For structural analysis the following apparatuses were used : the Perkin Elmer 577 IR spectophotometer ; X-ray difractometer Tur M-62 with goniometer HZG-3 ; the Universal Pol-Carl Zeiss optical microscope. The physico-mechanical properties were measured with the Wolpert dynamometer.

Results and discussion

The results concerning tensile strenght (R) and breaking elongation ($\Delta l\%$) in the studied films are represented in Figure 1. It could be seen that the mechanical properties of the films depend on the drawing ratios as well as on the temperature. Since the physico-mechanical properties of the films are determined by their structure, there results important modifications caused by drawing conditions /3, 4/. Figure 2 shows birefringence variation (Δn) depending on the drawing conditions. The rise of the birefringence with increasing draw ratios show the growing of the macromolecular alignement to film axis, in agreement with the physico-mechanical properties.

From IR spectra in non-polarized light of PP films, using absorbance bands of 846, 975, 1000 and 1170 cm^{-1} one has determined the following characteristics /5, 6/ :

— the cristallinity parameters

$$I_c = \frac{A_{846}}{A_{1170}} \qquad \text{and } I_c' = \frac{A_{1000}}{A_{975}}$$

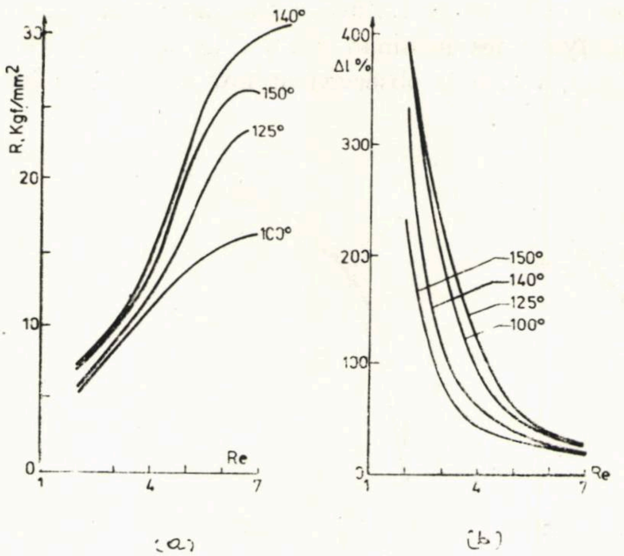

Fig. 1

The change of tensile strenght (a) and breaking elongation (b) in function of drawing ratio and temperature.

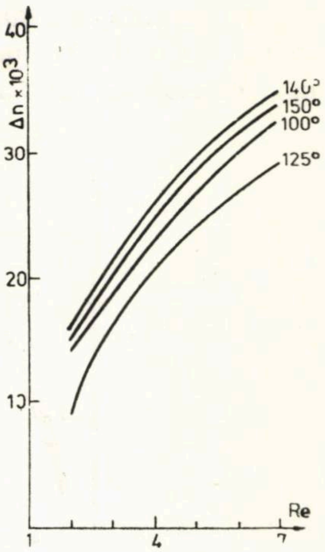

Fig. 2

The change of birefringence in function of drawing ratio and temperature.

$$K_x\% = \frac{990\, I_c + 80}{13{,}6}$$ (Heinen-Bouriot relation obtained from IR and density measurements)

where A_ν = the band absorbance at ν wavenumber, expressed in cm^{-1}; I_c, I'_c = crystallinity indices ; $K_x\%$ -crystallinity percentage

— the parameters of general orientation

$$R_G = R_{975} = \left\{\frac{A_{\parallel}}{A_{\perp}}\right\}_{975} \qquad R'_G = R_{1170} = \left\{\frac{A_{\parallel}}{A_{\perp}}\right\}_{1170}$$

$$f_G = \frac{R_G - 1}{R_G + 2} = \frac{R_{975} - 1}{R_{975} + 2} \qquad f'_G = \frac{R'_G -}{R'_G + 2} = \frac{R_{1170} -}{R_{1170} + 2}$$

where $A_{\parallel}$, $A_{\perp}$ represent the absorbances in the paralel and perpendicular polarized light towards the film drawing direction; R_G, R'_G - dichroic rations ; f_G, f'_G = factors of general orientation.

— the parameters of crystalline orientation

$$R_c = R_{1000} = \frac{A_{\parallel}}{A_{\perp}}\,_{1000}$$

$$f_c = \frac{R_c - 1}{R_c + 2} = \frac{R_{1000} - 1}{R_{1000} + 2}$$

where R_c = dichroic ratio and f_c = factor crystalline orientation.

The drawing conditions particularly influence the molecular orientation, while the crystallinity varies in small limts (Fig. 3, 4, 5). The mild decrease of crystallinity, which is observed at low drawing ratios

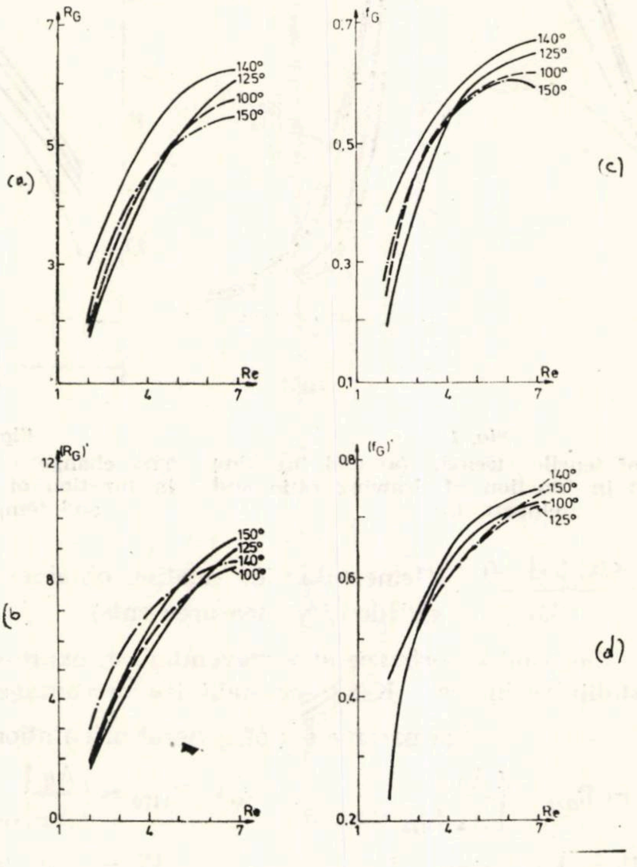

Fig. 3

The change of paremeters of general orientation : dichroic ration R_G (a), R'_G (b) and factors of general orientation f_G (c) f'_G (d) in function of drawing ratio and temperature.

(R_e = 3—4) is probably due to the fact that crystallities from undrawn films behave as "vulcanizing" zones of the polymer system. These zones form a network which restricts the macromolecular segments orientation. In the initial phase of the drawing, the partial destruction of the undrawn film structure and the macromolecular segments orientation undergo. At high drawing ratios, preferential orientation is sufficiently large to allow the recrystallization.

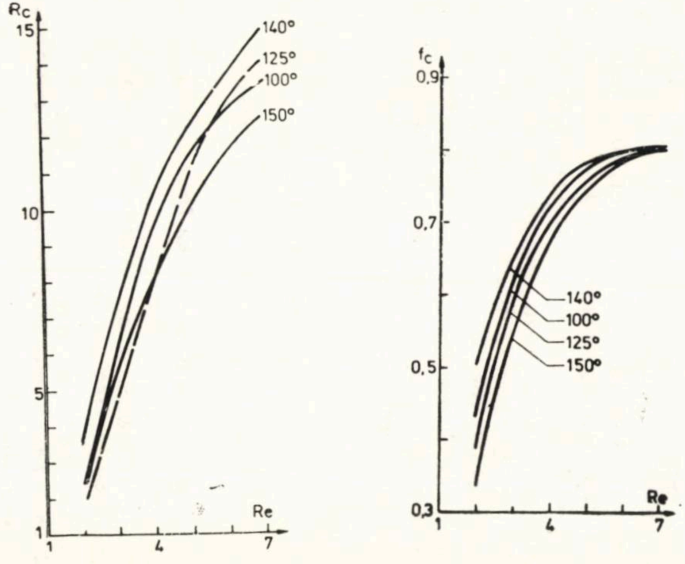

a *b*

Fig. 4

The change of parameters of crystalline orientation : dichroic ratios R (a) and factor of crystalline orientation f_c (b) in function of drawing ratio and temperature.

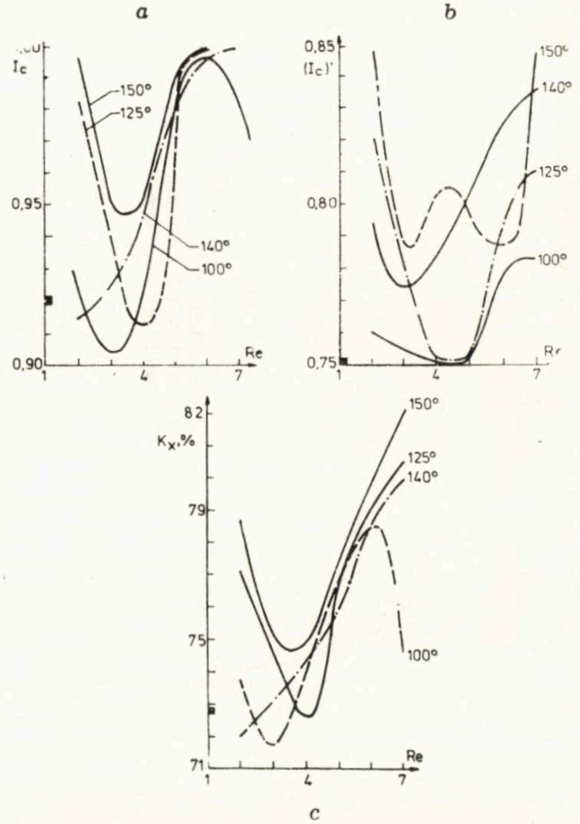

Fig. 5

The change of crystallinity paremeters : crystallinity indices I_c (a), I_c (b) and crystallinity percentaje $K_x\%$ (c) in function of drawing ratio and temperature.

The factor of crystalline orientation f_c^x, determined by X-ray diffraction, noticeable increases with R_e (Fig. 6).

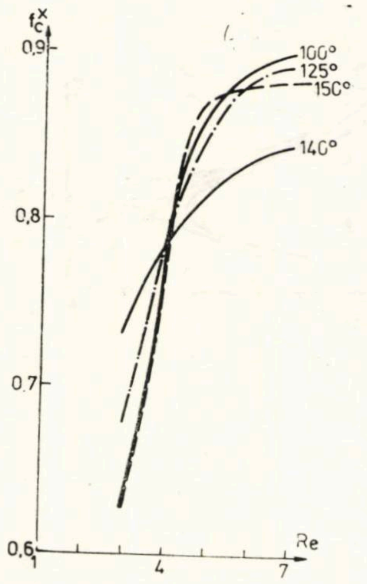

Fig. 6
The change of factor of crystalline orientation (X-ray) f in function of drawing ratio and temperature.

In the drawing process of PP films, the structural modifications become obvious especially in the molecular orientation, which mostly influence the physico-mechanical properties. By comparing the physico-mechanical properties of the studied films, one can find that at drawing ratio of 5, the best values of the tensile strength are recorded in case of films drawn at 140°C, elongation at breaking being about unchanged. Increasing of the drawing temperature results in a decrease of tensile strenght. This fact is a consequence of the plastic component of deformation increase, which results in a polymer orientation decrease.

The experimental results show that in the case of analyzed patterns at high drawing ratios and at the temperature of 140°C high strenght and orientation of films were obtained.

REFERENCES

1. R. ZBINDEN, *Infrared Spectroscopy of High Polymers*, Acad. Press, New York, 1964.
2. D. DECHANT, *Ultrarot-Spektroskopische Untersuchungen an Polymeren*, Akademie Verlag, Berlin, 1972.
3. S. HOSHINO, J. POWERS, D. J. LEGRAND, H. KAWAI and R. S. STEIN, J. Polym, Sci., 58, 166, 185, 1962.
4. R. J. SAMUELS, J. Polym. Sci., Part A, 3, 1741, 1965.
5. O. J. SWEETING, *The Science and Technology of Polymers Films*, vol. I., Interscience Publishers, New York, 1968.
6. P. BOURIOT, R. HAGEGE and N. SOTTON, Bull. Scient. ITF, 18, 139, 1976.

ANALELE UNIVERSITĂŢII BUCUREŞTI, FIZICA, XXXII, 1983, pag. 55—62

MÉTHODE D'ANALYSE DÉRIVATOGRAPHIQUE, DES MÉCANISMES THERMO-OXYDATIFS DANS LE POLYÉTHYLÈNE

E. BARNA, LIVIA IONESCU
Faculté de Physique, Université de Bucarest *

CARMEN RĂDULESCU, C. RĂDULESCU
Entreprise des Cables et Matériaux Electro-isolants — Bucarest

Résumé. Une nouvelle méthode de corrélation des mécanismes thermo-oxydatifs et de certains de leur effets au niveau de quelques structures macromoléculaires est présentée.

Dans ce cadre, des procès thermo-oxydatifs sont révélés par l'analyse thermique différentielle (DTA) et thermo-gravimétrie (TG) de certains échantillons de polyéthylène provenant de ICI, DFDM, UNIFOS, ICECHIM.

Des interdépendences thermo-mécaniques et électriques comprenant certains paramètres structuraux et des performances fonctionnelles de longue durée sont soulignées.

Procès thermo-oxydatifs dans le polyéthylène

On connait que le polyéthylène, stable dans des conditions de température spécifiquement adéquate a ses utilisations, sous vide ou dans une atmosphère inerte, soubit des modifications rapides, souvent irréversibles, en ce qui concerne les propriétés mécaniques, thermiques et électriques, s'il est exploité dans la présence de l'oxygène. Les proces élémentaires d'oxydation, de degration physico-structurale sont favorisés en champ thermique, menant à l'apparition de péroxydes, d'acides organiques et l'apparition secondaire quasi-catalytique des groupes carbonyle. Aux températures relativement élevées, a lieu une scission des chaînes avec dégagement de substances volatiles et la transformation du composé initial dans un produit final de type cire paraffinique, de masse moléculaire plus petite. [1]. On peut constater aussi que, sous l'influence conjuguée de la radiation lumineuse et thermique en milieu oxydant, sont accélérés les procès comprenant tant la formation des groupes carbonyle, que ceux de type $>C=C<$; ces effets, qui pratiquement ne sont pas souhaitables peuvent être prévenus par l'introduction de certaines soubstances antioxydantes, phénols ou amines, déstinées a limiter l'apparition des peroxydes, déterminant leur décomposition et favorisant ainsi la réticulation du polymère.

---

* Centre National de Physique, Măgurele, Bucarest. B.P. 5211. Roumanie.

La réaction commence à la surface du matériel et son avancement vers l'intérieur dépend du rapport de la phase cristalline et celle amorphe : le matériel cristallin, empaqueté plus sérré, s'oxyde difficilement.

La résistance des polymères à l'oxydation est appréciée d'après la „période d'induction“ (le temps nécessaire à l'acorçage de la réaction après l'éloignement de l'oxygène), ou bien d'après la hauteur des pics exothermes [2].

L'évalution des effets thermiques impliqués dans les transformations physiques et chimiques est basée sur certaines corrélations entre ceux-ci et la surface limitée par les pics DTA.

Pour un échantillon de masse égale à l'unité, qui soubit un simple cauffage, dans l'absence d'un effet thermique dû à un procès de transformation, l'équation du bilan thermique a la forme :

$$\frac{dQ_r}{dt} = C_{p,r}\frac{dT_r}{dt} \tag{1}$$

cependant que pour un procès de transformation, l'échantillon émet énergie calorique à la vitesse $\frac{dH}{dt}$ l'équation ayant la forme :

$$\frac{dH}{dt} + \frac{dQ_p}{dt} = C_{p,p}\frac{dT_p}{dt} \tag{2}$$

La théorie des systèmes d'analyse thérmique admet une dépendance linéaire entre le flux de chaleur et la différence de température :

$$\frac{dQ_i}{dt} = \frac{T_s - T_i}{R_i} \tag{3}$$

où l'indice i motre l'échantillon (p), ou la substance étalon (r). Admettant, dans une première approximation, R constant (la différence entre la capacité de diffusion thermique du matériel étalon et celle de l'échantillon étant négligeable) on peut formuler les équations décrivant les courbes DTA :

$$R\frac{dH}{dt} = \Delta T + R(C_{p,p} - C_{p,r})\frac{dT_r}{dt} + RC_{pp}\frac{d(\Delta T)}{dt} \tag{4}$$

L'étude comparative de la variation de certains paramètres des échantillons éxaminés, avec et sans oxydant, peut devenir concluant par suite d'une série d'expériences concernant l'absorption en I.R., l'émanation de substances volatiles etc.

Dans ce sens la méthode d'analyse thermique différentielle se montre efficiente, rapide et précise dans l'évaluation des paramètres physiques pour la degradition oxydative dans le polyéthylène. D'habitude, l'étude dérivatographique d'un matériel comporte la corrélation des variations en temps de certains paramètres significatifs, tels :

a) la température dans le centre de l'échantillon — la courbe de température T ;

b) la masse de l'échantillon — la courbe TG ;

c) la vitesse de variation de la masse de l'échantillon $\frac{dm}{dt}$ — la courbe DTG ;

d) la différence de témperature entre l'échantillon et le milieu environant ΔT — la courbe DTA.

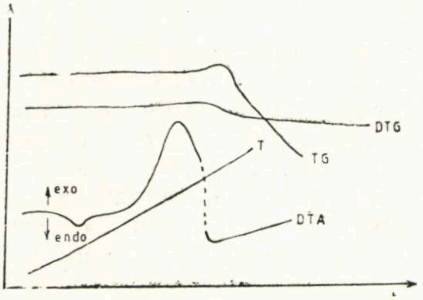

Fig. 1 — Les phases de la dérivatogramme obtenue pour un échantillon de polyéthylène.

Dans la figure 1 est donnée la dérivatogramme jusqu'à 500°C pour un échantillon de polyéthylène (inerte Al_2O_3), en distinguant les phases de transformation suivantes :

1) une réaction endotherme sans changement de masse ;

2) une réaction exotherme accompagnée au début d'une légère augmentation de la masse, suivie d'une diminution de celle-ci.

3) une réaction endotherme pendant que la masse diminue.

Ces phases de transformation successive peuvent être expliquées si on tient compte des procès accompagnant le traitement thermique, ou bien plus, mettant en évidence, leur température d'amorçage. La réaction initiale, endotherme, est associée ainsi au procès de dévitrification. La température de dévitrification (T_g) dépend des paramètres intrinsèques de l'échantillon, tels la masse moléculaire, le degré de cristallinité, le degré de reticulation.

La réaction exotherme est associée au procès de dégradation thermo-oxydative. L'augmentation initiale de la masse peut être expliquée par l'addition de l'oxygène aux chaînes de polyéthylène, en se formant ainsi des péroxydes et des groupes carbonyle. Ce phénomène est suivi, après un court moment, par un procès de dégradation de la chaîne, dû à l'ataque des péroxydes et au dégagement des composés gazeux ; la diminution de la masse devient ainsi évidente. Finalement, aux hautes températures apparait le procès de dégradation de la chaîne sous l'influence de l'agitation thermique (réaction endotherme). La réaction de thermo-oxydation du polyéthylène étant de type autocatalytique, un éventuel traitement thermique effectué antérieurement dans l'air modifiera les valeurs des températures des points d'amorçage mises en évidence.

La température de la réaction exotherme, ainsi que la température de l'addition d'oxygène (l'augmentation de la masse), seront controlées par la quantité d'antioxydant présente dans l'echantillon. Si pendant le traitement thermique a lieu „l'ttaque de l'oxygène“ sur le polyéthylène, la présence de celui-ci modifiera les températures d'apparition de l'exotherme et de l'augmentation de la masse sur la derivatogramme de l'échantillon traité.

Dans les expériences isothermes (DSC à température constante), l'apparition de la réaction thermo-oxydative est caractérisée par une „période d'induction“, en fait l'intervalle de temps jusqu'à l'apparition de l'oxydation. Dans cette méthode il este nécessaire de réaliser des thermogrammes à des températures différentes. En dérivatographie, la réaction d'oxydation est rapportée, en fait, à une variable bidimensionnelle continue température/temps, dont la norme est donnée par la vitesse de chauffage, une seule expérience étant suffisante pour caractériser le matériel.

La methode dérivatographique, mise au point de cette manière, permet donc d'obtenir les informations suivantes :

— caractérise la structure macromoléculaire du matériel.

— caractérise les performances initiales d'efficacité et persistence en temps de celles-ci pour le système antioxydant-polyéthylène.

Technique expérimentale

Les expériences ont été éffectuées avec un dérivatographe MOM 1500, dans les conditions suivantes :

— la masse de l'échantillon 1 g

— programme de temperature 500°C/2,5°C/min.

— l'erreur de la balance ± 0,5 mg

— sensibilité DTA 1/5

— sensibilité DTG 1/5 — creusets en platine.

Les granules de polyéthylène ont été laminées à froid, obtenant finalement des flocons de polyéthylène ; cette opération a eu pour but l'augmentation de la surface active. L'échantillon a été ensuite broye dans un mortier avec de l'oxyde d'aluminium, calcine à 100°C, en proportion de 50%, l'oxyde d'aluminium (Al_2O_3) a été choisi comme substance étalon (de référence).

Afin de déterminer l'efficacité de l'antioxydant, ont été effectuées des expériences sur les types suivants de polyéthylène : ICECHIM, UNIFOS, DFDM et ICI conditionnés à 100°C, en granules, laminés ultérieurement à froid.

Les durées des traitements thermiques ont été : nonconditionné, 7, 14, 28 et 48 jours (d).

Discussion des résultats

Les différentes sortes de polythylène ont été choisies parmi une gamme de produits, grâce aux propriétés de stabilité termique et mentien en temps de ceux-ci.

Dans la fig. 2 est montrée la variation de la température de dévitrification (Tg) des échantillons en fonction du temps de conditionnement.

Les échantillons non-conditionnés ($t = 0$) de polyéthylène ICI et ICECHIM ont les températures de dévitrification à 111°C, respéctivement 109°C, indiquant soit des masses moléculaires plus élevées, soit du degré de réticulation plus accentué de la chaîne par rapport aux polyéthylènes DFDM (105°C) et UNIFOS (106°C).

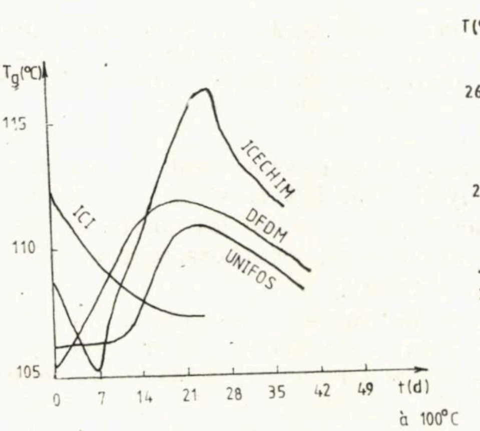

Fig. 2 — La variation de la température de vitrification (T) en fonction du temps de conditionnement de l'échantillon.

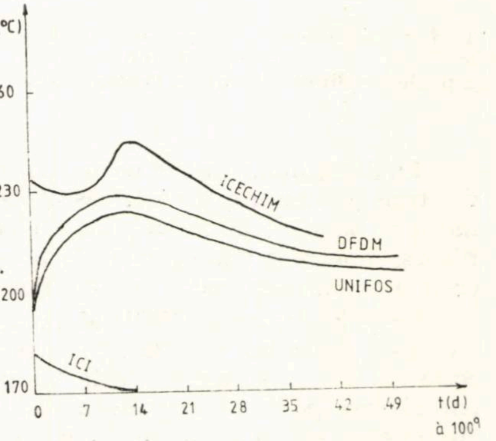

Fig. 3 — L'évolution de la température de début de la réaction thermo-oxydante en fonction du temps de conditionnement de l'échantillon.

L'évolution en temps des valuers de la température de dévitrification indique une degradation rapide de l'échantillon ICI, une réticulation pour les polyéthylènes DFDM et UNIFOS, et un procès en deux étapes pour le polyétylène ICECHIM. Ce procès comprend un phénomène de relaxation énergetique des chaînes (la durée ~ 7 jours) auivi de leur réticulation, phénomène qui indique l'action de l'antioxydant par rapport à l'attaque de l'oxygène.

Dans les figures 3, 4, 5 est présentée l'évolution des températures pour les phénomènes de thermo-oxydation.

Sur la fig. 3 est représentée aisi la température de début de la réaction de termo-oxydation, sur la fig. 4 — la température d'addition de l'oxygène, et sur la fig. 5 — la température correspondante au maximum de l'exotherme d'oxydation.

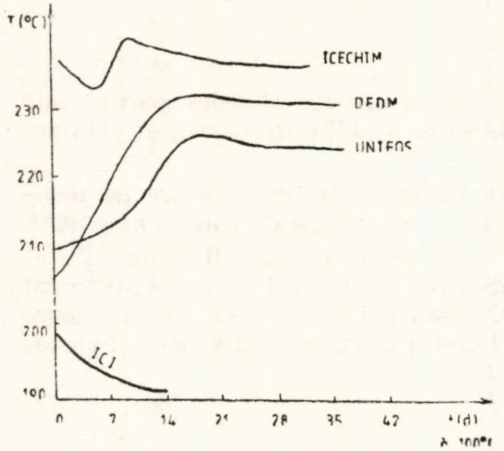

Fig. 4 — L'évolution de la température d'addition de l'oxygène en fonction du temps de conditionnement de l'échantillon.

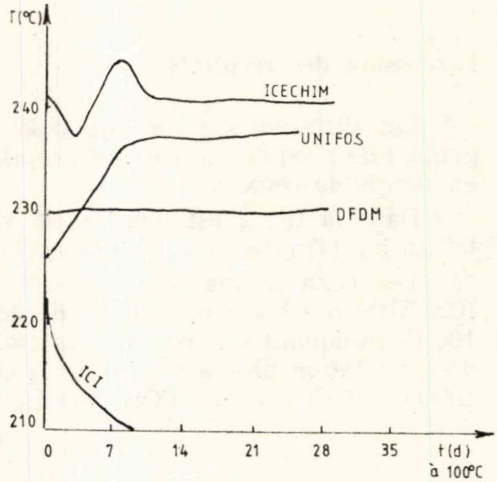

Fig. 5 — L'évolution de le température correspondante au maximum d'oxydation en fonction du temps de conditionnement de l'échantillon.

La diminution rapide en temps (après 14 jours seulement) des valeurs des trois paramètres dans le cas du polyéthylène ICI, ainsi que els valeurs initiales basses (182°, 199°, 122°C) par raport à celles des autres échantillons, montrent que ce type de polyéthylène est insuffiesament stabilisé et il a un niveau réduit et inefficace d'antioxydant.

Le polyéthylène ICECHIM présente les valueurs tehrmique les plus élevées à l'état initial (232°, 241°, respectivement 247°C' ; on observe que cette évolution en temps de la température est de même type que celle enrégistrée pour la température de dévitrification [3]. Ce fait impose l'hypothèse sur la présence des groupes carbonyle dans le matériel initial. Après 14 jours de traitement les valeurs thermiques commencent à diminuer.

Les pohlyéthylènes DFTM et UNIFOS présentent une augmentation des valeurs thermiques, partant d'un niveau initial plus réduit (199°, 205°, 229° — DFDM et 199°, 210°, 225°C — UNIFOS) augmentation qui atteint un palier maximum de saturation se maintenant même après 42 jours.

La croissance des valeurs tehrmiques dans les premières phases de l'expérience sont dûes, pour tous les cas, à l'action des antioxydonts. L'inhibition des péroxydes par des antioxydants mène à des réticulations sporadiques. En même temps, le traitement thermique au voisinage de la température de dévitrification (100°C) permet de réaliser — en augmentant le nombre de degrés de liberté intermoléculaire — des configurations et des conformations plus stables. Il en résulte un polymère stabilisé plus résistent à l'action des facteurs de thermodégradation. L'étude ultérieure des temperatures indique l'arret de l'action des antioxydants qui se trouvent en quantités suffisantes pour donner une bonne stabilité (199°, 210°, 225°C) et une constance convenable en temps de celle-ci.

Le polyéthylène ICECHIM o une masse moleculaire et un degré d'enchevêtrement des macromolécules plus élevés, contient une quantité plus grande d'antioxydant, mais il est d'un autre type (ou bien cette quantité trop élevée mène à une inhibition de l'action en temps), ce qui fait que l'éfficience et la fermeté de son activité diminuent aux traitements prolongés. Le polyéthylène ICI à une masse moléculaire élevée et une stabilite thermique réduite. L'hypothèse du procès par étapes dans le polyéthylène ICECHIM doit être confirmée par des études de spectroscopie I.R.

RÉFÉRENECES

1. R. ALLISON, *Polyethylene,* Intersci, Publishers, 1968.
2. C. VLAD, *Comportarea termică a polimerilor.* Edit. Academiei R.S.R., București, 1981.
3. K. OTONI, *Test raport of the basic characteristics of Roumanian polyethylenes,* Electric Co., 1980.

Reçu : le 5 février, 1982

ANALELE UNIVERSITĂŢII BUCUREŞTI, FIZICA XXXII, 1983, pag. 63—68

STRUCTURAL MODIFICATIONS AT THE SPINNING OF POLYPROPYLENE (PP) YARNS

GEORGE ERVANT GRIGORIU
Institute of Macromolecular Chemistry „P. Poni“ of Jassy *

AURELIA GRIGORIU
Polytechnic Institute of Jassy **

MIHAI LEANCĂ
Combine for Synthetic Fibers of Jassy ***

ION C. PETREA
Faculty of Physics, Bucharest University ****

Abstract. The influence of the spinning speed on the structure and properties of the PP yarns was investigated through IR spectroscopy, X-ray diffraction, birefringence determinations and physico-mechanical methods.

1. Introduction

The structure and physico-mechanical properties of yarns spinned from melting depend to a great extent on the conditions of their obtaining (melting temperature, flow capacity, spinning speed etc.). Depending on the crystallization speed, specific to every polymer, the spinned yarns can be amorphous or crystalline.

The spinned PP yarns have a high degree of crystallinity. The structure of PP yarns determines their subsequent remaking by drawing, with a view to obtaining superior characteristics.

---

* Alee Grigore Ghica-Vodă no. 41A, Jassy—6600.

** Calea 23 August no. 11, Jassy—6600.

*** Şoseaua Tuţora no. 29, Jassy—6600

**** National Center of Pysics, P. O. Box 5211, Măgurele Bucharest

This paper gives the experimental results about the influence of PP yarns structure on their deforming properties.

Experimental

The isotactic PP yarns studied in this paper were obtained in laboratory conditions, at a spinning speed ranging from 500 to 3000 m/min. The changes in ordonation and orientation were pursued by IR spectroscopy, X-ray diffraction and by birefringence determinations. To decrease the diffusion phenomenon the PP yarns were "reeled" on a distance placed between two KBr crystals /1/.

Results and discussion

The crystallinity parameters I_c, I'_c = indices of crystallinity ; K_x % = percentage crystallinity) were calculated /2—6/ using pick bands 846, 975, 1000 and 1170 cm^{-1} of IR spectra in non-polarized light.

The results presented in figure 1 show small variations in the crystalline content depending on the spinning speed.

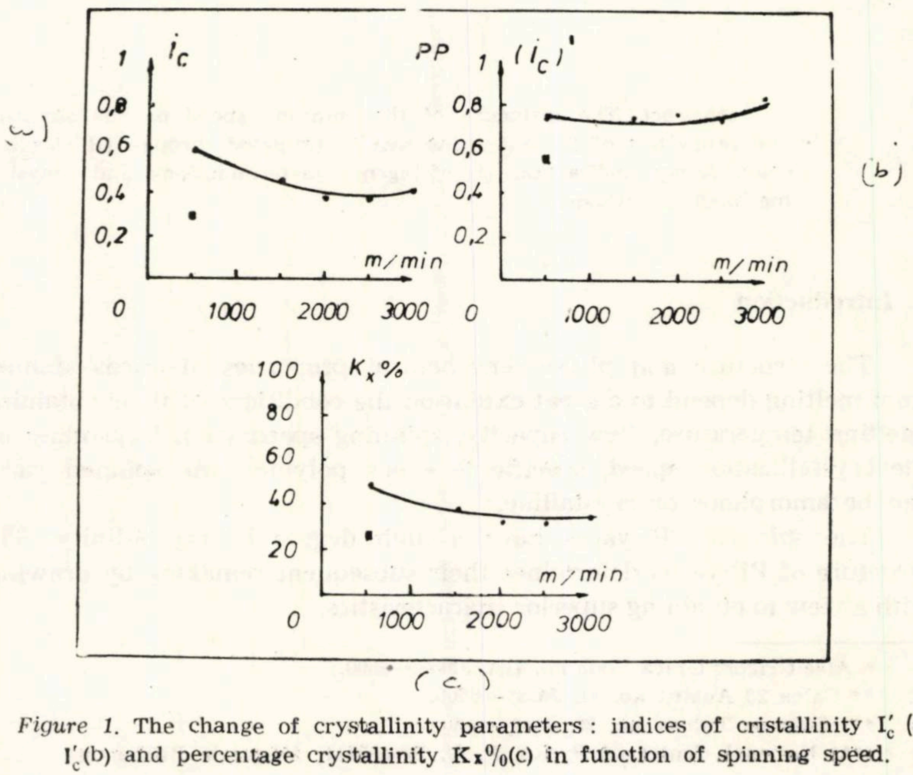

Figure 1. The change of crystallinity parameters : indices of cristallinity I'_c (a), I'_c(b) and percentage crystallinity $K_x\%$(c) in function of spinning speed.

By IR spectra in polarized light, using the same bands were determined : a) the parameters of general orientation (fig. 2 : R_G. R'_G = dichroic ratios ; f_G, f'_G = factors of general orientation) ; b) the parameters of crystalline orientation (Fig. 3 : R_c = dichroic ratio ; f_c = factor of crystalline orientation) ; c) the parameters of amorphous orientation (Fig. 3c : f_A = factor of amorphous orientation). For comparison, the same parameters were calculated for a PP yarns with suitable physico-mechanical properties (spinned at 500 m/min and then drawn).

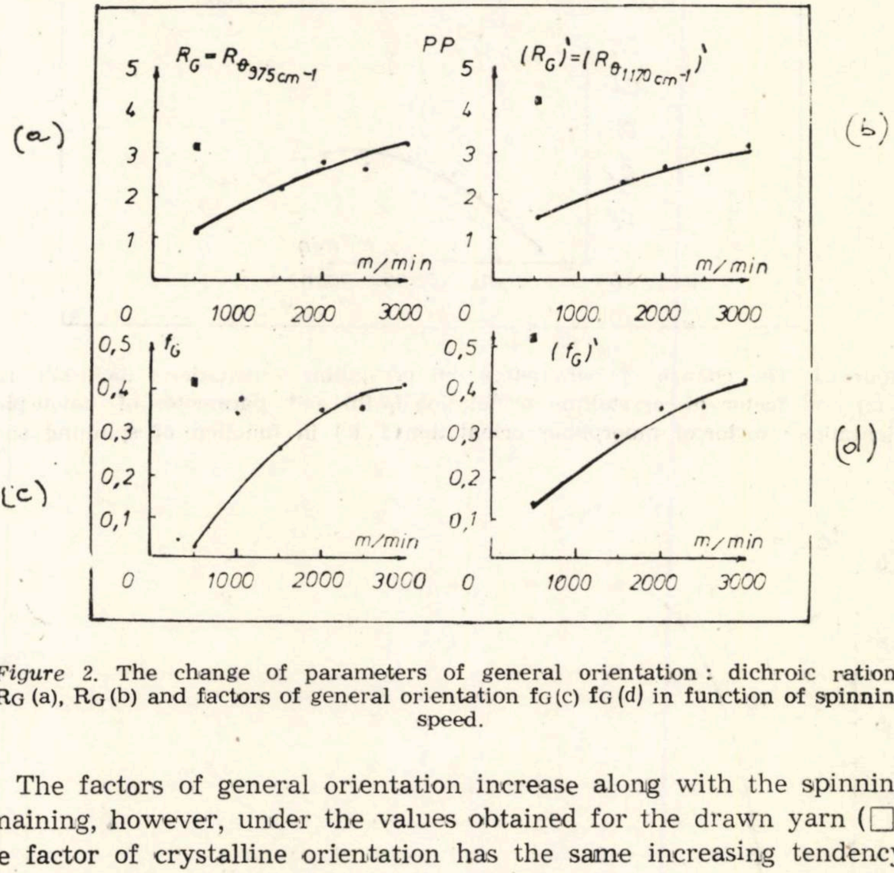

Figure 2. The change of parameters of general orientation : dichroic rations R_G (a), R_G (b) and factors of general orientation f_G (c) f_G (d) in function of spinning speed.

The factors of general orientation increase along with the spinning remaining, however, under the values obtained for the drawn yarn (☐), The factor of crystalline orientation has the same increasing tendency, the spinned yarn at a speed of 3000 m/min showing a crystalline orientation nearly similar to that of the drawn yarn. The factor of amorphous orientation of the spinned yarns remains significantly under the value obtained for the drawn yarn.

In the figure 4 the crystalline orientation factor f_c^x (determined by X-ray) presents a tendency to reach the maximum values of a spinning speed, higher than 2500 m/min.

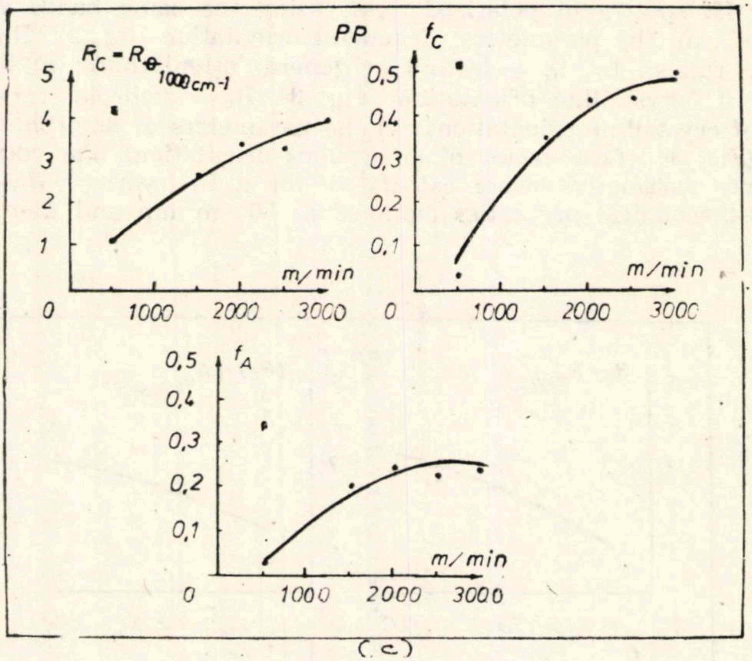

Figure 3. The change of parameters om crystalline orientation : dichronic ratio R_C (a) and factor of crystalline orinetation f_C (b) and parameter of amourphous orientation : factor of amorphous orientation f_A (c) in function of spinning speed.

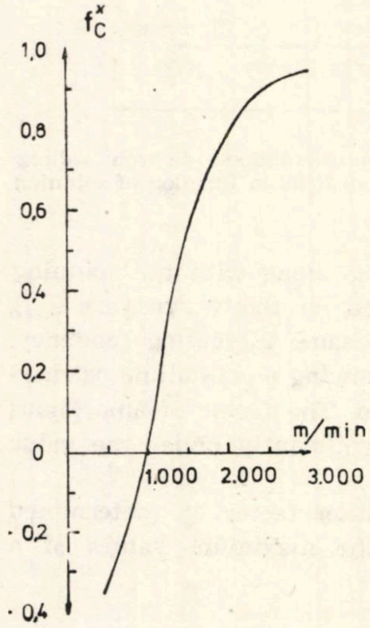

Figure 4. The change of crystalline factor f_C^X (X-ray) in function of spinning speed.

The variation of birefringence (fig. 5), depending on spinning speed, is in agreement with the bahaviour of the general orientation factors determined by IR.

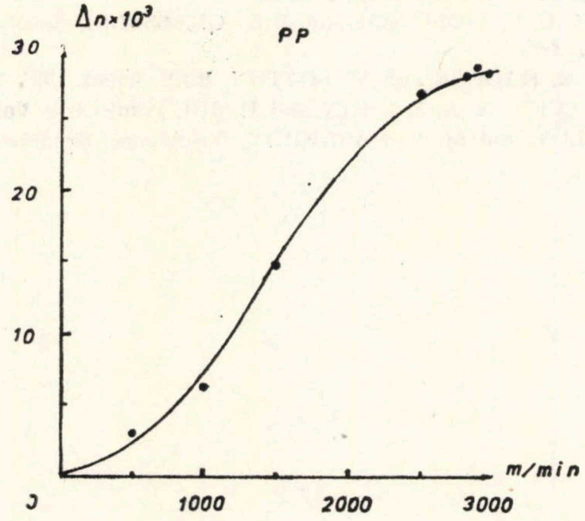

Figure 5. The change of birefringence Δ n in function of spinning speed.

The noticeable differences of the orientation of analysed spinned yarns are also reflected in their behaviour et deformation (fig. 6: tenacity, breaking elongation Δ 1%).

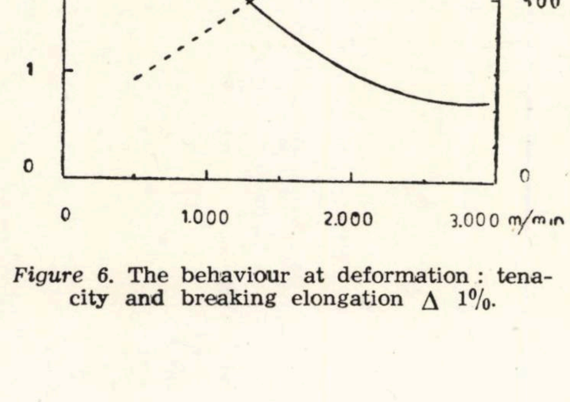

Figure 6. The behaviour at deformation : tenacity and breaking elongation Δ 1%.

REFERENCES

1. G. A. TIRPAK and J. P. SIBILIA, Appl. Polym. Sci., 17, 2, 643, 1973.
2. O. J SWEETING, *The Science and Technology of Polymers Films*, vol. I, Interscience Publ. New York, 1968.
3. J. L. KOENIG, L. E. WOLFRAM and J. G. GRASSELLI, Spectrochim. Acta, 22, 1242, 1966.
4. P. BOURIOT, R. HAGÈGE and M. SOTTON, Bull. Scient. ITF, 5. 139, 1976.
5. N. I. MAKAREVICI, A. A. KONKIN and U. JUI, Himiceskie Volokna, 5, 9, 1964.
6. N. V. MIHAILOV and M. V. SABLÎGHIN, Visokomol. Soedineniya, A, 4, 1155, 1962.,

ANALELE UNIVERSITĂŢII BUCUREŞTI, FIZICA, XXXII, 1983, pag. 69—86

E.S.R. STUDIES ON LIQUID CRYSTALS

L. GEORGESCU, SAEED BAFAYAD *, V. POPA-NIŢĂ
Faculty of Physics, University of Bucharest **

M. I. CHIPARĂ, R. MOLDOVAN
Institute for Physics and Technology of Materials ***

L. BUCŞA
National Institute for Gerontology and Geriartrics ****

Abstract. Electron spin resonance investigations on ordered fluids are briefly reviewed. The calculus necessary to evaluate the order parameters from resonance lines positions are derived in detail, in an elementary description. Some important applications of e.s.r. spectroscopy to liquid crystals are discussed.

1. Introduction

Ordered fluids are represented by a collection of assymmetrical molecules * which, under certains circumstances (in a range of temperature for thermotropic fluids or in a range of concentration for liotropic fluids) exhibit an ordered distribution of (long) molecular axis orientations (Fig. 1). In every layer, molecules tend to align their long axis on a given direction, defined as director /1—3/, as may be observed in Figures 1a — 1c. However, molecular axis' directions may change as are going from one layer to another one (Fig. 1c).

Electric or magnetic field as well as intermolecular interactions between fluid's molecules and container's molecules may align molecular axis of the liquid crystal. Usually, intermolecular interactions (anchoring) are neglected so that external fields (electric, magnetic, mechanic or a combination of these) define the direction of the director.

---

* On leave from Physics Department, University of Aden, D.P.R. Yemen.

** National Center for Physics, Măgurele-Bucharest, P. O. Box MG—11, R—76900. Romania.

*** National Center for Physics, Măgurele-Bucharest, P. O. Box MG—7, R—76900, Romania.

**** M. Căldăruşani Av., Bucharest, R—78178.

* The condition of assymmetrical molecules is sometimes too strong (a good example is the D smectic phase / 2, 3/).

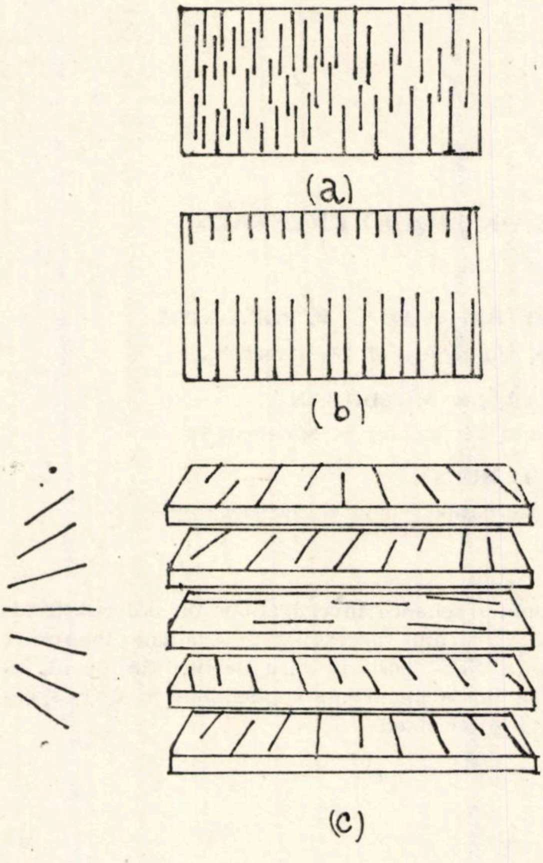

Fig. 1. Order in fluids· a. Nematic like order ; b. Smectic-like order c. Cholesteric-liker order.

Because most commercial available spectrometer are operating in X frequency band (about 9 GHz) or in higher frequency bands (K band about 24 GHz, Q band about 27 GHz...), the external magnetic field is higher than 0.3 T so that in most cases, liquid crystals are ordered by the external magnetic field, H_0. In general, the effect of magnetic fields (in gausses). is comparable to the effect of electric fields (in volts per centimeter) /3/.

Almost all papers dealing with e.s.r. applications to liquid crystals, concern nematic phases or in few cases smectic phases. Little progress has been reported in the e.s.r study on cholesterics.

2. Rudiments of E.S.R. spectroscopy

We shall discuss briefly and from an elementary point of view, the electron spin resonance (e.s.r.) phenomenon. As only few papers on liquid crystals concern a detailed analysis of resonance linewidth /4, 3/, we shall focus our attention on resonance lines positions and consequently on spin Hamiltonian description /6—8/.

E.s.r. phenomenon consists in the resonant absorption of energy from a collection of uncoupled electronic spins, in interaction each with other and/or with external systems and placed in an external magnetic field of intensity H_0 /6—8/. The external magnetic field, raises the degeneracy upon the quantum magnetic number M_s (Fig. 2), splitting the energy level in sublevels, known as Zeemann levels.

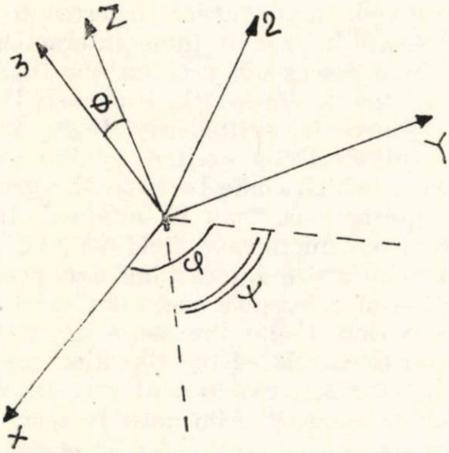

Fig. 2. Molecular and laboratory refe_ rence frames

The condition of resonant absorption from the electromagnetic field requires an adequate frequency ν_0, corresponding to the separation between the energy of Zeemann levels ΔE (Fig. 3). For a collection of uncoupled electronic spins, the resonance condition is,

$$h\nu_0 = g\mu_0\mu_r\beta H\Delta M_s \tag{1}$$

where h is Planck constant, β is Bohr magneton (for electron), μ_0 is the vacuum permeability and μ_r is the relative permeability of spins' collection. For most commercially available spectrometers, the magnetic component of electromagnetic field and the external magnetic field, of intensity H_0 are at right angles, the sample beeing located in regions of high magnetic field intensity and low electric field (component) intensity. Under these circumstances, magnetic dipole transitions, characterized by $\Delta M_s = 1$ as selection rule, are induced. These spectrometers operate usually in the microwave region of electromagnetic radiation, in the range 10^9—10^{11} Hz and requires magnetic fields of intensity 0.1—10. T.

As long as spin collection is perfectly isolated and there are no interactions among spins, resonant absorption of energy occurs till the population of Zeemann levels is equalized by transitions induced by the microwave field. Starting from this instant, because spins collection cannot dissipate their energy, no net absorption of electromagnetic energy will be measured. Interactions among uncoupled spins as well as (and/or) interactions between spins system and other systems, usually known as spin-spin interactions and spin-lattice interactions respectively, provides to uncoupled electronic spins ways to dissipate their energy, via various relaxation mechanisms (divided in two large classes; spin-spin relaxation mechanism and spin-lattice relaxation mechanisms according to the type of the interaction). Consequently, a net absorption of energy will be observed. In conclusion, in order to record a resonance spectrum of finite linewidth, one of these interaction must be present, at least. This qualitative discussion pointed out that relaxation mechanisms dominate the resonance linewidth. However, if the power of electromagnetic energy source is sufficiently high, then an equilibrium between the number of electrons excited by the microwave field and the number of electrons which come back on the ground level via spin-spin or spin-lattice interactions, may be attained. In this case, no net absorption of energy from microwave field will be measured, although spin — spin or/and spin-lattice interactions are present. This situation is known as "saturation of resonance spectrum" and is overcomed reducing the microwave power. Using the same argument as before, it is evident that saturation is correlated to relaxation mechanisms. However, in order to make a corrrect experiment on relaxation mechanisms, another technique, known as spin-echo must be used /9/.

From a macroscopic, elementary point of view, the resonance phenomena may be described by the complex evolution of a macroscopic vector, sample magnetization, using Bloch equations /8, 9/. From a simple quantum point of view, we may writte the Hamiltonian of the spin assembly in both fields ("static" external magnetic field of intensity H_0 and microwave field). Usually the higher terms as well as small terms in comparison to the "energy window" investigated by e.s.r. spectroscopy are neglected, a "spin Hamiltonian" /8/ beeing obtained. In general, the spin Hamiltonian is;

$$H = \beta^{(e)} \sum_{u} H g^{(e)} S_u + \beta^{(e)} \sum_{u} H L_u + \sum_{u} S_u P S_u + \beta^{(n)} \sum_{v} H g^{(n)} I_v + \lambda \sum_{u,v} L_u S_v + \\ + \sum_{u,v} S_u A I_v + \sum_{v} I_v Q I_v + \sum_{u',u''}{}' S_{u'} J S_{u''} \qquad (2)$$

where: $\beta^{(e)}$ is electronic Bohr magneton, $\beta^{(n)}$ is nuclear Bohr magneton, $g^{(e)}$ is the electronic g factor (tensor), $g^{(n)}$ is the tensor associated to the nuclear g factor, λ is the spin-orbit coupling constant, H is the magnetic field (including both static and microwave contributions), $\vec{S}$ is the electronic spin operator, $\vec{I}$ is the nuclear spin operator and $\vec{L}$ is the operator associated to electron's angular momentum. L, I, and S are vectorial operators. P represents the tensor of electronic dipolar interaction (containing two independent terms denoted as D and E in its proper reference frame /7, 8/, Q is the nuclear quadrupolar tensor, A is the hyperfine structure tensor and J is the exchange tensor.

The sommation in (2) is performed over electronic spins denoted by the subscript u (or u' and u") and over nuclear spins, denoted by the subscript v. The prime index after the double sommation in (2) signifies that this sommation is performed only for $u' \neq u''$ (the terms with $u' = u''$ are in the third term of (2)). It is customery, in e.s.r. spectroscopy, to use the effective spin concept, roughly given by /8/ ;

$$S = \sum_{u} S_u ; \quad I = \sum_{u} I_u ; \quad L = \sum_{u} L_u \tag{3}$$

Therefore, equation (2) turns to ;

$$H_s = \beta^{(e)} \vec{H} \hat{g}^{(c)} \hat{\vec{S}} + \beta^{(e)} \vec{H} \hat{\vec{L}} + \hat{\vec{S}} \hat{P} \hat{\vec{S}} + \beta^{(n)} \vec{H} \hat{g}^{(n)} \hat{\vec{I}} + \lambda \hat{\vec{L}} \hat{\vec{S}} + \hat{\vec{S}} \hat{A} \hat{\vec{I}} + \\ + \hat{\vec{I}} \hat{Q} \hat{\vec{I}} + \sum_{u', u''}' \hat{\vec{S}}_{u'} \hat{J} \hat{\vec{S}}_{u''} \tag{4}$$

Let we discuss the significance of the terms occuring in the right hand of equations (2) or (4). The first term represents the energy associated to the (effective) uncoupled electronic spin $\hat{\vec{S}}$, in a magnetic field $\vec{H}$. It is known as Zeemann term (energy) and usually it is the largest term. The magnetic field $\vec{H}$ may take into account both the contribution of static and microwave magnetic fields. The second term given the interaction energy between angular momentum L and magnetic fields H. In solids and often in ordered fluids the angular momentum is quenched /6—8/, so that the contribution of this term is zero or negligible. The second term is associated to interactions among electronic spins belonging to the same nucleus. It leads to the fine structure of resonance spectrum and it is a traceless tensor. Therefore, in the proper reference frame for P, only two components are independent (D and E). This term is nonzero only if the effective spin is higher than 1/2. The fourth term represents the nuclear Zeemann energy as it describes the interaction between nuclear spin and magnetic fields. Because the nuclear magneton is three order of magnitude smaller than the electronic magneton, this term is generally neglected. The fifth term is associated to the energy of interaction between angular momentum and electronic spin. In solids this term is usually negligible /7, 8/. The sixth term represents the energy associated to the interaction between nuclear and electronic spins. It leads to he hyperfine structure of the resonance spectrum. The seventh term represents the energy of quadrupolar interactions between nuclear spins. It is nonzero only if the nuclear spin is higher than 1/2. Usually, this term is negligible even if the nuclear spin is higher than 1/2 but not too large. The contribution of this term is particularly large for Mn^{2+} or V^{4+} ions /6, 8/. The last term is associated to the exchange interactions among different electrons. In most cases, the contribution of this term is negligible.

Usually, in e.s.r. spectroscopy the contribution of second and fourth term is neglected (sometimes even in the liquid state). If the electronic spin is 1/2, as in the case of most spin labels or spin probes, and if the concentration of spin probe or spin label is sufficiently low to neglect exchange interactions, the third and the last term in equation (4) are negligible. In general, the contribution of the fifth term is negligible for organic probes and for some probes containing transition-metal ions. In some cases (for example Cu^{2+} /8/) the contribution of spin-orbit coupling is not negligible. If the nuclear spin is nonzero but its value is no very high, the contribution of nuclear quadrupolar interactions is negligible. However, it is necessary to take into account the seventh term in (4) for systems in which the uncoupled electron is delocalized over a (or more) nucleus with a large spin as in the case of vanadium and manganese /8/ ions.

In consequence, most e.s.r. applications to liquid crystals are described by a truncated spin-Hamiltonian H_s

$$H_s = \beta^{(e)} \vec{H}\hat{g}^{(e)} \hat{\vec{S}} + \hat{\vec{S}}\hat{A}\hat{\vec{I}} \tag{5}$$

The resonance spectrum of an uncoupled electronic spin ($S = 1/2$) delocalized over a nucleus characterized by the nuclear spin I consists in $(2I + 1)$ resonance lines, equally spaced, with the same intensity. Most e.s.r. studies on nitroxides probes dissolved in liquid crystals use this spin Hamiltonian.

In the case of a spin probe containing paramagnetic ions of vanadium or manganese, the appropriated spin Hamiltonian is ;

$$H_s = \beta^{(e)} \vec{H}\hat{g}^{(e)}\hat{\vec{S}} + \hat{\vec{S}}\hat{A}\hat{\vec{I}} + \hat{\vec{I}}\hat{Q}\hat{\vec{I}} \tag{6}$$

In these cases, the effective electronic spin is $S = 1/2$ but the nuclear spin is high (5/2 for manganese and 7/2 for vanadium). The resonance spectrum consists still of $(2I + 1)$ lines, but the lines are no longer equally spaced, due to the presence of the quadrupolar (nuclear) interaction term. As the quadrupolar interaction may mixt states with different nuclear magnetic number, forbidden transitions characterized by $\Delta M_I = 1$ or even 2, are observed. In the case of the spin Hamiltonian (5) the allowed transition requires $\Delta M_S = 1$ and $\Delta M_I = 0$. According to the relative orientation between molecular and laboratory frames, nuclear dipolar interactions may reduce the separation between outer lines or between inner lines /6, 7/. If these frames have the same orientations (coincide) the nuclear quadrupolar interaction does not affect resonance lines positions.

In few cases the contribution of spin-orbit coupling is considered. One of these cases may be related to probes containing Cu^{2+} ions and described by the following spin hamiltonian ;

$$H_s = \beta^{(e)}\vec{H}\hat{g}^{(e)}\hat{\vec{S}} + \beta^{(e)}\vec{H}\hat{\vec{L}} + \hat{\vec{S}}\hat{A}\hat{\vec{I}} + \lambda\hat{\vec{L}}\hat{\vec{S}} \tag{7}$$

Usually, the second term is neglected, excepting the cases in which the g factor is evaluated with a high accuracy. The spin orbit interaction affects the resonance line position and therefore the g factor.

Sometimes, probes dissolved in liquid crystals are characterized by effective spin higher than 1/2. The most commonly cases concerns biradicals or systems with strong ferromagnetic exchange interactions described by an efective spin $S = 1$ and transition metal ions (for example Fe^{3+} in the high spin state has an effective spin equal to 5/2). Fe^{3+}, in the high spin state is described by the following Hamiltonian ;

$$H_s = \beta^{(e)}\vec{H}\hat{g}^{(e)}\hat{\vec{S}} + \hat{\vec{S}}\hat{P}\hat{\vec{S}} \tag{8}$$

The dipolar interaction tensor (among electrons) is a traceless tensor so that in the proper reference frame of P, only 2 independent components characterize the dipolar interactions. Usually this tensor is split in a diagonal tensor (denoted as D /6—8/) which describe the situations in which axial symmetry occurs and a nondiagonal tensor (term), denoted as E and associated to distortions from the axial symmetry. Sometimes, for systems with a large effective spin, higher term in electronic spins are taken into account in the spin Hamiltonian. Using D and E, Hamiltonan (8) turns to ;

$$H_s = \beta^{(e)}\vec{H}\hat{g}^{(e)}\hat{\vec{S}} + D\left(\hat{S}_z^2 - \frac{1}{3}S(S+1)\right) + E(\hat{S}_x^2 - \hat{S}_y^2) \tag{9}$$

If the external magnetic field H (including the microwave field) is zero, the Hamiltonian reduces to the dipolar interaction term, known as zero-field term /6, 10/. Therefore, the energy levels are splitted by the dipolar interaction term, which raises totally or partially the degeneracy upon M_s.

In a case of a nitroxide biradical, the spin Hamiltonian has the following form ;

$$H_s = \beta^{(c)}\vec{H}\hat{g}^{(c)}\hat{\vec{S}} + \hat{A}\hat{\vec{I}}\hat{\vec{S}} + D\left(\hat{S}_z^2 - \frac{1}{3}S(S+1)\right) + E(\hat{S}_x^2 - \hat{S}_y^2) \tag{10}$$

In the case of a strong exchange interaction, between nitroxides radicals for example, the spin Hamiltonian is ;

$$H_s = \beta^{(c)}\vec{H}\hat{g}^{(e)}\hat{\vec{S}}_1 + \hat{A}\hat{\vec{I}}\hat{\vec{S}}_1 + \beta^{(e)}\vec{H}\hat{g}^{(c)}\hat{\vec{S}}_2 + \hat{A}\hat{\vec{I}}\hat{\vec{S}}_2 + \hat{\vec{S}}_1\hat{J}\hat{\vec{S}}_2 \tag{11}$$

where $S_1 = S_2 = 1/2$ (because no electronic dipolar term appears in 11). If we introduce the effective spin $S = S_1 + S_2$ for a ferromagnetic-like exchange interactions, equations (11) turns to ;

$$H_s = \beta^{(e)}\vec{H}\hat{g}^{(e)}\hat{\vec{S}} + \hat{A}\hat{\vec{I}}\hat{\vec{S}} + \hat{\vec{S}}_1\hat{J}\hat{\vec{S}}_2 \tag{12}$$

If the electronic spin is higher than 1/2, equation (12) becomes ;

$$H_s = [\beta^{(c)}\vec{H}\hat{g}^{(e)}\hat{\vec{S}}_1 + \beta^{(c)}\vec{H}\hat{g}^{(c)}\hat{\vec{S}}_2 + \hat{A}\hat{\vec{I}}\hat{\vec{S}}_1 + \hat{A}\hat{\vec{I}}\hat{\vec{S}}_2 + \hat{\vec{S}}_1\hat{J}\hat{\vec{S}}_2 + D\left(\hat{S}_{1z}^2 - \right.$$

$$\left. - \frac{1}{3}S_1(S_1 + 1)\right) + D\left(\hat{S}_{2z}^2 - \frac{1}{3}S_2(S_2 + 1)\right) + E(\hat{S}_{1x}^x - \hat{S}_{1y}^2) + E(\hat{S}_{2x}^2 - \hat{S}_{2y}^2) \tag{13}$$

It is important to notice that equations (2—13) are not written in a single reference frame. The tensors $g^{(e)}$, $g^{(n)}$, A, P and Q are defined in the molecular frame whereas spins S and I as well as the angular momentum L are defined in the laboratory frame, as the static external magnetic field is a natural axis of quantization. The Euler angles between these frames are θ, $\varnothing$ and ψ (Fig. 2). In order to writte equations (2—13) in a single reference frame, it is important to notice that all tensors occuring in these equations are second order tensors. Their components change upon rotations according to the transformations :

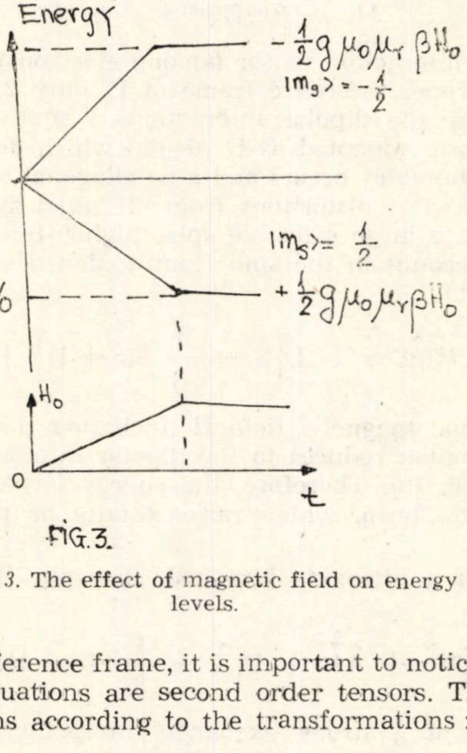
Energy
W_0
$-\frac{1}{2}g\mu_0\mu_r\beta H_0$
$|m_s\rangle = -\frac{1}{2}$
$|m_s\rangle = \frac{1}{2}$
$-W_0$
$+\frac{1}{2}g\mu_0\mu_r\beta H_0$
H_0
0
t

FIG.3.

Fig. 3. The effect of magnetic field on energy levels.

$$g_{ab} = R_{ai}R_{bj}g_{ij} \tag{14}$$

where (a, b) = (x, y, z) denotes laboratory frame's axis (i, j) = 1, 2, 3) denotes molecular frame's axis. R_{ai} respectively R_{b1} represents the rotation matrix /7/. Therefore, in the laboratory frame, equation (2) turns to :

$$H_s = \beta^{(c)}(\sum_u \vec{H}\hat{R}\hat{R}\hat{g}^{(e)}\hat{\vec{S}}_u + \sum_u \vec{H}\hat{\vec{L}}_u) + \sum_u \hat{\vec{S}}_u\hat{R}\hat{R}\hat{P}\hat{\vec{S}}_u + \beta^{(n)}\sum_v \vec{H}\hat{R}\hat{R}\hat{g}^{(n)}\hat{\vec{I}}_v +$$

$$+ \lambda\sum_{u'u''}\hat{\vec{L}}_{u'}\hat{\vec{S}}_{u''} + \sum_u\sum_v \hat{\vec{S}}_u\hat{R}\hat{R}\hat{A}\hat{\vec{I}}_v + \sum_v \hat{\vec{I}}_v\hat{R}\hat{R}\hat{Q}\hat{\vec{I}}_v + \sum_{u'}\sum_{u''}{}' \hat{\vec{S}}_{u'}\hat{R}_0\hat{R}_0\hat{J}\hat{\vec{S}}_{u''} \tag{15}$$

The exchange tensor J has been rotated by another rotation R_0 because it is not generally evident that this tensor is defined in the molecular frame, too.

In order to find resonance lines positions, the time independent Schrodinger equation, associated to (15) must be solved. The matrix representation of (15) is in general, an irreducible representation /7/, as electronic spin wavefunction $/B_S)$, electronic angular wavefunctions $/B_L)$ and nuclear spins wavefunctions $/B_I)$ are mixed so that the wavefunction of (15) may be considered as the direct (tensor) product of these components ;

$$/B) = /B_S) \bigcirc /B_L) \bigcirc /B_I) \qquad (16)$$

The spin orbit interaction term mixes orbital wavefunction $/B_L)$ with mixes spin electronic wavefunction $/B_S)$ with nuclear spin wavefunction electronic (spin) wavefunction $/B_S)$ and the hyperfine interaction term $/B_I)$. If the spin-orbit interaction is negligible, the representation of (15) becomes reducible and only spins provides an irreducible representation. The eigenvalues E_n (M_S, M_I, N_L) need to be estimated from the time independent Schrodinger equation associated to (15). The resonance lines positions are easily derived imposing the dipole magnetic selection rule ;

$$\Delta M_S = 1, \quad \Delta M_I = 0, \quad \Delta N_L = 0, \qquad (17)$$

so that ;

$$E_n(M_S, M_I, N_L) - E_K(M'_S, M'_I, N'_L)\delta(M_S - M'_S - 1)\delta(M'_I - M_I)\delta(N'_L - N_L) =$$
$$= h\nu_0 = g^{(eff)}\,\beta^{(e)}H(M_S - M'_S) \qquad (18)$$

From equation (18), the effective g value ($g^{(eff)}$) is obtained. However, we must recognize that the resonance spectrum depends on molecular axis orientation so that what we really obtaine in an experiment is an average upon all possible molecular orientations. Therefore, in order to evaluate the g factor, the eigenvalues obtained as solutions of equations (2—16) must be averaged over all possible molecular orientations. These calculations are performed up to every detail in Appendix 1. The situation is even more complicated in ordered or partially ordered fluids and leads to the introduction of order parameter tensor. Consequently, e.s.r. spectroscopy leads to the estimation of order parameter tensor.

According to the calculus performed in Appendix 1, the effective values of the g factor and hyperfine splitting A, repectively, are ;

$$g^{(eff)} = g^{(e)} - (g^{(e)} - g^{(e)}_{zz})\sigma_{zz} + \frac{1}{3}(g_{xx} - g_{yy})(\sigma_{xx} - \sigma_{yy}) \qquad (19)$$

$$A^{(eff)} = A - (A - A_{zz})\sigma_{zz} + \frac{1}{3}(A_{xx} - A_{yy})(\sigma_{xx} - \sigma_{yy}) \qquad (20)$$

For a nitroxide spin probe or spin radical, the spin Hamiltonian (5) is ;

$$H_s = \left[\left(g^{(e)} - (g^{(e)} - g^{(e)}_{zz})\sigma_{zz} + \frac{1}{3}(g_{xx} - g_{yy})(\sigma_{xx} - \sigma_{yy})\right)\right]\beta^{(e)}\underset{o}{H}S_z +$$
$$+ S_zI_z\left[\left(A - (A - A_{zz})\sigma_{zz} + \frac{1}{3}(A_{xx} - A_{yy})(\sigma_{xx} - \sigma_{yy})\right)\right] \qquad (21)$$

where σ_{xx}, σ_{yy}, σ_{zz} are the diagonal components of the order tensor. The order tensor has supposed to be diagonal, and because it is a traceless tensor, only 2 independent components are sufficient to characterize it. We shall suppose that $\sigma_{xx} - \sigma_{yy}$ an σ_{zz} are these components.

$$(\sigma_{xx} - \sigma_{yy}) = 3\,\frac{(A^{eff} - A)(g^{(e)} - g^{(e)}_{zz}) - (A_{zz} - A)(g^{(e)} - g^{(eff)})}{(A - A_{zz})(g_{xx} - g_{yy}) + (g^{(e)} - g^{(e)}_{zz})(A_{xx} - A_{yy})} \tag{22}$$

and,

$$\sigma_{zz} = \frac{g^{(e)} - g^{(eff)}}{g^{(e)} - g^{(e)}_{zz}} +$$

$$+ \frac{(g^{(e)}_{xx} - g^{(e)}_{yy})\,[(A^{(eff)} - A)\,(g^{(e)} - g^{(e)}_{zz}) - (A_{zz} - A)\,(g^{(e)} - g^{(eff)})]}{(g^{(e)} - g^{(e)}_{zz})\,[(A - A_{zz})\,(g^{(e)}_{xx} - g^{(e)}_{yy}) + (g^{(e)} - g^{(e)}_{zz})\,(A_{xx} - A_{yy})]} \tag{23}$$

In the case in which all tersors $g^{(e)}$, P, Q, A and σ have an axial symmetry, the relation between effective values and theoretical values of $g^{(e)}$, P, A, and Q order parameter σ_{zz} is,

$$\sigma_{zz} = \frac{3}{2}\,\frac{g^{(eff)} - g^{(e)}}{g^{(e)}_{||} - g^{(e)}_{\perp}} = \frac{3}{2}\,\frac{A^{(eff)} - A}{A_{||} - A_{\perp}} = \frac{3}{2}\,\frac{Q^{(eff)} - Q}{Q_{||} - Q_{\perp}} =$$

$$= \frac{3}{2}\,\frac{P^{(eff)} - P}{P_{||} - P_{\perp}} \tag{24}$$

Equation (24) may be also writteen as follows ; ,

$$\sigma_{zz} = \frac{g^{(eff)} - g}{g_{zz} - g} = \frac{\Delta g}{g_{zz} - g} = \frac{\Delta A}{A_{zz} - A} \tag{25}$$

As, in the case of the axial symmetry, a single order parameter is independent, a single e.s.r. measurement (of g factor or of hyperfine splitting) is sufficient to estimate this independent order parameter, σ_{zz}.

In more complex cases, in which the order tensor may be supposed to be diagonal but is no longer axial, two order parameters, σ_{zz} and $\sigma_{xx} - \sigma_{yy}$ are independent so that two measurements are necessary in order to evaluate both σ_{zz} and $\sigma_{xx} - \sigma_{yy}$. Under these circumstances, hyperfine splitting measurement and g value measurement are suffficient for the evaluation of order parameters. Inserting the experimental data in equations (22) respectively (23), $\sigma_{xx} - \sigma_{yy}$ respectively σ_{zz} are easily obtained. (It is necessary to mentioned that g_{xx}, g_{yy}, g_{zz}, and g are theoretical values).

At the end of this section we shall review some important e.s.r. applications in the study of liquid crystals. For nitroxides spin probes, the order parameter is evaluated from equation (25), measuring the g value shift and supposing that g $= 2.00238$, with an accuracy better than 20% (up to 10%). The accuracy of the data obtained by e.s.r. spectroscopy using this crude approximation is good in some cases /10—14/.

If the order tensor parameters are diagonal but do not exhibit an axial symetry, measurements of $g^{(eff)}$ and $A^{(eff)}$ values permitt the estimation of order parameters /15—20/.

D.P.P.H., a standard e.s.r. marker for line position has been used to estimate the order parameters. Roughly speaking, the spin Hamiltonian used to interpret experimental data, corresponds to the spin Hamiltonian (5) for both D.P.P.H. or nitroxides probes.

Vanadium paramagnetic ions, have been used as spin probes in liquid crystals /21—24/. In this case, the spin Hamiltonian is given by equation *(6)*.

Manganese and iron (high spin Fe^{3+} ions) have been used as spin probes in liquid crystals /1/. These systems are described by the spin Hamiltonian (7) respectively (9).

Biradicals, have been used as probes dissolved in liquid crystals and these systems are described by the spin Hamiltonian (11) or (12). These systems (named also triplet state systems) are of particular importance in the investigation of photochemically excited states /25—32/.

Electric fields have been used to investigate liquid crystals and therefore to evaluate order parameters dependence on the angle between electrostatic field and the external magnetic field /33—34/. The director is align by the applied electric field in most cases /35—37/.

An interesting example of e.s.r. applications to liquid crystals and model phases concerns the investigations of solid modifications of liquid crystals /40, 41/. The resonance spectrum changes when liquid crystal phase change from isotropic fluid to liquid crystal, polycrystalline phase, single (mono) crystalline phase or even amorphous solid state phase.

A major line of developments concerns biologycal applications of liquid crystals are model phases for biologycal membranes /42, 43/. In figure 4, some resonance spectra on D.P.P.H. dissolved in M.B.B.A. in the isotropic and ordered phases as well as some resonance spectra on a nitroxide spin-probe in isotropic, ordered phases of a liquid crystal (including spectra of nitroxide spin probe in a polymer, in both glassy and high elastic state) are presented /44/.

Appendix 1.

In this appendix we shall evaluated the resonance lines positions in e.s.r. experiments on ordered systems. As, we are interested only in lines positions, the spin Hamiltonian description offers an adequate framework. In order to find the position of resonance lines, the Schrodinger equation associated to the spin Hamiltonian 15 must be solved. For simplicity, we shall use time independent Schrodinger equation to estimate the energy levels ;

$$H_s/B) = \beta^{(e)}\vec{H}\hat{R}\hat{g}^{(e)}\hat{R}^{+}\hat{\vec{S}}/B) + \beta^{(e)}\vec{H}\hat{\vec{L}}/B) + \lambda\hat{\vec{L}}\hat{\vec{S}}/B) + \hat{\vec{S}}\hat{R}\hat{P}\hat{R}^{+}\hat{\vec{S}}/B) +$$
$$+ \beta^{(n)}\hat{\vec{H}}\hat{R}\hat{g}^{(n)}\hat{R}^{+}\hat{\vec{I}}/B) + \hat{\vec{S}}\hat{R}\hat{A}\hat{R}^{+}\hat{\vec{I}}/B) + \hat{\vec{I}}\hat{R}\hat{Q}\hat{R}^{+}\hat{\vec{I}}/B) + \sum_{u',}\sum_{u''}{}' \hat{\vec{S}}_{u'}\hat{R}_0\hat{J}\hat{R}^{\pm}\hat{\vec{S}}_{u''}/B) \qquad \text{(A—1)}$$

where $\hat{R}\hat{R}^{+} = \hat{R}^{+}\hat{R} = \hat{E}$ ($\hat{E}$ is the unit matrix). The eigenvalues of (15) may be obtained averaging the spin Hamiltonian over all electronic and nuclear coordinates:

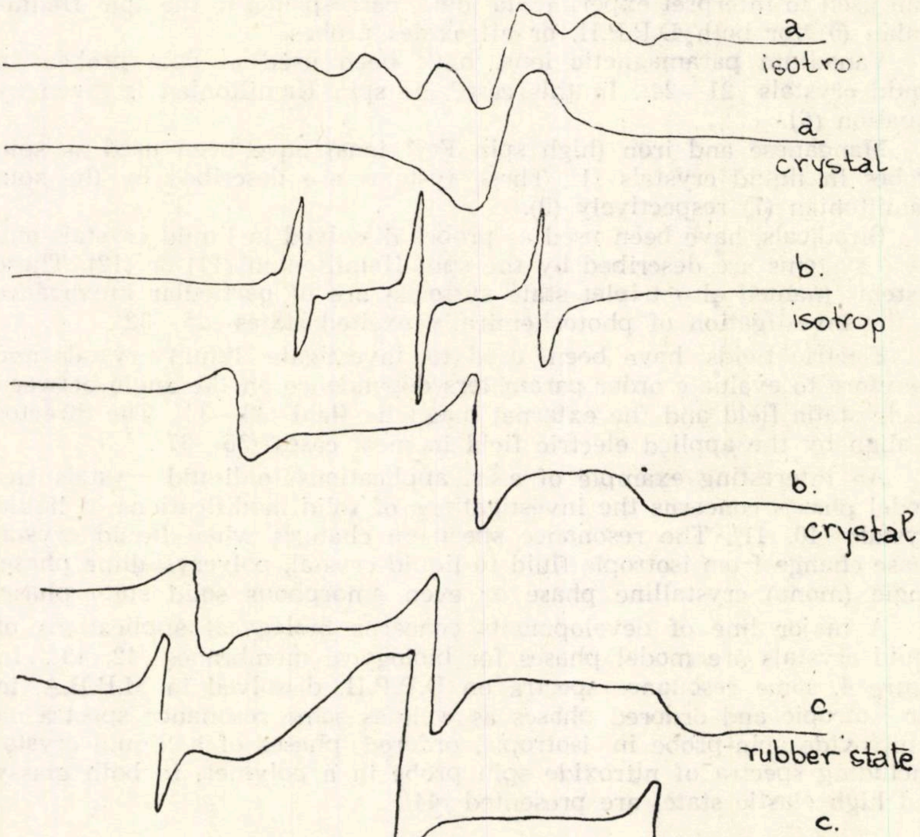

Fig. 4. Electron spin resonance spectra of probes in liquid crystals a) D.P.P.H. dissolved in liquid crystal (MBBA); b) TEMPONE spin probe dissolved in MBBA; c) TEMPONE spin probe dissolved in a polymer.

$$(B/E(M_S, M_I, N_L)/B) = [(B/\beta^{(e)}\vec{\hat{H}}\hat{R}\hat{g}^{(e)}\hat{R}^{+}\vec{\hat{S}}/B) + (B/\beta^{(e)}\vec{H}\vec{\hat{L}}/B) + (B/\lambda\vec{\hat{L}}\vec{\hat{S}}/B) +$$

$$+ (B/\beta^{(n)}\vec{H}\hat{R}\hat{g}^{(n)}\hat{R}^{+}\vec{\hat{I}}/B) + (B/\vec{\hat{S}}\hat{R}\hat{A}\hat{R}^{+}\vec{\hat{I}}/B) + (B/\vec{\hat{I}}\hat{R}\hat{Q}\hat{R}^{+}\vec{\hat{I}}/B)] \qquad (A-2)$$

In equation (A—2), the spin exchange interaction term has been neglected and the wavefunctions /B) fulfills the condition;

$$(B/B) = 1 \qquad (A-3)$$

However, we must recognize that e.s.r. spectroscopy averages over all possible orientations of molecular axis, so that in fact, equation (A—2) must be writte as follows ;

$$E(M_S, M_I, N_L) = \int [(B/\beta^{(e)} H\hat{R}\hat{g}^{(e)}\hat{R}^{+}\hat{\vec{S}}/B) + (B/\beta^{(e)} H\hat{\vec{L}}/B) + (B/\lambda\hat{\vec{L}}\hat{\vec{S}}/B) + \\ + (B/\beta^{(n)} H\hat{R}\hat{g}^{(n)}\hat{R}^{+}\hat{\vec{I}}/B) + (B/\hat{\vec{S}}\hat{R}\hat{A}\hat{R}^{+}\hat{\vec{I}}/B) + (B/\hat{\vec{I}}\hat{R}\grave{Q}\hat{R}^{+}\hat{\vec{I}}/B)]\, f(\Omega)\, d\Omega \qquad (A\text{—}4)$$

Where $f(\mathbf{\Omega})$ is the distribution function for molecular axis orientations. In an isotropic fluid this function has the following expression ;

$$d\Omega f\Omega = \sin\theta d\theta d\varphi \qquad (A\text{—}5)$$

where θ and φ are the angles measured in spherical polar co-ordinates

where θ and φ are the angles measured in spherical polar co-ordinates

/1 ; 3/. In the case of an ordered fluid the distribution functions becomes more complicated /1 ; 3/.

$$f(\mathbf{\Omega})d\mathbf{\Omega} = (\exp w\cos^2\theta)\ \sin\theta d\theta d\varphi \qquad (A\text{—}6)$$

We must recognize that R is a complex rotation matrix, allowing to three rotations about three axis and it may be represented as follows ;

$$R = R(\psi)R(\theta)R(\varphi) \qquad (A\text{—}7)$$

where ;

$$\hat{R}(\psi) = \begin{pmatrix} \cos\psi & \sin\psi & 0 \\ -\sin\psi & \cos\psi & 0 \\ 0 & 0 & 1 \end{pmatrix}, \qquad \hat{R}(\theta) = \begin{pmatrix} 1 & 0 & 0 \\ 0 & \cos\theta & \sin\theta \\ 0 & -\sin\theta & \cos\theta \end{pmatrix}$$

and

$$\hat{R}(\varphi) = \begin{pmatrix} 0 & 0 & 1 \\ \cos\varphi & \sin\varphi & 0 \\ -\sin\varphi & \cos\varphi & 0 \end{pmatrix} \qquad (A\text{—}8)$$

In order to find the relations between tensors expressed in the molecular frame, tensors expressed in the laboratory frame and order tensor, the products $\hat{R}\hat{T}\hat{R}^{+}$ must be evaluated, where $\hat{T}$ is a second order tensor ($\hat{g}^{(e)}$, $\hat{g}^{(n)}$, $\hat{A}$, $\hat{P}$, $\hat{Q}$). If x, y, z denotes laboratory frame and 1, 2, 3 denotes molecular frame, the relation between the components of a second order tensor in differrent frames is fairly complicated ; for example the element t_{xx} in laboratory frame and the components of this tensor in the molecular frame t_{ab} are related through,

$$t_{xx} = t_{11}(\cos^2\varphi\cos^2\psi - \cos\theta\sin\varphi\cos\varphi\sin\psi\cos\psi - \cos\theta\sin\varphi\cos\varphi\ \sin\psi\cos\psi + \\ + \cos^2\theta\sin^2\varphi\sin^2\psi) + t_{12}(\sin\varphi\cos\varphi\cos^2\psi - \cos\theta\sin^2\varphi\sin\psi\cos\psi + \\ + \cos\theta\cos^2\varphi\sin\psi\cos\psi - \cos^2\theta\sin\varphi\cos\varphi\sin^2\psi) + t_{13}(\sin\theta\cos\varphi\sin\psi\cos\psi - \\ - \sin\theta\cos\theta\sin\varphi\sin^2\psi + t_{21}(\sin\varphi\cos\varphi\cos^2\psi - \sin^2\varphi\cos\theta\sin\psi\cos\psi + \\ + \cos\theta\cos^2\varphi\sin\psi\cos\psi + \cos^2\theta\cos^2\varphi\sin^2\psi) + t_{22}(\cos\theta\sin\varphi\cos\varphi\sin^2\psi + \\ + \sin^2\varphi\cos^2\psi + \cos\theta\sin\varphi\cos\varphi + \sin\psi\cos\psi + \cos^2\theta\cos^2\varphi\sin^2\psi) + \\ + t_{23}(\sin\theta\sin\varphi\sin\psi + \sin\theta\cos\theta\cos\varphi\sin^2\psi) + t_{31}(\sin\theta\cos\varphi\sin\psi\cos\psi -$$

$+\ \sin\theta\cos\theta\sin\varphi\sin^2\psi) + t_{32}(\sin\theta\sin\varphi\sin\psi\cos\psi + \sin\theta\cos\theta\sin^2\psi) +$
$+\ t_{33}\sin^2\theta\sin^2\psi$

In fact we must found the relation between the average of T in both references frames and the order tensor. However, we may average every component of T in the laboratory frame, using a distribution function. If the distribution function (A—6) is used, then ;

$$\begin{aligned}(\sin\varphi)_0 &= (\cos\varphi)_0 = 0\\ (\sin^2\varphi)_0 &= (\cos^2\varphi)_0 = 1/2\end{aligned} \qquad \text{(A—10)}$$

If second order tensors are diagonal in both reference frames and the local symmetry is axial, the average implies,

$$\begin{aligned}&(\sin^2\varphi)_0 = (\cos^2\varphi)_0 = (\sin^2\psi)_0 = (\cos\psi^2)_0 = 1/2 \text{ and}\\ &(\sin\varphi)_0 = (\cos\varphi)_0 = (\sin\psi)_0 = (\cos\psi)_0\end{aligned} \qquad \text{(A—11)}$$

where $(\ \ )_0$ signifies an average over all molecular orientations. However in the case of equation (A—11) the distribution function is no longer appropriate, a distribution function as (A—5) beeing used. Introducing (A—11) in (A—9) results ;

$$t_{xx} = t_{11}(1/4)(1 + \cos^2\theta) + t_{22}(1/4)(1 + \cos^2\theta) + \frac{t_{33}}{2}(\sin^2\theta) \qquad \text{(A—12)}$$

Using the definition of order parameter and introducing it in (A—12) results ;

$$t_{xx} = \left((t_{11} + t_{22} + t_{33}) - \sigma\left(\frac{t_{11} + t_{22}}{2} + t_{33})\right)(1/3)\right) \qquad \text{(A—13)}$$

This equation may be extended to he general case, in which, for simplicity, it is supposed that only the nondiagonal terms of the order tensor in laboratory frame are negligible. Under these circumstances, equation (A—13) becomes,

$$\begin{aligned}(t_{xx})_0 &= (1/3)[\sum_a (t_{aa})_0 - \sum_{a,b}\sigma_{ab}(t_{ab})_0]\\ (t_{yy})_0 &= (1/3)[\sum_a (t_{aa})_0 - \sum_{a,b}\sigma_{ab}(t_{ab})_0]\\ (t_{zz})_0 &= (1/3)[\sum_a (t_{aa})_0 + 2\sum_{a,b}\sigma_{ab}(t_{ab})_0]\end{aligned} \qquad \text{(A—14)}$$

Therefore, equation (A—4) turns to ;

$$\begin{aligned}&[(B/H_s/B)]_0 = \beta^{(e)}[B/(H_x\hat{L}_x + H_y\hat{L}_y + H_z\hat{L}_z)_0/B] + [B/(\hat{L}_x\hat{S}_x + \hat{L}_y\hat{S}_y +\\ &+ \hat{L}_z\hat{S}_z)_0/B] + \frac{1}{3}\beta^{(e)}(B/\{H_x[\sum_a(g^{(e)}_{aa})_0 - \sum_{a,b}\sigma_{ab}(g^{(e)}_{ab})_0]S_x + H_y[\sum_a(g^{(e)}_{aa})_0 -\\ &- \sum_{a,b}\sigma_{ab}(g^{(e)}_{ab})_0]S_y + H_z[\sum_a(g^{(e)}_{aa})_0 + 2\sum_{a,b}\sigma_{ab}(g^{(e)}_{ab})_0]\}|B) + (1/3)[\beta/\hat{S}_x(\sum_a(P_{aa})_0 -\\ &\qquad - \sum_{a,b}\sigma_{ab}(P_{ab})_0]\hat{S}_x + \hat{S}_y[\sum_a(P_{aa})_0 - \sum_{a,b}\sigma_{ab}(P_{ab})_0]\hat{S}_y + \hat{S}_z[\sum_a(P_{aa})_0 +\end{aligned}$$

$$+2\sum_{a,b}\sigma_{ab}(P_{ab})_0]\hat{S}_z|B)+(1/3)\beta^{(n)}(B/H_x[\sum_{a}(g^{(n)}_{aa})_0-\sum_{a,b}\sigma_{ab}(g^{(n)}_{ab})_0]\hat{I}_x+$$

$$+H_y[\sum_{a}(g^{(n)}_{aa})_0-\sum_{a,b}\sigma_{ab}(g^{(n)}_{ab})_0]\hat{I}_y+H_z[\sum_{a}(g^{(n)}_{aa})_0+2\sum_{a,b}\sigma_{a,b}(g^{(n)}_{ab})_0]\hat{I}_z/B)+$$

$$+(B/[S_x(\sum_{a}(A_{aa})_0-\sum_{a,b}\sigma_{ab}(A_{ab})_0)\hat{I}_x+\hat{S}_y[\sum_{a}(A_{aa})_0-\sum_{a,b}\sigma_{ab}(A_{ab})_0]\hat{I}_y+$$

$$+\hat{S}_z(\sum_{a}(A_{aa})_0+2\sum_{a,b}\sigma_{ab}(A_{ab})_0)I_z]/B)(1/3)+(1/3)(B|[\hat{I}_x(\sum_{a}(Q_{aa})_0-$$

$$-\sum_{a,b}\sigma_{ab}(Q_{ab})_0)\hat{I}_x+\hat{I}_y(\sum_{a}(Q_{aa})_0-\sum_{a,b}\sigma_{ab}(Q_{ab})_0)\hat{I}_y+$$

$$+\hat{I}_z(\sum_{a}(Q_{aa})_0+2\sum_{a,b}\sigma_{ab}(Q_{ab})_0)\hat{I}_z]/B) \qquad (A-15)$$

Usually $\hat{g}^{(e)}$, $g^{(n)}$, $\hat{P}$, $\hat{A}$ and $\hat{Q}$ tensors are supposed to be diagonal tensors in the laboratory frame. Moreover, as the amplitude of the static external field H_0 exceeds by few order of magnitude the amplitude of microwave's magnetic field and because we are not interested in the study of time dependent phenomena (accordingly, we are investigating the eigenvalues of time independent Schrodinger equation), it is possible to suppose that;

$$H_x=H_y=0; \qquad H_z=H_0 \qquad (A-16)$$

Consequently, magnetic spins (electronic and nuclear) are aligned by this external fields. In the ideal case, the components of electronic and nuclear spins, in the laboratory frame, are;

$$\hat{S}_x=\hat{S}_y=0; \quad \hat{I}_x=\hat{I}_y=0; \quad \hat{I}_z\neq 0; \quad \hat{S}_z\neq 0 \qquad (A-17)$$

Under the circumstances expressed by equations (A—16), (A—17), equation (A—15) becomes;

$$(B/H_s/B)_0=\beta^{(e)}[B/(H_z\hat{L}_z)_0/B]+\lambda[B/\hat{L}_z\hat{S}_z)_0/B+$$

$$(1/3)(B/\beta^{(e)}\sum_{a}(g^{(e)}_{aa})_0(1+2\sigma_{aa})H_z\hat{S}_z/B)+[(B/3)S_z\sum_{a}(P_{aa})_0(1+2\sigma_{aa})H_z\hat{I}_z/B)+$$

$$+(1/3)(B/\hat{I}_z\sum_{a}(Q_{aa})_0(1+2\sigma_{aa})\hat{I}_z/B) \qquad (A-18)$$

The Zeemann term from (A—10) may be written as follows;

$$\beta^{(e)}g^{(eff)}H_z\hat{S}_z/B)=(1/3)\beta^{(e)}\sum_{a}(g^{(e)}_{aa})_0(1+2\sigma_{aa})H_z\hat{S}_z/B) \qquad (A-19)$$

therefore,

$$g^{eff}=(1/3)\sum_{a}(g^{(e)}_{aa})_0(1+2\sigma_{aa}) \qquad (A-20)$$

where g^{eff} is the g value measured by electron spin resonance spectroscopy. Let we introduce the notation;

$$\begin{aligned} g &= (1/3)(g_{xx} + g_{yy} + g_{zz}) \\ A &= (1/3)(A_{xx} + A_{yy} + A_{zz}) \\ P &= (1/3)(P_{xx} + P_{yy} + P_{zz}) \\ Q &= (1/3)(Q_{xx} + Q_{yy} + Q_{zz}) \end{aligned} \qquad \text{(A—21)}$$

Consequently, (A—20) becomes,

$$g^{eff} = g + (2/3) \sum_a \sigma_{aa} g_{aa} \qquad \text{(A—22)}$$

where the sigus for electron "(e)" and orientational werage "($)_0$" have been droped. In analogy with (A—21) is obtained :

$$\begin{aligned} P^{eff} &= P + (2/3) \sum_a \sigma_{aa} P_{aa} \\ A^{eff} &= A + (2/3) \sum_a \sigma_{aa} A_{aa} \\ Q^{eff} &= Q + (2/3) \sum_a \sigma_{aa} Q_{aa} \end{aligned} \qquad \text{(A—23)}$$

Let we change slightly the last term in equation (A—22)

$$(2/3)(\sigma_{xx}g_{xx} + \sigma_{yy}g_{yy} + \sigma_{zz}g_{zz}) = (1/3)(2\sigma_{xx}g_{xx} + 2\sigma_{yy}g_{yy} + 3\sigma_{zz}g_{zz} - \sigma_{xx}g_{zz} + \sigma_{xx}g_{zz} - \sigma_{yy}g_{zz} + \sigma_{yy}g_{zz} - \sigma_{zz}g_{zz}) = (1/3)(g_{xx}\sigma_{xx} + g_{yy}\sigma_{yy} + \sigma_{yy}g_{yy} + \sigma_{zz}g_{yy} + \sigma_{xx}g_{xx} + \sigma_{zz}g_{xx}) - (1/3)(g_{xx} + g_{yy} + g_{zz} - 3g_{zz})\sigma_{zz} \qquad \text{(A—24)}$$

Therefore,

$$(2/3)\sum_a g_{aa}\sigma_{aa} = -(g - g_{zz})\sigma_{zz} + (1/3)(\sigma_{xx}g_{xx} + \sigma_{yy}g_{yy} + \sigma_{yy}g_{yy} + g_{yy}\sigma_{zz} + g_{xx}\sigma_{xx} + g_{xx}\sigma_{zz}) \qquad \text{(A—25)}$$

Supposing that the order parameter is diagonal, because the order tensor is traceless, results ;

$$\sigma_{xx} + \sigma_{yy} + \sigma_{zz} = 0 \qquad \text{(A—26)}$$

Introducing (A—26) in (A—25) is obtained :

$$(2/3) \sum_a \sigma_{aa}g_{aa} = -(g - g_{zz})\sigma_{zz} + (1/3)(\sigma_{xx}g_{xx} + \sigma_{yy}g_{yy} + \sigma_{yy}g_{yy} - \sigma_{xx}g_{yy} - \sigma_{yy}g_{yy} - \sigma_{xx}g_{xx} - \sigma_{yy}g_{xx} + \sigma_{xx}g_{xx}) = (1/3)((g_{xx} - g_{yy})\sigma_{xx} - (g_{xx} - g_{yy})\sigma_{yy}) - (g - g_{zz})\sigma_{zz} \qquad \text{(A—27)}$$

Accordingly, (A—22) becomes,

$$g^{eff} = g - (g - g_{zz})\sigma_{zz} + (1/3)(g_{xx} - g_{yy})(\sigma_{xx} - \sigma_{yy}) \qquad \text{(A—28)}$$

By analogy ;

$$\begin{aligned} A^{eff} &= A - (A - A_{zz})\sigma_{zz}(1/3)(A_{xx} - A_{yy})(\sigma_{xx} - \sigma_{yy}) \\ P^{eff} &= P - (P - P_{zz})\sigma_{zz} + (1/3)(P_{xx} - P_{yy})(\sigma_{xx} - \sigma_{yy}) \\ Q^{eff} &= Q - (Q - Q_{zz})\sigma_{zz} + (1/3)(Q_{xx} - Q_{yy})(\sigma_{xx} - \sigma_{yy}) \end{aligned} \qquad \text{(A—29)}$$

As the order parameter satisfies (A—26), we must recognize that only σ_{zz} and $\sigma_{xx} - \sigma_{yy}$ are independent variables. If these tensors have an axial symmetry, $g_{xx} = g_{yy} = g_{\perp}, g_{zz} = g_{\parallel}, A_{xx} = A_{yy} = A_{\perp}, A_{zz} = A_{\parallel}$

In these conditions, equations (A—22) and (A—23) change to ;

$$\begin{aligned} g^{eff} &= g + (2/3)(g \parallel - g_{\perp})\sigma_{zz} \\ A^{eff} &= A + (2/3)(A \parallel - A_{\perp})\sigma_{zz} \\ P^{eff} &= P + (2/3)(P - P)\sigma_{zz} \\ Q^{eff} &= Q + (2/3)(Q \parallel - Q_{\perp})\sigma_{zz} \end{aligned} \qquad (A—30)$$

If both g^{eff} and g^{eff} may be evaluated, then :

$$\begin{aligned} g^{eff} &= g_{\perp} \ (1 + 2\sigma_{zz}) \\ g^{eff} &= g_{\parallel} \ (1 - \sigma_{zz}) \end{aligned} \qquad (A—31)$$

If the order tensor has an axial symmetry, i.e. $\sigma_{xx} - \sigma_{yy} = 0$ and $\sigma_{zz} = -(1/2)\sigma_{xx}$, only one order parameter is independent. Therefore,

$$\begin{aligned} g^{eff} &= g - (g - g_{zz})\sigma_{zz} & A^{eff} &= A - (A - A_{zz})\sigma_{zz} \\ P^{eff} &= P - (P - P_{zz})\sigma_{zz} & Q^{eff} &= Q - (Q - Q_{zz})\sigma_{zz} \end{aligned} \qquad (A—32)$$

REFERENCES

1. G. DE GENNES, *The physics of liquid crystals,* Clarendon Press, Oxford, 1974.
2. S. CHADRASEKHAR, *Liquid crystals,* Cambridge Monographs on Physics, Cambridge University Press, 1977.
3. G. W. GRAY, *Molecular structure and the properties of liquid crystals,* Academic Press, New York, 1962 ; G. W. GRAY, P. A. WINSOR, *Liquid Crystals and plastic crystals,* vol. 1, 2, Halsted Press, New York 1974 ; G. MEIER, E. SACKMANN, G. GRABMAIER, *Applications of Liquid Crystals,* Springer-Verlag, 1975.
4. I. URSU, *La resonance paramagnetique electronique,* Dunod, Paris, 1968.
5. J. W. ORTON, *Electron Paramagnetic Resonance,* Illfe Books Ltd. London, 1968 ; A. NICULA. *Rezonanța magnetică,* Editura Didactică și Pedagogică, București, 1980.
6. A. ABRAGAM, *The principles of Nuclear Magnetism,* Clarendon Press, Oxford, 1961.
7. CH. SLICHTER, *Principles of Magnetic Resonance,* Harper & Row, New-York, 1963.
8. G. E. PAKE, *Paramagnetic Resonance,* W. A. Benjamin, New York 1962.
9. GH. POOLE, *Electron Spin Resonance,* Interscience Publishers Inc., New York (1967).
10. J. D. MEMORY, *Quantum Theory of Magnetic Resonance Parameters,* Mc Graw Hill Book Co., New-York, 1968.
11. K. MOBIUS, H. HAUSTEIN, M. PLATO, Z. Naturforsch. 23, 1626, (1968).
12. G. HALL, *A. Hardison,* Proc. Roy. Soc. (London) 278 A, 129, (1964).
13. A. J. STONE, Mol. Phys., 6, 509, (1963).
14. A. J. STONE, Mol. Phys., 7, 311. (1964).

15. H. R. FALLE, G. R. LUCKHURST, J. Mag. Res., 3, 161, (1970).
16. H. R. FALLE, G. R. LUCKHURST, Mol. Phys., 11. 299, (1966).
17. S. H. GLARUM, J. M. MARSHALL, J. Chem. Phys., 44, 2884, (1969).
18. W. MAIER, A. SAUPE, Z. Phys. Chem., 6. 327, (1956).
19. L. C. SNYDER, J. Chem. Phys., 43, 4041, (1965).
20. A. SAUPE, Z. Naturforsch A 19, 161, (1969).
21. I.ZUPANCIC, M. VILFAN, M. SENTJURC, M. SCHARA, F. PUSNIC, J. PIRS, R. BLINC in Liquid Crystals and ordered fluids, vol. 2, p. 525 (J. F. Johnson, R. S. Porter — Editors), Plenum Press, New York, 1978.
22. G. R. LUCKHURST, Mol. Cryst. 2. 363, (1969).
23. A. CARRINGTON, G. R. LUCKHURST, Mol. Phys., 12, 55, (1967).
24. S. H. GLARUM, J. H. MARSHALL, J. Chem. Phys., 46, 55, (1967).
25. H. R. FALLE, G. R. LUCKHURST, N. LEMAIRE, Y. MARECHAL, A. RASSAT. P. REY, Mol. Phys., 2, 11, 4 9(1968).
26. P. KREBBS, E. SACKMANN, J. VOSS, Chem. Phys. Lett.. 8, 417, (1972).
27. P. KOITTIS, R. LEFEBVRE, J. Chem. Phys.. 41, 3660, (1964).
28. J. VAND DER WAALS, M. S. DE GROOT, Mol. Phys., 3, 196, (1960).
29. P. KOTTIS, Ann. Phys., 4, 458, (1960).
30. A. R. FORRESTER, R. H. THOMSON, G. R. LUCKHURST, J. Chem. Soc. B, 1311, (1968).
31. I. AGRANAT M. RABINOWITZ, H. R. FALLE, G. R. LUCKHURST, J. N. OCKWELL, J. Chem. Soc. B. 294 (1970).
32. C. SCHWERDFEGER, P. DIELL, Molec. Phys., 17, 417 (1969).
33. P. DIEHL. C. F. SCHWERDTFEGER, Molec. Phys. 17, 423, (1969).
34. J. C. ROWELL, W. D. PHILLIPS, L. R. Melby, M. Panar J. Chem. Phys., 43, 3442 (1965).
35. D. H. CHEN, G. R. LUCKHURST, Mol. Phys., 16, 91, (1969).
36. L. C. SNYDER, T. AMOS, J. Chem. Phys., 41. 1773, (1964) and 42, 3670, (1965).
37. K. P. DINSE, R. BIEHL, K. MOBIUS, H. HAUSTEIN, Chem. Phys. Let., 12, 399, (1971).
38. F. E. CARR, E. A. HOAR, W. T. MAC DONALD, J. Chem. Phys., 48, 2822, (1960).
39. C. A. HUTCHINSON, B. W. MAGNUM, J. Chem. Phys., 29, 958, (1958).
40. A. E. STILLMAN, L. J. LORETTA, R. N. SCHWARTZ, B. L. BALES, *Liquid Crystals and Ordered Fluids*, vol. 3. 1978.
41. A. BERMAN, E. GELERINTER, G. C. FRYBURG, G. H. BROWN, in *Liquid Crystals and orderd fluids*, vol. 2, p. 23, 1974.

ANALELE UNIVERSITĂŢII BUCUREŞTI, FIZICA, XXXII 1983, pag. 87—90

DETERMINATION OF THE FOG INTRINSIC PARAMETERS BY MEANS OF THE LASER RADIATION EXTINCTION

D. BORŞAN, SABINA ŞTEFAN
University of Bucharest, Faculty of Physics *

1. Introduction

The fog is a colloidal system made out of an agglomeration of water drops, ice crystals or a mixture of these, to be found in the air, in a state of suspension. This system is the outcome of the condensation or sublimation of water vapours contained in an air layer close to the ground level. The immediate consequence of fog formation is a reduced visibility along the horizontal direction at values lower than one kilometer.

Function of its formation conditions the fog falls into the following classes : advection fog, evaporation fog, radiation fog. According to the physical structure, the fog may be classified as : fog made up of water-drops, fog made up of ice crystals and fog of mixed componence. It is the object of this paper to deal with fog made up of water drops only.

The micro-physical structure of fog is determined by the physical formation conditions and has the following main characteristics :

- the dimensional range of particles and the system of magnitudes characterizing this range ;
- the particle concentration — N ;
- the liquid water contents — q ;
- the visibility distance, or the meteorological visibility — S_m.

It is important to know the microphysical characteristics in the study of the physical processes leading to fog formation and dissipation, respectively. The determination of these characteristics is performed by direct measurements or indirectly by measuring two of them and determining the remaining two on account of the relationships betwwen them.

In this paper the microstructural characteristics of fog were determined making use of the laser radiation extinction through fog and the dimensional range of drops measured by the impact method [1].

The laser radiation extinction through a polydisperse environment, as it is the case of fog, takes place due to absorbtion and diffusion on the water drops within fog. Quantitatively speaking, extinction may be characterized by the volumetric extinction coefficient in the extinction law:

$$I = I_0 \exp(-\alpha h) \qquad 1$$

---

* National Centre of Physics, C.P. 5211, Măgurele, Bucharest.

where h is the depth of the homogeneous layer covered by radiation. The expression of α for a radiation of wavelenght in a polydisperse environment consisting in spherical water drops and characterized by the distribution function according to radius f(x) is given by the Mie theory [2]:

$$\alpha(\lambda) = N\int_0^\infty Q(x, m)\pi r^2 f(r)\,dr \tag{2}$$

where $Q(x, m)$ is the effective extinction factor of a water drop, $x = \frac{2\pi r}{\lambda}$, r is the radius of the spherical water drop, m is the complex refraction index of the drop material. In the limit case of smallest drops $Q(x, m) \cong 4\left|\frac{m^2 - 1}{m^2 + 1}\right| x^4$ while with largest drops $Q(x, m) \cong 2$.

For the particles the dimensions of which are comparable with λ, $Q(x, m)$ may be tabled for various values of r and λ. For certain practical purposes one may use the effective average extinction factor $F(\lambda)$ defined as below, instead of $Q(x, m)$

$$F(\lambda) = \frac{\alpha(\lambda)}{S} = \frac{\int_0^\infty Q(x, m)\pi r^2 f(r)dr}{\int_0^\infty \pi r^2 f(r)dr} \tag{3}$$

where $S = N\int_0^\infty \pi r^2 f(r)dr$ stands for the efficient section of the volume units. Making use of the average effective extinction factor $F(\lambda)$, the following relationships may be established between $\alpha(\lambda)$, N, q and S_m :

$$\begin{aligned} \alpha(\lambda) &= k_N(\lambda)\cdot N \\ \alpha(\lambda) &= k_q(\lambda)\cdot q \\ \alpha(\lambda) &= k_s(\lambda)\cdot S_m \end{aligned} \tag{4}$$

Coefficients k_N, k_q and k_s are called correspondence coefficients and are defined by the following expressions :

$$k_N = F(\lambda)\int_0^\infty \pi r^2 f(r)dr = \pi r_2 F(\lambda)$$

where r_2 is the average square radius of the waterdrops ;

$k_q = \frac{3}{4\,a_q\rho}$ where $a_q = \frac{{r_3}^2}{{r_2}^2}$, r_3 standing for the average cubic radius of the water drops and ρ for the water density ; k_q coefficient is constant for a given λ. For a $\lambda = 0.6328\mu$ is considered equal with 3.91.

Working method

The fog was produced in a fog chamber of a cylinder shape, 1.54 m long and 50 cm in diameter, by the adiabatic relaxation of humid air under a pressure of about 1.5 atm.

The volume extinction coefficient was measured by a differential method. This lies in recording the signal generated by a photodiode which receives the radiation emitted by a He-Ne laser ($\lambda = 0.6328\ \mu$) across the chamber. The measured voltage is proportional with the intensity of the received radiation : $U_0 = kI_0$. When the laser radiation crosses the chamber where fog was produced, the signal received by the photodiode is $U = kI$.

During measurements the stability of the quantic generator was provided.

The volume extinctor coefficient was computed according to relation:

$$\alpha = \frac{1}{L} \ln \frac{U_0}{U}$$

During the recording, samples were taken in order to establish the fog microstructure. In sample taking the impact method was employed. The air containing fog drops is absorbed at a constant speed through a tube provided with a nozzle. In front of the nozzle there is a glass blade covered with a thin layer of oil and petroleum jelley. The water drops run against the blade and sink into the mixture layer which prevents their evaporation. The samples are photographed at a microscope which enlarges 200—300 times.

Outcomes of the study. Conclusions

From the images obtained by an adequate statistical processing the dimensional particle range is reached. The average radius is also determined

$$r_1 = \frac{1}{N} \sum_i N_i r_i = \int_0^\infty r f(r)\, dr$$

as well as the average square radius

$$r_2 = \sqrt{\frac{\sum_i N_i r_i^2}{N}} = \sqrt{\int_0^\infty r^2 f(r) dr}$$

and the average cubic radius

$$r_3 = \sqrt[3]{\frac{\sum_i N_i r_i^3}{N}} = \sqrt[3]{\int_0^\infty r^3 f(r) dr}$$

Once and the structure parameters r_1, r_2 and r_3 known, the other structure parameters are determined :

1) the visibility distance $S_m = \dfrac{3{,}91}{\alpha}$,

2) the liquid water content $q = \dfrac{10\alpha r_1}{9}$, where ρ is water density,

3) the particle concentration $N = \dfrac{5}{6} \dfrac{\alpha}{\pi} \dfrac{r_1}{r_3^3}$ and

4) the A and b constants in the distribution function of the drops according to radius : $f(r) = Ar^2e^{-br}$ /3/

The A constant equals $\frac{1.61}{5r_1}$ while $b = \frac{3}{r_1}$.

The data obtained are listed in table no. 1. The measurements were taken for fog obtained under various physical conditions and therefore the dimensional range is different. The results reached spotlight the fact that there is a proportionality relationship between the volume extinction coefficient and the q liquid water content or the N concentration of particles. The proportionality coefficient depends on the fog structure (i.e. on r_1 ; r_2 and r_3) and olso on the wave length.

Table 1

No.	α (m^{-1})	S_m(m)	r_1(μ)	r_2^2(μ^2)	r_3^3(μ^3)	q(g/m^3)	N(cm^{-3})	A (μ^{-6})	b(μ^{-1})
1.	0.36	10,86	3.3	17.45	110.6	1.32	0.00286	0.00011	0.91
2.	0.47	8.319	1.31	2.17	5.81	0.684	0.0281	0.168	2.290
3.	0.48	8.146	1.91	4.04	12.82	1.019	0.0189	0.366	1.571
4.	0.49,	7.980	1.24	2.11	5.33	0.675	0.0302	0.168	2.290
5.	0.5	7.82	1.14	1.63	3.44	0.633	0.0439	0.802	2.632
6.	0.74	5.284	2.31	6.20	20.13	1.899	0.0225	0.317	2.205
7.	0.79	4.950	1.59	3.04	8.22	1.396	0.0405	0.137	1.887
8.	0.86	4.546	1.17	1.94	4.56	1.118	0.0584	0.488	1.276
9.	1.045	3.742	1.75	3.46	9.34	2.032	0.0518	0.076	1.714
10.	1.09	3.587	1.36	2.35	6.66	1.647	0.0574	0.317	2.205

The experimental data led to the conclusion that the dimensional range and the distribution function according to radius (r) are similar to other relations to be found in the literature in the field [3].

The study of the dimensional range and of the characteristic fog parameters may be extended to the natural fog by means of the same method. Such studies are of great importance in approaching the proper means in atmospheric fog dissipation.

BIBLIOGRAPHY

1. LEVIN, L. M. a.o., *Aerozolnie lovuşki primenianie v Elbruskoi expediţii*, 1957.
2. HULST VAN, H.C., *Light diffusion with small particles (Russian)*, 1961.
3. HRIGHIAN, A. H., MAZIN, I. P., Trudî Ţentr. Aerol. Obs. nr. 7, 1952.

ANALELE UNIVERSITĂŢII BUCUREŞTI, FIZICA, XXXII, 1983, pag. 91—94

CORRELATED ANALYSIS OF PARTICLE CONCENTRATION AND METEOROLOGICAL PARAMETERS ON THE MĂGURELE PLATFORM

ELENA DECU, ŞT. LASCU
Faculty of Physics, University of Bucharest *

Abstract. In this paper we tried to point out the correlative relation between different measures hat characterize the particle concentration in the air, as well as between these and the meteorogical parameters. The calculation of the correlation coefficients, together with their characterization as significant or not, reveal a series of linear correlations for which the respective regressive straigth lines were written. The existence of some insignificant correlation coefficients asserts the lack of linear correlations between the respective measures, emphasizing the need of finding some other types of correlation.

Introduction

The study of the dependence of some magnitudes measured in terms of different factors, without knowing some precise physical laws, claims the use of some statistic laws. Some results concerning the manner in which some meteorogical factors influence particle concentration in the atmosphere were obtained in [2]. In paper [3, 4] the way in which the particle concentration on the Măgurele Platform verifies the laws of a normal distribution has also been studied.

The correlation between the different magnitudes of the measured particle concentration, as well as between them and different meteorological parameters is searched for in the following.

As it is known, within the linear correlation the dependences are expressed by regressive straight lines that intersect each other in a point

---

* National Center of Physics, P.O. BOX 5211, Măgurele, Bucharest.

called regressive point (x, y) whose angle characterizes the correlation degree : the smaller the angle, the closer the correlation.

The equations of the regressive straight lines are :

$$\begin{aligned} y - \overline{y} &= m\,(x - \overline{x}) \\ x - \overline{x} &= m'\,(y - \overline{y}) \end{aligned} \qquad (1)$$

in which m is the regressive coefficient of y on x and represents the inclination of the respective stright line towards the ox axis, and m′, the regressive coefficient of x on y, being the inclination of the second straight line towards oy.

The expressions of the regressive coefficients m and m′ in relation to the series of values of the two magnitudes are :

$$m = \frac{\Sigma\,(x_i - \overline{x})\,(y_i - \overline{y})}{\Sigma\,(x_i - \overline{x})^2}, \qquad m' = \frac{\Sigma\,(x_i - \overline{x})\,(y_i - \overline{y})}{\Sigma\,(y_i - \overline{y})^2} \qquad (2)$$

Taking into account the definition of the coefficient of linear correlation

$$r = \frac{\Sigma\,(x_i - \overline{x})\,(y_i - \overline{y})}{N \cdot \sigma_x \cdot \sigma_y} \qquad (3)$$

and also the expressions of the standard deviation σ_x, σ_y of the two series of values, the result will be :

$$m = r\,\frac{\sigma y}{\sigma x}, \qquad m' = r\,\frac{\sigma x}{\sigma y} \qquad (4)$$

The correlation coefficient r is an adimensional magnitude, with $|r| \leqq 1$, and its values characterize the degree of connection between the two variables x, y, thus :

$r \in (-1, 1) \setminus 0$, correlation
$r \in \{-1, 1\}$, functional connection
$r = 0$, independence between the variables

Since in the calculations of the empirical coefficient of correlation, as a consequence of the aleatory spreading of the variables, even in case of independence r can be defined by zero, or in case of functional connection r can not be rigorously equal with the unity, there arises the necesity to verify the significance of the correlation coefficient by comparing the calculated product $H = |r|\,\sqrt{N-1}$ with its critical value for a given confidence level.

1. Calculation of the empirical correlation coefficient and its significance.

We considered the series of measured particle concentration on the soil of the Măgurele Platform in 1976, divided into the four dimensional domains : this is the series for which studies upon normality were carried out in papers [3, 4].

If we calculate the correlation coefficients (3) for different combinations of concentrations : Aitken particles C , big and huge particles C_G, C_1, C_3, C_5 ($C_G = C_1 + C_3 + C_5$), as well as the combinations between the particle concentrations and the values of the meteorological parameters : wind speed, temperature, humidity, the values represented in Table were obtained. These magnitudes r were used to determine calculated H, which were compared to critical H taken out of [1, 6], for a near probability $P = 0.99$ (or $P = 0.999$), all of them being encountered in Table 1 ; the magnitudes r also help to draw some conclusions on the significance of the coefficient correlation r.

In Table obtained it is easy to note that some values of r are insignificant, which means that between the respective magnitudes there is no linear dependence ; still a non-linear dependence is possible as a measure of such a dependence, that is the concentration of some experimental points round the regressive curves ; thus the correlation ratio must be also calculated.

The significant coefficients of correlation were found between the magnitudes C_G and t ; G_G and C_1 ; C_G and C_3 ; C_G and C_5 ; C_1 and C_3 ; C_3 and C_5 ; C and C_1, for which the regressive coefficients were calculated with the relations (2).

2. Equations of the empirical regressive straight lines.

We wrote down the equations of the regressive straight lines for the cases with significant correlation coefficient r.

The correlation between the concentration C_G and t has $r = 0.3340$, the positive value of the correlation coefficient showing that the concentriation of big and huge particles increases when the temperature increases.

The equation of the regressive straight line is :

$$C_G = 3.518\ t + 255.1 \tag{5}$$

To the positive correlation between the concentration of big and huge particles C_G (0.1—5 μ) and the concentration C_1(0.1—1μ) having $r = 0.977$, the corresponding straight line is :

$$C_G = 1.129\ C_1 + 15.82 \tag{6}$$

The large positive correlation between C_G and C_5 (1—3 μ) with $r = 0.6748$ shows that the increase of one of the magnitudes leads to the increase of the other one, the equation of the regressive straight line being :

$$C_G = 3.277\ C_3 + 175 \tag{7}$$

Between the C_G and C_5 (3—5 μ) concentration there exists a positive correlation coefficient, $r = 0.3171$; the regressive straight lines hat the form :

$$C_G = 5.836\ C_5 + 246 \tag{8}$$

Between the C_1 and C_3 concentrations there exists a positive correlation coefficient $r = 0.5252$ which yields the regressive straight line :

$$C_1 = 2.207\ C_3 + 168 \tag{9}$$

Between the concentrations C_3 and C_5 there also exists a positive correlation coefficient, $r = 0.4427$; there results the following regressive straight line :

$$C_3 = 1.678\ C_5 + 22.65 \tag{10}$$

Given the negative correlation that exists between C_1 and the concentration of the Aitken nuclei C , having $r = 0.2998$, that is relatively high, it means that the increase of the C_1 concentration is occasioned also by the fusion of the Aitken particles, their concentration being lowered. In this case, the regressive straight line is :

$$C_A = -\ 35.29\ C_1 + 38.580 \tag{11}$$

Conclusions

The equations (5) — (11), as well as the data in Table 1 show that between the majority of the studied magnitudes there exists a linear correlation. These correlations expressed by the respective regressive straight lines permit the determination of a variable in terms of the value experimentally found for the other variable at a certain moment, or a possible prognosis in case a rate of variation is determined for one of them.

Table obtained also points out insignificant r coefficients, that is the absence of linear correlation between the respective variables ; this fact evinces the necessity of further studies for revealing some possible non-linear correlations or some possible non-dependences.

REFERENCES

1. CONSTANTINESCU I., GOLUMBOVICI D., MILITARU C. — *Prelucrarea datelor experimentale cu calculatoarele numerice*, București, 1980.
2. DECU ELENA, LASCU ŞT., EŞEANU D. — Anal. Univ. Buc., Fizică, XXVII, 1978, p. 97—101.
3. DECU ELENA, LASCU ŞT. — Anal. Univ. Buc., Fizică, XXVIII, 1979, p. 117—121.
4. DECU ELENA, LASCU ŞT., DIACONU OTILIA — Anal. Univ. Buc., Fizică, XXX, 1981, p.
5. FACY L. — Rev. Assoc. prev. poll. atm., 1959.
6. RUMŞISKI Z. L. — *Prelucrarea matematică a datelor experimentale*, Buc., 1974.
7. YULE G. U., KENDALL M. G. — *Introducere în teoria statisticii*, Buc., 1969.

Received January, 1982

ANALELE UNIVERSITĂŢII BUCUREŞTI, FIZICA, XXXII, 1983, pag. 95—104

CONSIDERATIONS UPON THE VARIATION OF THE SEISMIC WAVE VELOCITY BENEATH THE VRANCEA ZONE

ŞT. LASCU, ELENA DECU
Faculty of Physics, University of Bucharest *

Abstract. By using the residuals of the P wave travel times we can point out the azimuthal variation of the P wave velocity beneath the Vrancea seismic zone. As this variation presents certain differences from one stratum to another, considering the five strata the upper mantle beneath the Vrancea is divided in, in the present study we suggest the idea that in this zone the subduction process is complex and associated with a torsion of the subduct plate together with a lateral displacement.

We also point out that the plate has a small displacement or naught of advance, being crushed by the three adjacent tectonic plates that have a convergent movement in this zone.

Introduction

The study of the distribution of the seismic wave velocities in terms of the depth they reach in the inner part of the earth, pointed out, for most of the active seismic zones, regional variations as against the adopted standard model which is characterized by the travel time tables used in determining the focuses. The study has revealed the existence of a low velocity stratum, especially for the S waves ; as for the P waves the existence of this stratum has been more difficult to establish. For certain seismic zones characterized by the producing of earthquakes as a consequence of a subduction process, the existence of some anomalies both in the seismic wave velocities and in the attenuation of the seismic energy in the upper mantle has been noticed, these anomalies being characterized by high velocities of the seismic waves [19] and reduced attenuations of energy [20].

---

* National Center of Physics, Măgurele, Bucharest, P.O. Box 5211.

The Vrancea seismic zone, in which the earthquakes are generated by a subduction process too, has been intensely studied from this point of view ; the existence of some strata in which the velocity does not increase with the depth, in accordance with the model [5, 6, 11, 12, 13, 17, 18, 21], and whose upper and lower limits are to be found at various depths has been pointed out, the latter ones being dependent on the observation data and the methods used.

In the following we try to evince the existence of some lateral non-homogeneities of the medium beneath the Vrancea zone that implies the existence of some lateral anomalies for the seismic wave velocities which are largely responsible for the disagreements noticed in the limits of faster or slower increase of the wave velocities with the depth.

Data Employed

As in the most of the similar studies we used as observation data the travel times of the P waves produced by the stronger earthquakes beneath the Vrancea zone to be found in table 1) and recorded in the seismic stations all over the world.

These travel times are compared to the standard ones given by the two tables more important, i.e. the Jeffreys-Bullen [14] and the Herrin et. al. [9] tables, obtaining what seismologists call the residuals of the travel times.

Table 1

Earthquake		H h m s	φ^o_N	λ^o_E	h km
1	1929 XI 1	06 57 14	46.0	26.1	160
2	1940 VI 24	00 57 27	45.7	26.8	115
3	1940 X 22	06 36 57	45.7	26.8	122
4	1940 XI 8	12 00 44	45.7	26.7	145
5	1940 XI 10	01 39 07	45.7	26.8	134
6	1940 XI 11	06 34 16	45.7	26.8	134
7	1940 XI 19	20 27 12	45.7	26.8	134
8	1940 XI 23	14 49 53	45.7	26.8	150
9	1945 III 12	20 51 46	45.7	26.8	125
10	1945 IX 7	15 48 26	45.7	26.8	75
11	1945 XII 9	06 08 45	45.7	26.8	80
12	1948 V 29	04 48 58	45.9	26.7	140
13	1950 I 16	04 25 01	45.7	26.8	120
14	1955 V 1	21 22 52	45.5	26.3	134
15	1963 I 14	18 33 25	45.8	26.8	134

The residuals of the travel times can be affected by more factors :

a. *The imperfect localization of the focuses.* The systematic differences between the used travel time tables in terms of the epicentral distance as well as of the imperfect distribution in the epicentral distance and the azimuth of the recording stations lead to the imperfect localization of the focuses. The studies made for the earthquakes in the Tonga-Kermadec [19] point out that the earthquakes hypocentres determined by Herrin's tables together with the station corrections suggested by Herrin and Toggart [10] differ by 5 km at the most from the hypocentres of the same earthquakes determined by the Jeffreys-Bullen tables without any corrections. For the Vrancea earthquakes under study when trying to represent graphycally the frequency of the residual distribution for three values of depth namely : h — the earthquake depth, and two neighbouring depths, h — 0.001 R and h + 0.001 R, we came to the conclusion that the curve nearest to the gauss one is that corresponding to the depth h ; this reason induced us to overlook the modification of the depths.

b. *Errors in determining the origin times.* The given systematic differences between the two travel time tables (fig. 1) will lead to systematic differences in the origin times determined and consequently in the travel times noticed. The residuals calculated in relation to the same tables for determining the hypocentres are practically independent the tables employed. For avoiding errors in determining the origin time we did not use the individual values of the residuals but the mean values of all the earthquakes under study ; the data were collected from more stations, excluding the ones which did not record all the earthquakes. In this way the sum of the errors in determining the origin times maintains constant for all the distances and azimuths, without affecting the obtained curves shape, possibly displacing them in relation to the ordinates axis.

c. *The lateral non-homogeneity of the mantle.* As already known the majority of the travel time tables are fully concordant for large epicentral distances ; that is why we accept that the low mantle is homogeneous enough from the view point of the azimuthal distribution of the seismic wave velocity. Jeffreys [15] and Carter [2], when studying the travel times of nuclear explosions in the Pacific, found their azimuthal variations very small or zero. Chinnery and Toksoz [3], Hales et al. [8] consider that the travel times in the lower mantle can not be perfectly symmetrical, but Hales et al. 's data suggest that the azimuthal variations, even if existent, are very small and at the same time very difficult to separate from the variations in the upper mantle.

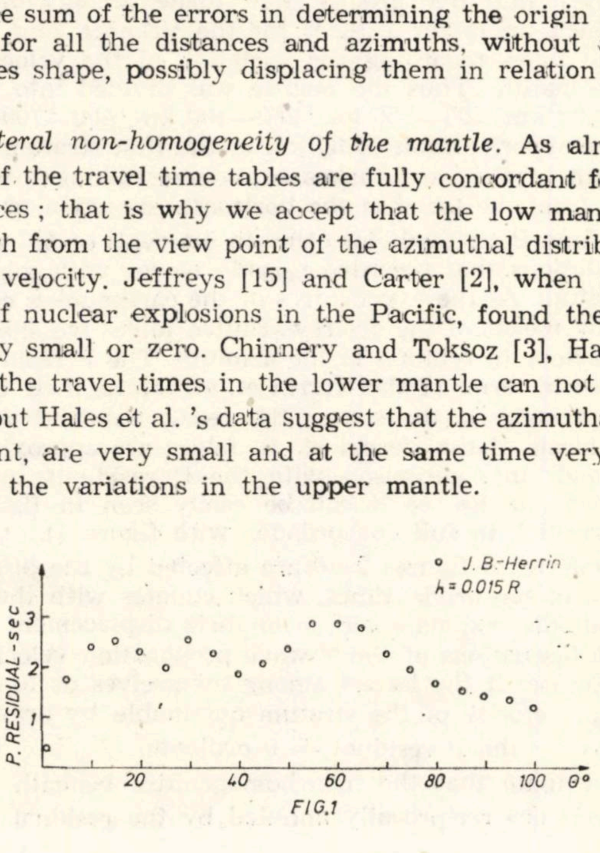

FIG.1

So, in accordance with Herrin [10], Mitronovas [19] the existence of some asymmetries in the travel times noticed will be considered in the present study too as a consequence of the existence of some lateral anomalies of the seismic waves in the upper mantle beneath the Vrancea zone, superposed on the effect of the erroneous localization of hypocentres resulting from the non-uniform distribution of the recording seismic stations.

Results

For evaluating the distribution of the seismic wave velocity beneath the Vrancea zone, in terms of the azimuth for different depths we divided the recording stations into five groups according to the maximum dept to which the seismic rays had penetrated into the inner part of the earth, and we noted with h_p the depth of the seismic rays minimum. A division of these stations according to the epicentral distance only would have been wrong because the depth h of the earthquakes considered varies from 0.007 R to 0.020 R and for the same epicentral distance the seismic rays from an earthquake having its depth $h = 0.007$ R have their minimum at a h_p depth smaller than that of the corresponding seismic rays of an earthquake with its depth $h = 0.02$ R. This division of the stations into five groups was made taking into account the results obtained up to the present for the Vrancea zone as well as for other seismic zones regarding the variation of the velocity against the depth in the mantle. Thus the mantle was divided into five concentric strata : 80—200 km, 200—250 km, 250—400 km, 400—700 km and 700—2900 km ; the superior limit of 80 km of the first stratum represents the minimal depth of the earthquakes considered, taking into account only seismic rays from the focus in the horizontal direction or downward.

The medium P residuals for azimuth intervals of 30° were calculated for all the stations that recorded seismic waves with minimal depth in the same stratum. As the hypocentres of the earthquakes considered were determined by means of the Jeffreys-Bullen tables we shall discuss their residual behaviour in relation to the azimuth. The P residuals have been still calculated in terms of the Herrin et. al. tables, their coordinates and origin times remaining the same ; the result obtained was that the P residuals in terms of the Herrin et. al. tables are approximately greater by 2—3 seconds in comparison with the P residuals in terms of the Jeffreys-Bullen's tables, as it can be easily seen in figures 2—6 (the curves are parallel, in full concordance with figure 1).

All the curves in figures 2—6 are affected by the possible incorrect determination of the origin times, which equates with the addition of a constant to all the residuals and so to their displacement as against the ordinate ; the discussions of the P wave propagation velocities will focus on the comparison of the latters among themselves or to their comparison to a mean velocity of the stratum obtainable by drawing a parallel to the axis ox by the P residual = 0 ordinate.

If we postulate that the non-homogenities beneath the recording seismic stations are reciprocally annuled by the residual mediation and

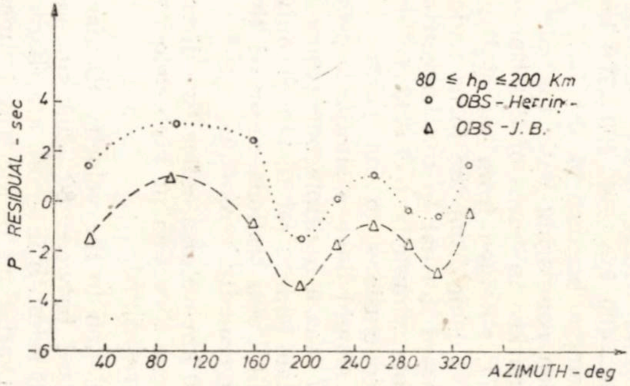

Fig. 2

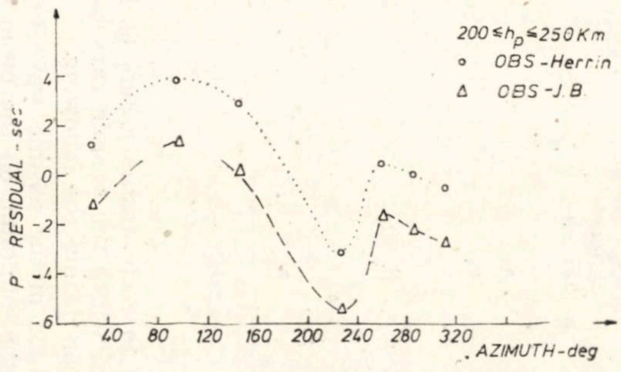

Fig. 3.

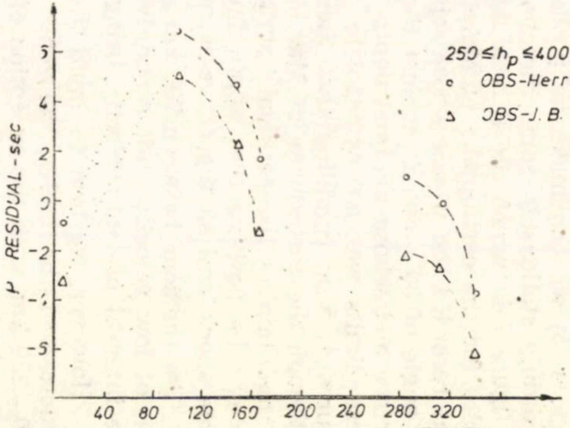

FIG. 4

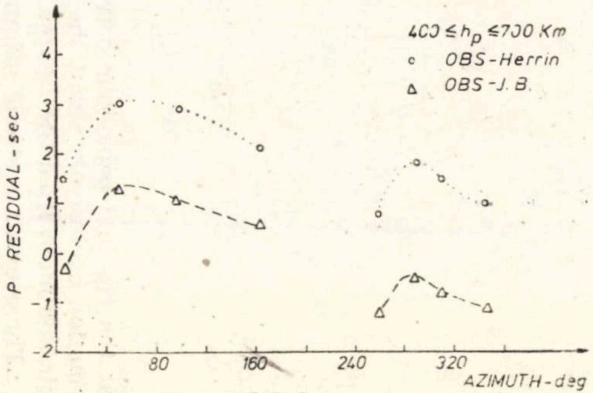

FIG. 5

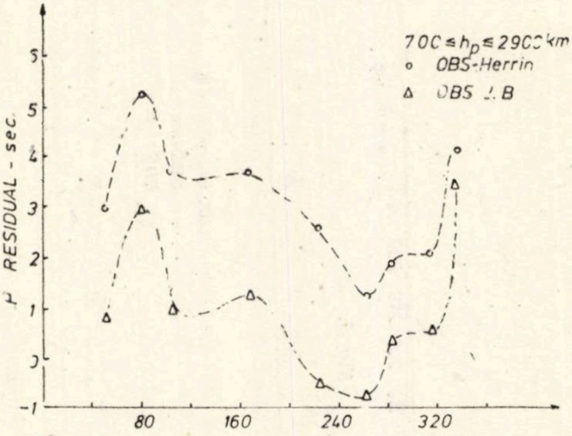

FIG. 6

that the residual behaviour corresponding to each stratum offers us information exclusively about the stratum in which the seismic rays have their minimum from the figures 2—6 we can deduce the following.

There exists a strong azimuthal variation of the seismic wave velocity characterized by low velocities with the minimum on the mean direction of 100° and by high velocities whose maximum is to be found within larger limits between 200°—260°.

In the strata 80—200 km and 200—250 km the velocity presents two directions of minimum and two of maximum which, indeed, are not equal (figs 2, 3), while for the strata 250—400 km and 400—700 km (figs. 4, 5) we can make no positive statement because of the lack of recording stations in some directions. When comparing with the curve in figure 7 in which the P residuals are marked in terms of the Harrin tables for the earthquake of March 4, 1977, obtained from the stations that recorded the waves whose seismic rays come from the focus under an angle of 30°—60° as against the downward normal to the terrestrial surface and whose minimal depth h_p is approximatelly included within these limits we can extrapolate these conclusions to the curves in figures 4, 5 on condition that these ones should have a similar aspect. Although the earthquake of March 4, 1977 was a multiple phenomenon, by maintaining the residuals' within certain epicentral distances only, we can be positive that approximately all these stations recorded the same shock and so the curve is not exaggeratedly erroneous.

For the zone between 700 km and 2900 km we also notice two direction of low velocity and, certainly, only one direction of high velocity, the interval of high velocity being more restricted.

However, we bear in mind that in relation to the velocity standard structure of the tables, the zones comprised between 80—200 km and 200—250 km, with the exception of a small azimuth interval, are characterized by higher velocity, with 6 seconds' variations of the travel times. Within the 250—400 km zone, an marked decrease of velocity on the ≈ 100° azimuth direction is noticed, together with the existence of a

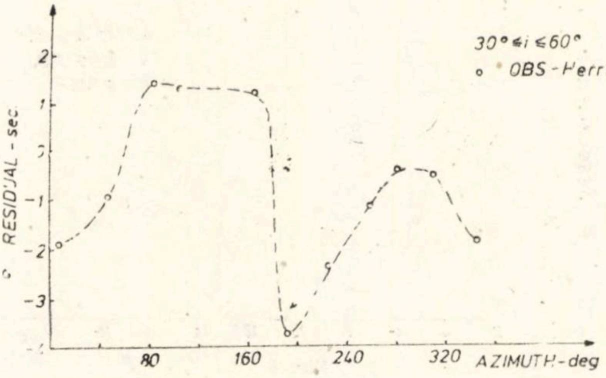

Fig. 7.

high velocity for azimuths of about 360° ; the absence of observation data between 180° and 280° do not allow us to appreciate the direction of about 240°. If in the 400—700 km stratum the curves become evidently levelled producing the impression of a certain lateral homogeneity, in the lower part of the mantle, 700—2900 km, the discordance between velocities reappears, the residuals, variations from minimum to maximum are of about 6 seconds one should further notice that for the majority of the azimuthal directions the wave velocity is reduced. As in figures 2, 3, 4 the curve in figure 7 obtained for the earthquake whose coordinates are determined by the Herrin tables points out, besides the azimuthal asymmetry of the velocities, the fact that for most of the directions the velocities are higher.

Figures 2—6 emphasize the displacement of the direction of high velocity to big azimuth, while the direction of low velocity displaces to reduces azimuths while the azimuthal interval of lower velocity is restricted. Such a displacement can be accounted for only by the torsion and changing of the subduction direction of the subduct plate, bearing strong evidence that in this zone the subduction process is more complex, consisting of a downward displacement of the subduct plate combined both with its lateral torsion and displacement.

In figures 8, 9, 10 we represent the residuals in terms of the Jeffreys-Bullen tables in relation to the epicentral distance ; the residuals were calculated only from earthquakes having the same depth, separately for all the earthquakes mith the dept about 0.015 R and for those with h = 0.007 R. Two fixed directions were chosen, one for the azimuth of about 100° corresponding to the lom velocity, the other one for azimuth of about 300° corresponding to the interval with higher velocity. For the earthquakes having a small depth h = 0.007 R there are nont enough data corresponding to the direction of 100°. The direction of high velocity, the azimuth of about 250° would have been more indicated but figures 4 and 5 show that there are not enough data for some strata of the mantle corresponding to this azimuth. The curves are drawn down to epicentral distances a little over 20°, corresponding to some penetrating depths of the seismic ray inferior to 600 km.

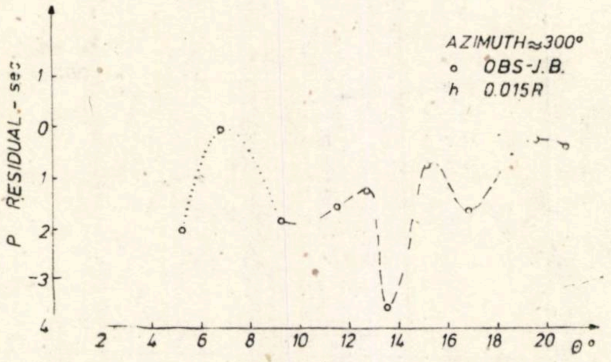

Fig. 8.

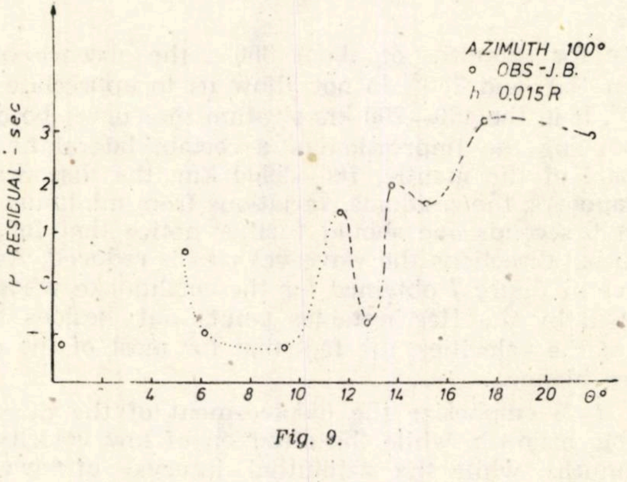

Fig. 9.

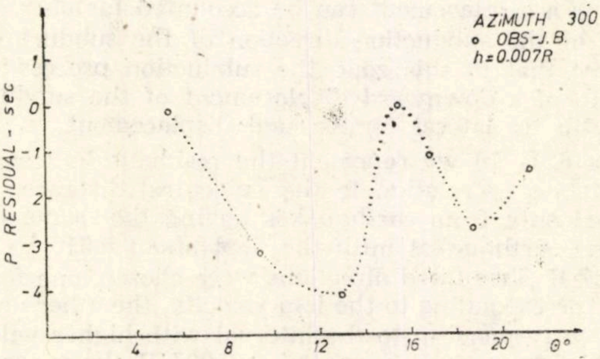

FIG. 10

The different shape of the curves for the direction of 100° as against the direction of 300° for epicentral distances smaller than 13° is obvious, consequently for depths that are a little longer than 200 km. The three curves (figs. 8, 9, 10) are not similar, helping the conclusions of some different velocity structures on different directions. The non-concordance of the curves in figures 8 and 10 built up for the same direction but derived from earthquakes with different depths is explained by the fact that as the deepest point of the seismic ray reaches greater depths, it also moves away from the vertical line passing through the epicentre of the earthquakes having a distance with the same order of magnitude and so, although the curves 8 and 10 give information about the seismic wave velocity for the same depth and direction, they do not bring the information from the same points.

Conclusions

Synthesizing the results contained in figures 1—10 on the velocity distribution beneath the Vrancea zone we can state the following :

1. The curves that give the P residuals, calculated by using the Jeffreys-Bullen and Herrin tables are practically parallel for all the strata of the mantle, leading to the same conclusions on the lateral anomalies of the seismic wave velocity.

2. The changing of the hypocentre depth h by h ± 0.001 R does not lead to essential differences in the shape of the 2—6 curves ; it results that the erroneous localization of hypocenters is only slightly responsible for the azimuthal variation of the seismic wave travel times in this zone.

3. The existence of some low propagation velocities in the 80—100 azimuth interval, in contrast to the high velocities at azimuths of 200—280°, demonstrates that the subduct tectonic micro-plate is stronger than the adjacent material and that it is found at another temperature than this one.

4. The variation of the maximum velocity direction with the depth suggests the changing of the subduction direction of the subduct plate, associated with a change in the orientation of the principale tensions responsible for the producing of splits in the earthquakes focuses, being knomn that the lab experiments with rocks subject to pressures give maximum velocities on the maximum tennsion direction and small velocities on the minimum tension directions [7]. The change in the direction orientation of the material's crystallization can also be a cause of change in the high velocity direction ; the azimuthal variation of the velocity can be also explained by the crystal orientation in the medium [1].

5. The behaviour of the travel time residuals together with the results of the studies on the focal mechanism for the earthquakes in the Vrancea zone [4] and on the direction of the fault plane for plain-producing earthquakes at the mestern part of the subduction plate [22] lead us to the idea that not the microplate of the Black Sea is moving towards the Nord-West penetrating the Transylvania plate but that the three plates, in their convergent displacement, swallow, by subduction, the microplate of the Black Sea. This conclusions is justified by the existence of some profound faults too [6, 23] that are parallel to the subduction

direction and which betray the existence of some compression tensions generated by the two adjacent, convergent plates, as demonstrated by the experiments [7].

Thus the movement of the plate which is subdeued may be considered either as an up or down movement producing the mentioned faults and accounting for the superior width of the crust beneath this plate in comparison with the medium crust in Europe as well as for the variation by leaping of the depths of the Conrad and Moho surfaces [5, 6, 23].

REFERENCES

1. BABUŠKA V., 1972 — J. Geophys. Res., 77, 6955.
2. CARDER D. S., 1964 — Bull. Seismol. Soc. Amer., 54, 2271.
3. CHINERY M. A. and TOKSOZ M. N., 1967 — Bull. Seismol. Soc. Amer., 57, 199.
4. CONSTANTINESCU L., ENESCU D., 1963 — Studii şi Cercet. de Geofiz., 1, 51.
5. CONSTANTINESCU L., CORNEA I., ENESCU D., 1972 — Rev. Roum. Geophys., 16, 3.
6. GAVĂT I., et. al., 1963 — Studii şi Cercet. de Geofiz., 1, 7.
7. GUPTA I., 1973 — J. Geophys. Res., 78, 6936.
8. HALES A. L., CLEARY S. R., ROBERTS J. L., 1968— Bull. Seismol. Soc. Amer., 58, 1975.
9. HERRIN E. (Chairman), 1968 — Bull. Seismol. Soc. Amer., 58, 1193.
10. HERRIN E., TOGART J., 1968 — Bull. Seismol. Soc. Amer., 58, 1325.
11. IOSIF T., 1965 — Rev. Roum. Geophys., 9, 1, 13.
12. IOSIF T., 1966 — Rev. Roum. Geophys., 10, 1, 33.
13. IOSIF T., 1968 — Rev. Roum. Geophys., 12, 23.
14. JEFFREYS H., BULLEN K. E., 1948 — Seismological Tables-British Association for the Advancement of Sciences, London.
15. JEFFREYS H., 1962 — Geophys. J., 7, 212.
16. KEBEASY M. R., 1970 — Bull. Earth. Inst., 48, 381.
17. LASCU ŞT., 1975 — Anal. Univ. Buc., Fizică, XXIV, 41.
18. LASCU ŞT., 1980 — Anal. Univ. Buc., Fizică, XXIX, 107.
19. MITRONOVAS W., ISAKS B., 1971 — J. Geophys. Res., 76, 7154.
20. OLIVER J., ISACKS B., 1967 — J. Geophys. Res., 72, 4529.
21. PETRESCU G., RADU C., LASCU ŞT., 1965 — Rev. Roum. Geophys., 9, 129.
22. RADU C., 1965 — Rev. Roum. Geophys., 9, 1, 49.
23. SOCOLESCU M. et al., 1964 — Rev. Roum. Geophys., 8, 3.

Received, January, 1982

Abonamentele în țară se pot contracta la oficiile P.T.T.R., agenții poștali și factorii poștali.

Cititorii din străinătate se pot abona, adresîndu-se la ILEXIM Departamentul Export-Import Presă, P.O. Box 136—137, telex: 11229, București, str. 13 Decembrie nr. 3.

Lei 35